WORLD METEOROLOGICAL ORGANIZATION

GLOBAL ATMOSPHERE WATCH

WORLD DATA CENTRE FOR GREENHOUSE GASES

WMO WDCGG DATA SUMMARY

WDCGG No. 49

GAW DATA

Volume IV-Greenhouse and Related Gases

PUBLISHED BY
JAPAN METEOROLOGICAL AGENCY
IN CO-OPERATION WITH
WORLD METEOROLOGICAL ORGANIZATION

AUGUST 2025

CONTENTS

Page

PREFACE ---------- 1

1. CARBON DIOXIDE ---------- 3

2. METHANE ---------- 9

3. NITROUS OXIDE ---------- 15

4. HALOCARBONS AND OTHER HALOGENATED SPECIES ---------- 21

5. CARBON MONOXIDE ---------- 29

APPENDICES ---------- 35

A ANALYSIS ---------- 36

B CALIBRATION AND STANDARD SCALES ---------- 38

C LIST OF OBSERVATIONAL STATIONS ---------- 61

D LIST OF CONTRIBUTORS ---------- 72

E LIST OF ABBREVIATIONS ---------- 96

F LIST OF WMO/ WDCGG PUBLICATIONS ---------- 99

REFERENCES ---------- 101

PREFACE

Global observations of greenhouse gases are essential for understanding of the global carbon cycle and the role these gases play in driving climate change. The results of observations demonstrate accelerating increase of levels of major greenhouse gases in the atmosphere. Though the general trend is a result of the increased emissions of greenhouse gases to the atmosphere from anthropogenic activity (such as fossil fuel combustion, deforestation and agricultural activity) since the beginning of the industrial era in around 1750, the interannual changes are largely driven by natural variability. It is not easy to quantify spatial distribution of these changes given the limitations of the current observing network. The increasing greenhouse gas concentrations are driving detectable tropospheric warming. To avoid negative consequences of climate change, urgent actions should be taken towards reduction of greenhouse gas emissions based on scientifically robust information. It is also important to understand the feedbacks that are created in natural systems in response to climate change. Against this background, there is an increased demand for available and reliable greenhouse gas data to meet needs of scientific research and provide information for use by decision makers.

The World Data Centre for Greenhouse Gases (WDCGG) has been operated by the Japan Meteorological Agency (JMA) since 1990 in response to a request from the World Meteorological Organization (WMO). It holds the status of a World Data Centre (WDC) under the WMO Global Atmosphere Watch (GAW) programme and provides critical services to the community through data collection, analysis, archiving and distribution of data on greenhouse and related gases (such as CO) in the atmosphere over the land and oceans from surface stations, mobile platforms and certain satellites worldwide. WDCGG plays a critical role in the data management system of GAW. The data are provided online free of charge with a requirement for acknowledgment or offer of co-authorship when used in publications (see the WDCGG website for details). WDCGG implements an open data policy that is compliant with the WMO Unified Data Policy adopted in 2021. With the January 2025 site update, much of the data can be downloaded without user registration.

Information on the global state of major greenhouse gases in the atmosphere is regularly published in the WMO Greenhouse Gas Bulletin, to which WDCGG contributes via the calculation of globally averaged mole fractions, long-term trends and growth rates. The Bulletin has been used as a background document at the Conference of the Parties (COP) to the United Nations Framework Convention on Climate Change (UNFCCC) (https://unfccc.int/process/transparency-and-reporting/greenhouse-gas-data/greenhouse-gas-data-external-sources). The WMO WDCGG Data Summary in addition to reports on global averages covered in bulletins, also provides latitudinal or hemispheric averages and individual observational data used in global analysis. The Data Summary contains information on CO and certain halogenated species, which are not covered in the bulletins.

This issue of the Data Summary covers monthly mean observational data collected at surface stations and on certain ships for the period from 1968 to 2023 and submitted to WDCGG by September 2024. Observational data and the results of related analysis indicate that mole fractions of major greenhouse gases (CO_2, CH_4, N_2O, SF_6 and certain HCFCs and HFCs) are increasing, while those of certain ozone-depleting substances (e.g., CFCs) are not. The globally averaged mole fractions of CO_2, CH_4 and N_2O reached new highs of 420.0±0.1 ppm, 1934±2 ppb and 336.9±0.1 ppb in 2023, corresponding to 151%, 265% and 125% of pre-industrial levels, respectively. More detailed information is provided in the main text of this publication. The value-added analytical information presented in this Data Summary is expected to support scientific research, assessments and policy-making in relation to environmental issues.

WDCGG thanks all data contributors worldwide for their efforts in maintaining accurate long-term observations and for their ongoing data submissions. Contributors include the National Oceanic and Atmospheric Administration (NOAA) Global Monitoring Laboratory (GML) and its cooperative air-sampling network, the Advanced Global Atmospheric Gases Experiment (AGAGE), and a variety of other observational stations operating under the framework of GAW and other programmes as listed in Appendix D. All organizations submitting data to WDCGG are acknowledged as invaluable contributors to the Data Summary.

Mailing address:
WMO World Data Centre for Greenhouse Gases (WDCGG)
c/o Japan Meteorological Agency
3-6-9, Toranomon, Minato City, Tokyo 105-8431, Japan
E-mail: wdcgg@met.kishou.go.jp
Telephone: +81-3-3434-9127
Website: https://gaw.kishou.go.jp/

1.

CARBON DIOXIDE

(CO_2)

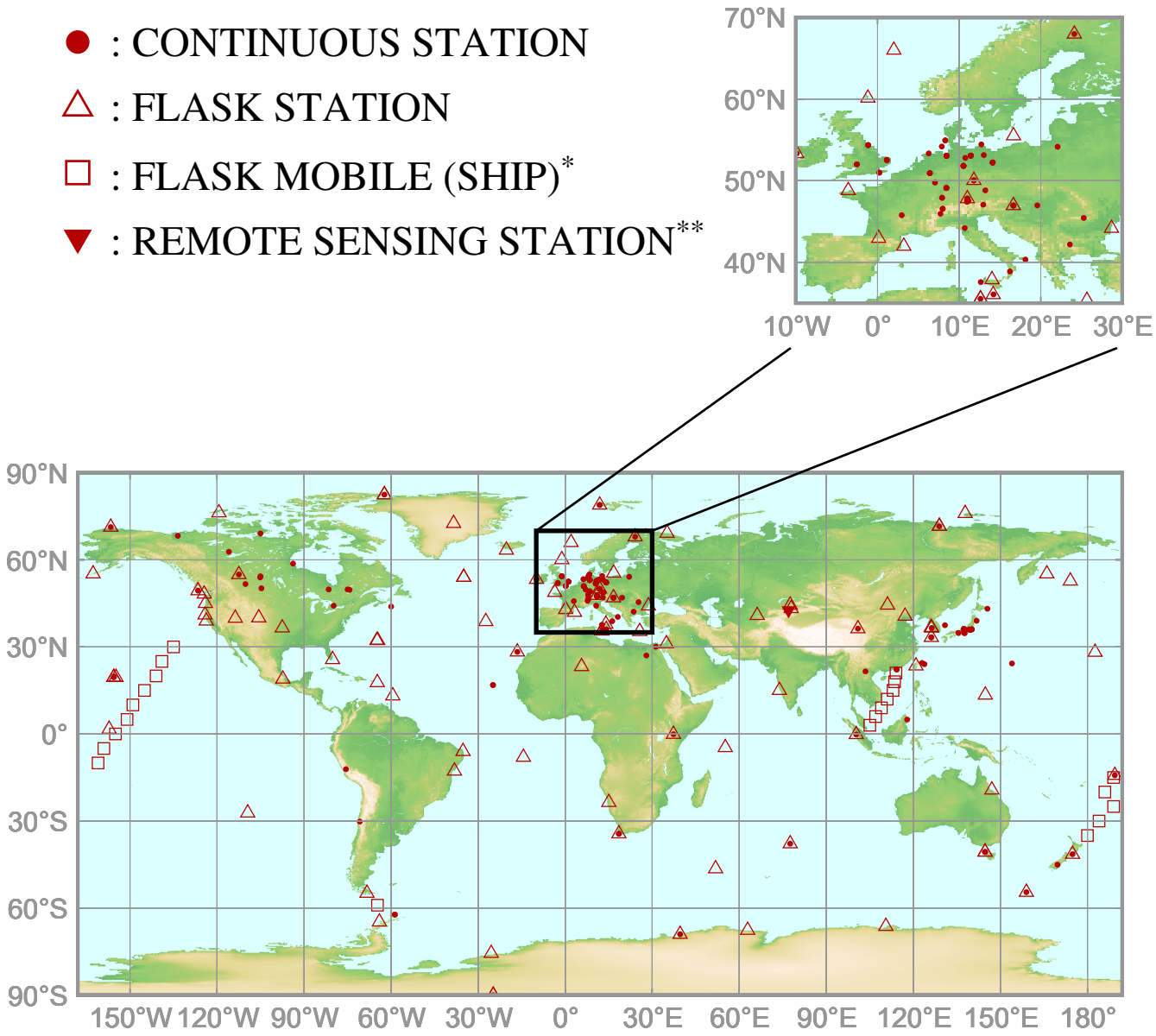

This map shows locations of the stations that have submitted data for monthly mean mole fractions.

* Only fixed point observations are shown in the figure. Other observational locations from mobile platform can be found at https://gaw.kishou.go.jp/search/mobile.

** The Issyk-Kul station is the only remote sensing station that submits data to WDCGG.

CO_2 Monthly Data

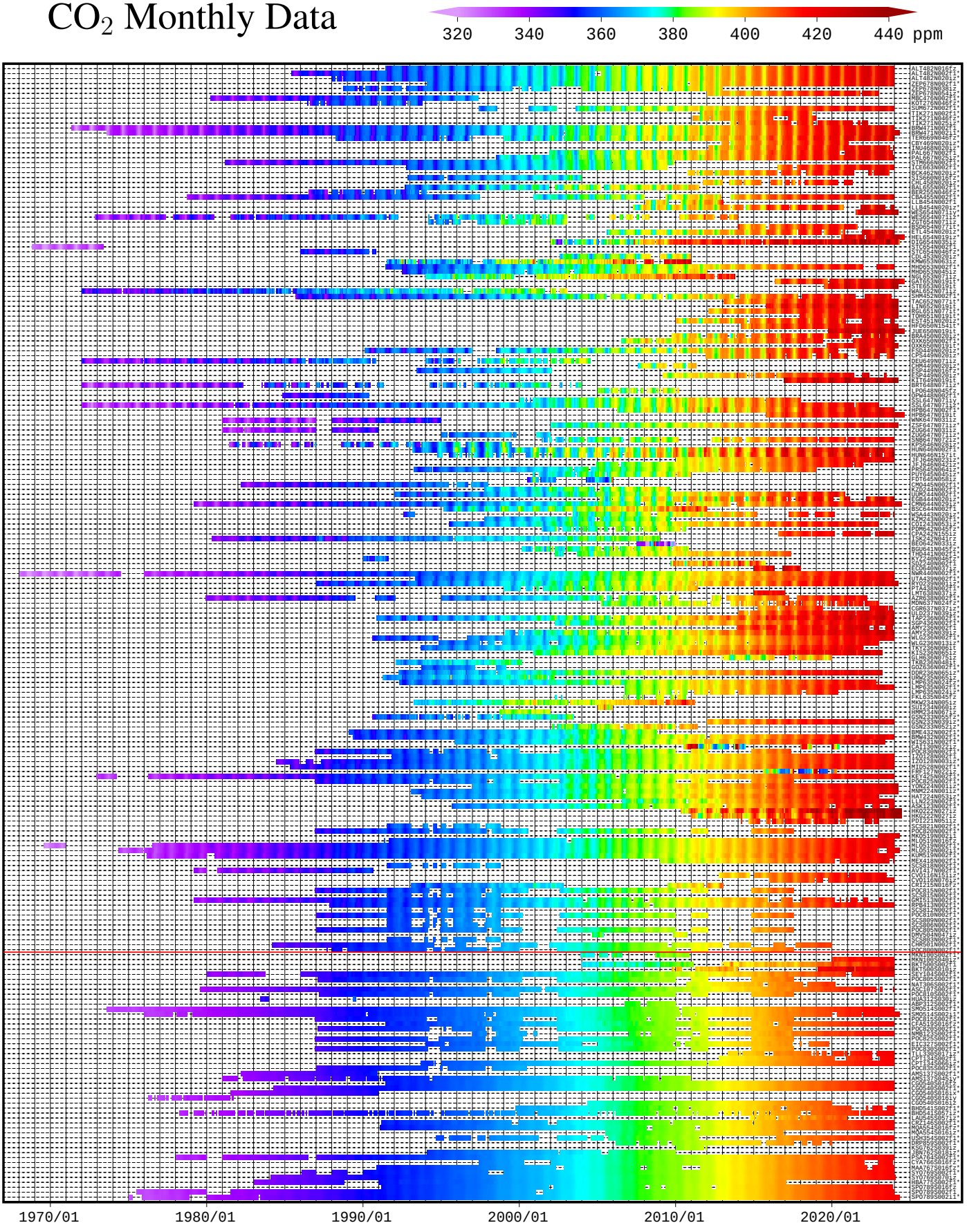

https://doi.org/10.50849/WDCGG_CO2_ALL_2024

Plate 1.1 Monthly mean CO_2 mole fractions that have been reported to the WDCGG. The mole fractions are illustrated in different colors. The sites are listed in order from north to south. The red line indicates the equator. In cases where data are reported for two or three different altitudes, only the data at the highest altitudes are illustrated. In cases where monthly means are not reported, the WDCGG calculates them from hourly or other mole fractions reported to the WDCGG by simple arithmetic mean. The data from the sites with an asterisk at the end of the station index were used for the analyses shown in Plate 1.2 (see Appendix A).

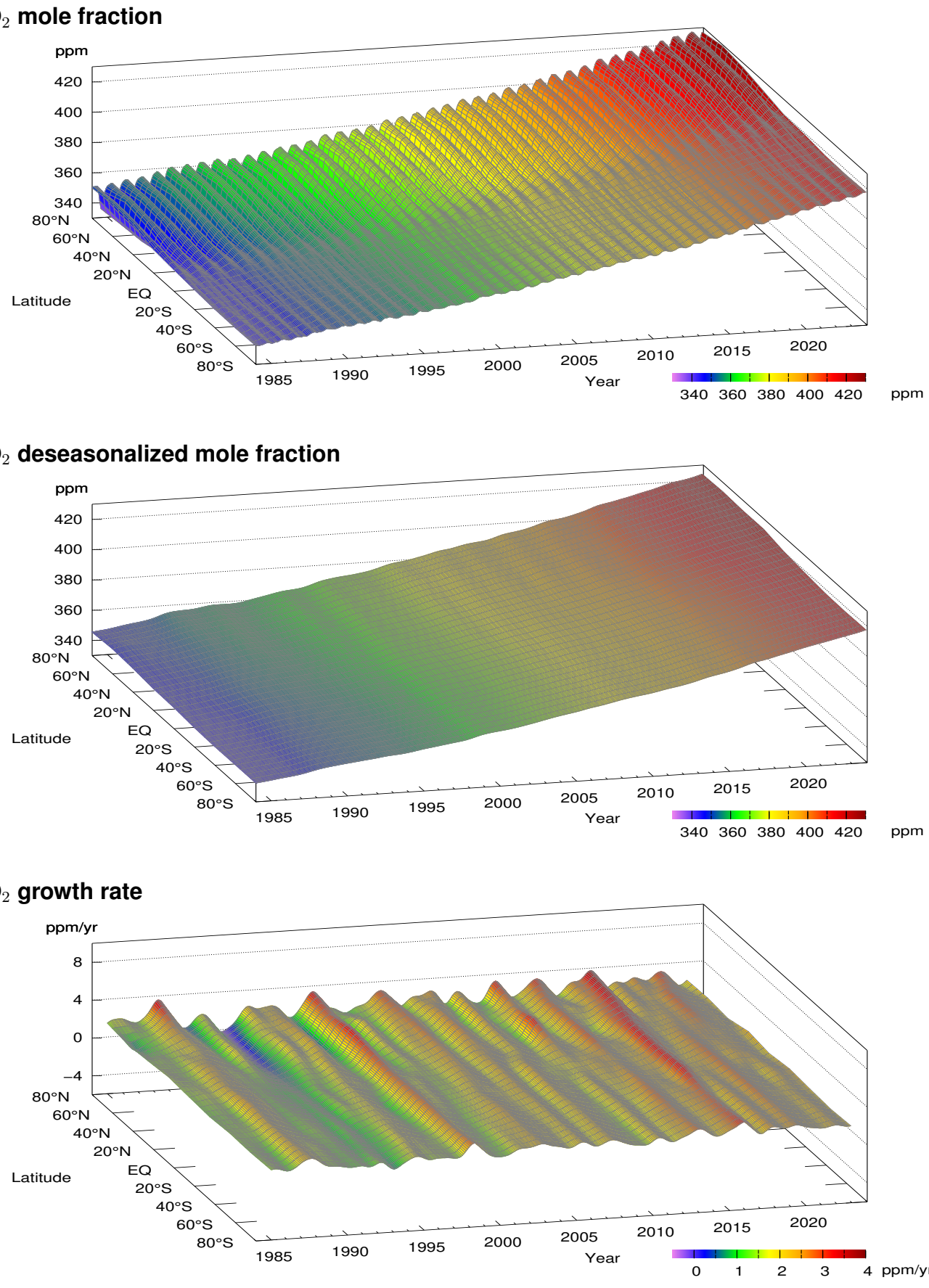

Plate 1.2 Variation of zonally averaged monthly mean CO_2 mole fractions (top), deseasonalized long-term trends (middle), and growth rates (bottom). The zonally averaged mole fractions were calculated for each 20° zone. The deseasonalized trends and growth rates were derived as described in Appendix A.

1. CARBON DIOXIDE (CO_2)

Atmospheric mole fractions of carbon dioxide (CO_2) – the most significant long-lived greenhouse gas related to anthropogenic activities – have been increasing since the beginning of the industrial era in around 1750. The globally averaged mole fraction of CO_2 reached a new high of 420.0±0.1 ppm in 2023, representing an increase of 2.3 ppm from the previous year. This increase marked the twelfth consecutive year with an increase greater than 2 ppm. The 2023 CO_2 mole fraction constitutes 151% of the pre-industrial level of 278.3 ppm as inferred from ice-core studies. CO_2 is responsible for around 66% of radiative forcing (relative to the pre-industrial era) caused by all long-lived greenhouse gases (WMO, 2024).

The increase in CO_2 mole fraction is primarily attributable to human activity, particularly fossil fuel combustion, cement production, land-use change and land management. Around half of anthropogenic CO_2 emissions are removed by the biosphere and oceans, and the rest remains in the atmosphere. The remaining fraction has been generally stable over the past 60 years (IPCC, 2021) though it experiences significant interannual variations. This determines the annual CO_2 increase in the atmosphere. The red columns in Fig. 1.1 show the observed growth rate for atmospheric CO_2 dry mole fraction, and the green line shows theoretical growth rates for CO_2 based on the assumption that all annual fossil fuel CO_2 emissions remain in the atmosphere. The lack of correlation between these time-series suggests that variations of the CO_2 growth rate are driven by the variability of the land and/or ocean sources and sinks. A comprehensive understanding of the mechanisms that control various CO_2 sources/sinks and their current states is of key importance in providing a scientific foundation for strategies to mitigate climate change. Data required for quantification of these processes are very limited.

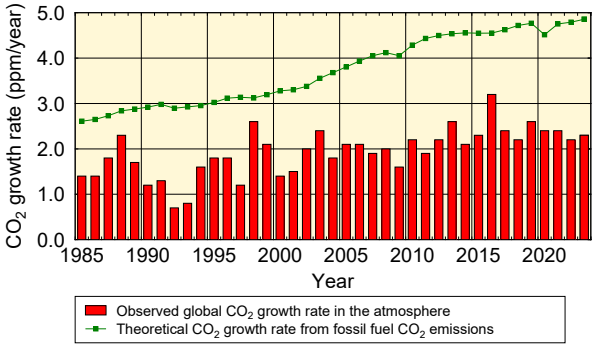

Fig. 1.1 Annual growth rates of CO_2 mole fraction in the atmosphere calculated from observational data (red columns), and theoretical rates derived from the data on fossil fuel emissions (green curve). The theoretical data were calculated taking CO_2 emissions as a proxy (from the Global Carbon Project (Friedlingstein *et al.*, 2025)), converted to mole fractions based on the conversion factor (2.124 PgC/ppm) (Ballantyne *et al.*, 2012). The observed growth rates were calculated by WDCGG.

Globally averaged mole fractions

The blue dots in Fig. 1.2 show globally averaged CO_2 monthly mean mole fractions (top) and their growth rates (bottom). The red line in the top panel shows the long-term trend after removal of seasonal cycles from the monthly means shown by the blue dots. Details of the analysis are provided in Appendix A.

Throughout the period for which observational data are available, the CO_2 mole fraction shows a continuous increase accompanied by characteristic seasonal cycle, with higher values from boreal winter to spring and lower values in summer. The seasonal cycle of CO_2 mole fraction (Fig. 1.5) is mainly driven by activity of the terrestrial biosphere, where plant photosynthesis is active in summer and large amounts of CO_2 are consumed, while plant respiration and organic-matter decomposition in soil become dominant in winter and emissions exceed the

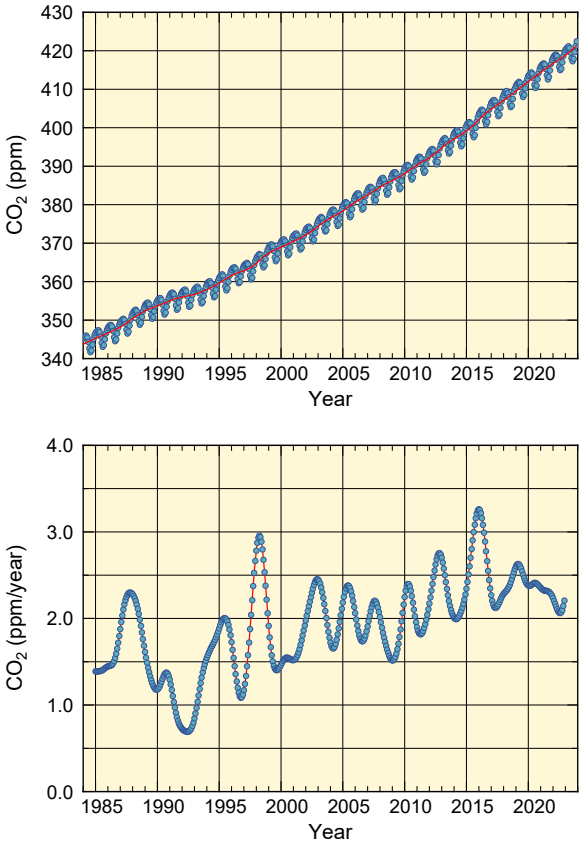

Fig. 1.2 Globally averaged monthly mean mole fraction of CO_2 (top) and its growth rate (bottom) from 1984 to 2023. Red line on the top panel presents the deseasonalized long-term trend.

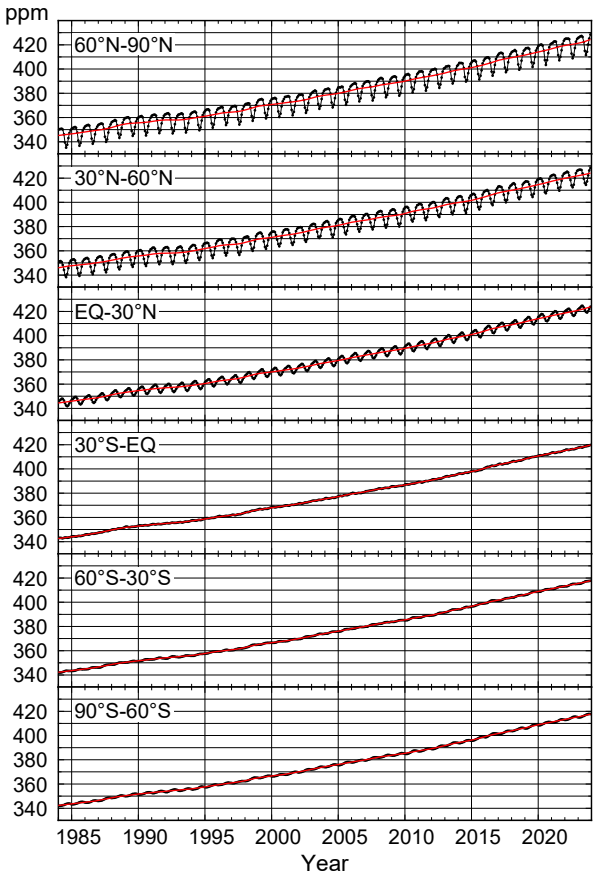

Fig. 1.3 Monthly mean mole fractions of CO_2 from 1984 to 2023 averaged over each 30° latitudinal zone (black) and their deseasonalized long-term trends (red).

amounts absorbed.

The activity of the terrestrial biosphere is characterized by significant interannual fluctuations, which are reflected in the CO_2 growth rate variations shown in the bottom panel of Fig. 1.2. The growth rate has been particularly high during El Niño events, such as those of 1986 – 1988, 1997/1998, 2002/2003, 2009/2010 and 2014 – 2016. El Niño conditions are usually associated with high temperatures and droughts in tropical land areas. High temperatures enhance plant respiration and organic-matter decomposition in soil, thereby increasing CO_2 emissions, while droughts suppress CO_2 uptake via plant photosynthesis, as for example, demonstrated for the European region in 2022 (van der Woude et al. 2023) and by the measurements of the stable carbon isotopic ratio, ^{13}C:^{12}C, in atmospheric CO_2 (Alden et al. 2010, Keeling et al. 1985). Enhanced forest/peat fires also contribute to direct CO_2 emissions. The CO_2 growth rate was exceptionally low during the El Niño event of 1991/1992, though this anomaly is largely attributed to the eruption of Mt. Pinatubo in June 1991, which caused low-temperature anomalies on a global scale leading to a terrestrial biosphere response opposite to the one described above.

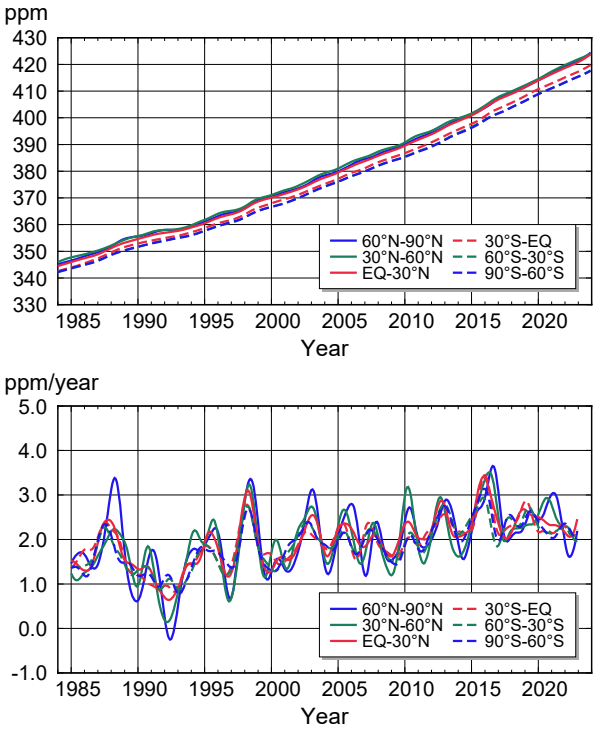

Fig. 1.4 Long-term trends of the CO_2 mole fractions for each 30° latitudinal zone (top) and their growth rates (bottom).

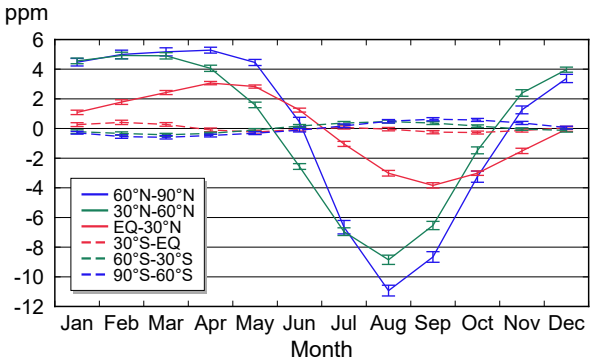

Fig. 1.5 Average seasonal cycles of the CO_2 mole fractions for each 30° latitudinal zone obtained by subtracting long-term trends from the zonally averaged time series. Vertical error bars represent the range of ±1σ which was calculated for each month (period 1984 to 2023).

Latitudinal dependence of mole fractions

The black lines in Fig. 1.3 show monthly mean CO_2 mole fractions averaged over six 30° latitudinal zones (60 – 90°N, 30 – 60°N, etc.). Long-term trends are shown by red lines. These trends are collectively presented at the top panel of Fig. 1.4. The bottom panel of Fig. 1.4 shows CO_2 growth rates in each latitudinal zone, and Fig. 1.5 shows average seasonal cycles of CO_2 mole fractions in the six respective zones. Figure 1.6 presents monthly mean CO_2 mole fractions for specific months of 2023 at individual stations, which were included in calculation of the global average mole fraction, as a function of latitude.

As shown in Fig. 1.4, CO_2 mole fractions are higher on average in the Northern Hemisphere, largely due to greater concentrations of human activity and the land mass areas there. However, the long-term trends are the same in all latitudinal zones. This suggests that, although the major sources and sinks of CO_2 are located in the Northern Hemisphere, changes in mole fractions occur on a global scale due to atmospheric transport.

Figure 1.5 indicates that seasonal cycle of CO_2 mole fraction has a large amplitude in northern regions, mainly because the Northern Hemisphere has larger continental areas and an extensive terrestrial biosphere. Pronounced lagging between seasonal minima in the different latitude zones is also seen.

Seasonal variations are evident at the individual sites in the Northern Hemisphere as shown in Fig. 1.6. In contrast, low seasonal variability is observed in the Southern Hemisphere. In the mid- and high southern latitudes, seasonal cycle of CO_2 mole fraction has an opposite phase to the one of the Northern Hemisphere.

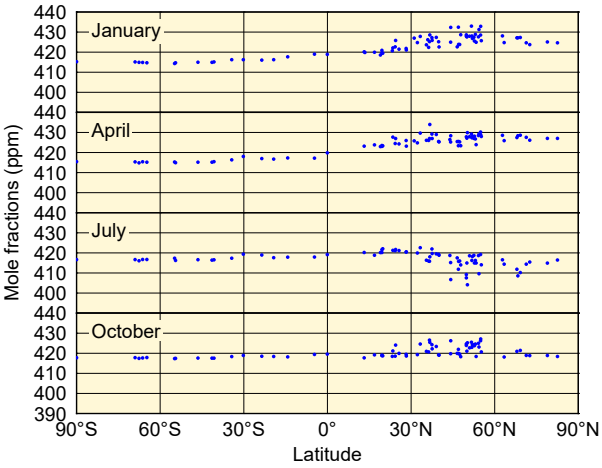

Fig. 1.6 Latitudinal distributions of the monthly mean mole fractions of CO_2 in January, April, July and October 2023 at individual stations.

2.

METHANE

(CH_4)

● : CONTINUOUS STATION

△ : FLASK STATION

□ : FLASK MOBILE (SHIP)*

▼ : REMOTE SENSING STATION**

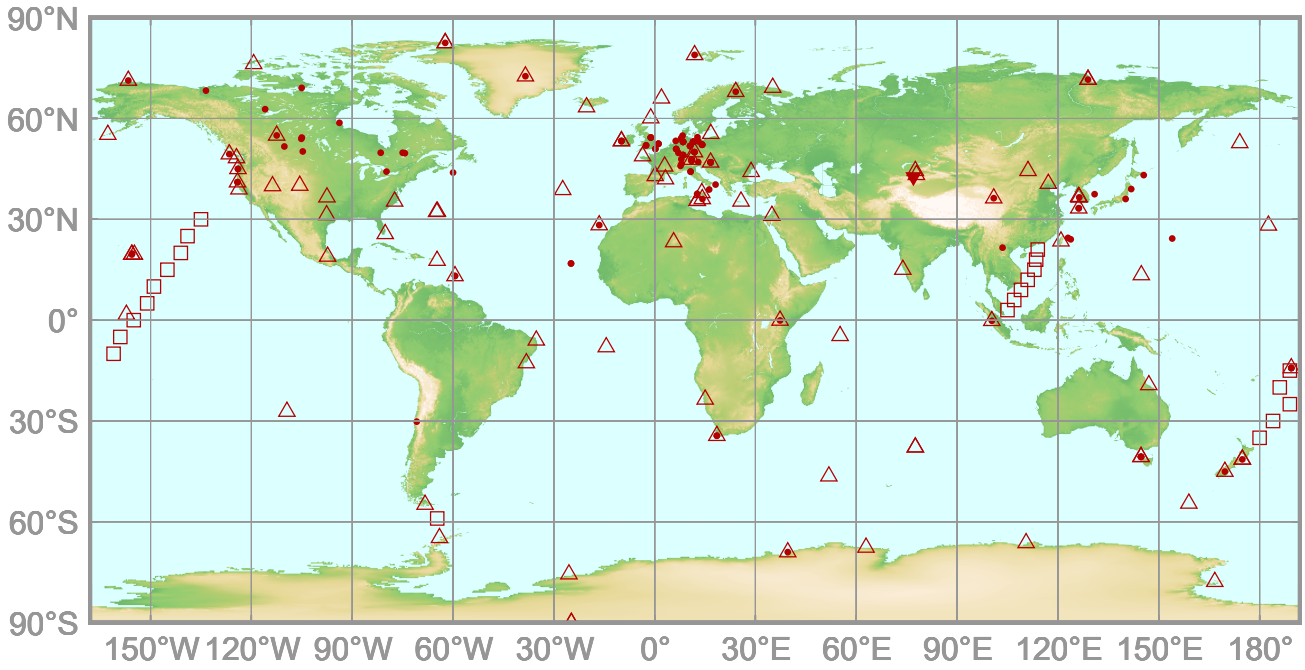

This map shows locations of the stations that have submitted data for monthly mean mole fractions.

* Only fixed point observations are shown in the figure. Other observational locations from mobile platform can be found at https://gaw.kishou.go.jp/search/mobile.

** The Issyk-Kul station is the only remote sensing station that submits data to WDCGG.

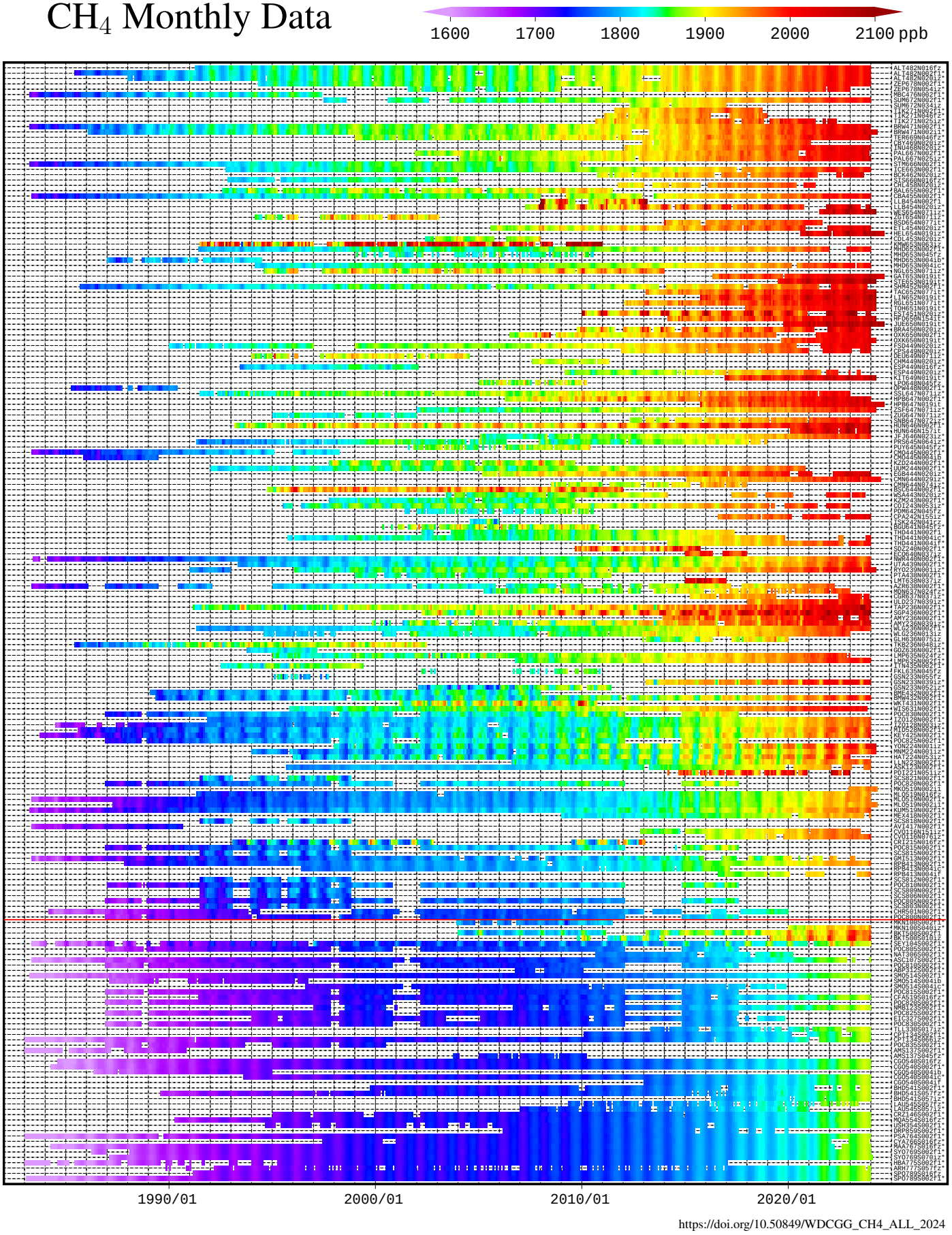

https://doi.org/10.50849/WDCGG_CH4_ALL_2024

Plate 2.1 Monthly mean CH_4 mole fractions that have been reported to the WDCGG. The mole fractions are illustrated in different colors. The sites are listed in order from north to south. The red line indicates the equator. In cases where monthly means are not reported, the WDCGG calculates them from hourly or other mole fractions reported to the WDCGG by simple arithmetic mean. The data from the sites with an asterisk at the end of the station index were used for the analyses shown in Plate 2.2 (see Appendix A).

CH_4 mole fraction

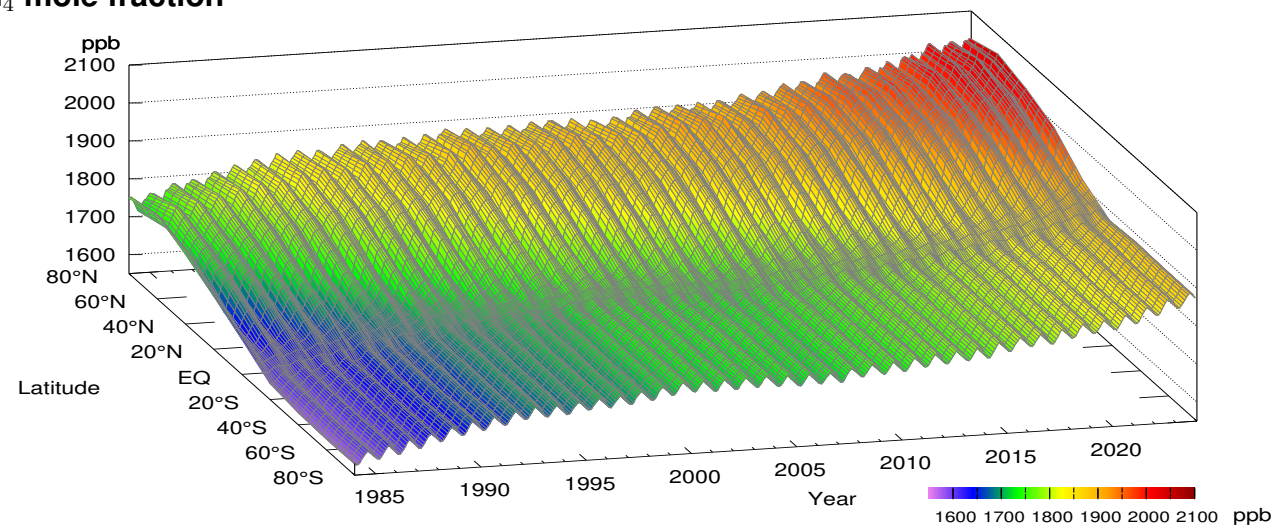

CH_4 deseasonalized mole fraction

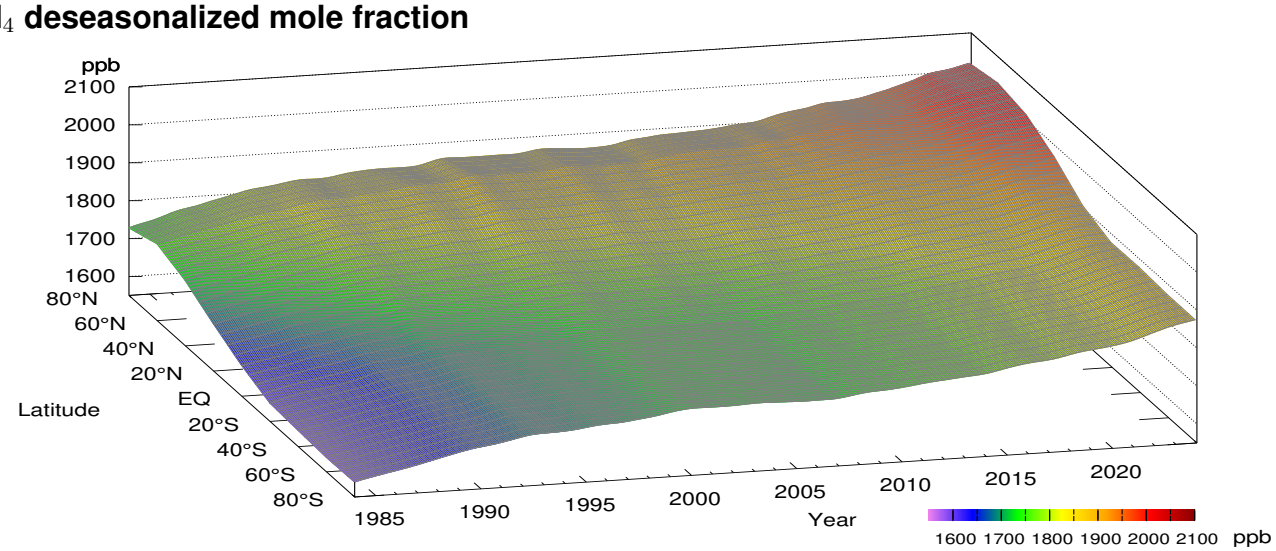

CH_4 growth rate

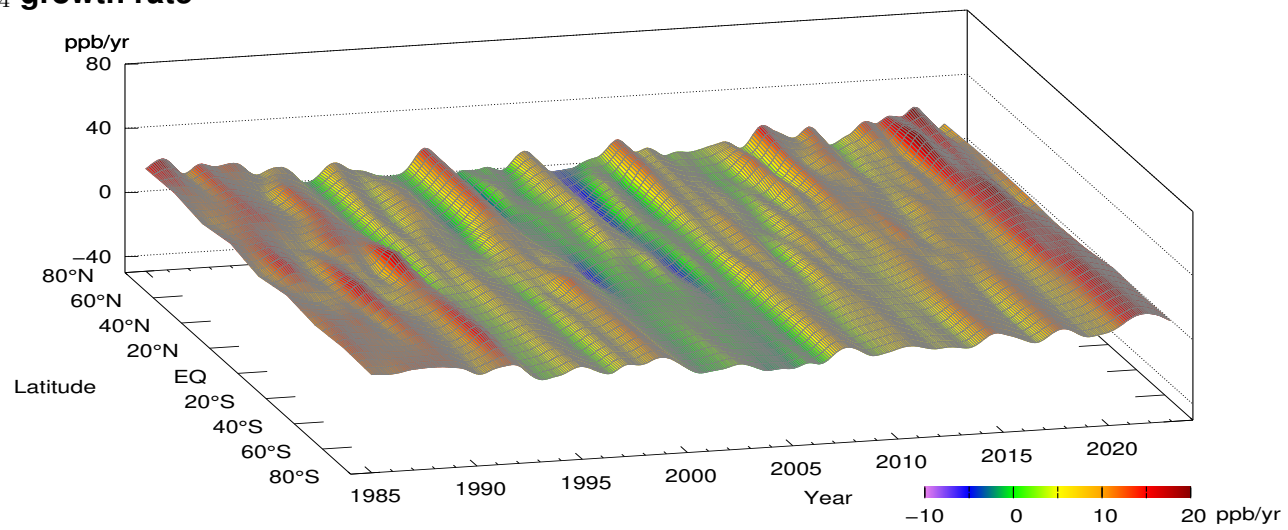

Plate 2.2 Variation of zonally averaged monthly mean CH_4 mole fractions (top), deseasonalized long-term trends (middle), and growth rates (bottom). The zonally averaged mole fractions were calculated for each 20° zone. The deseasonalized trends and growth rates were derived as described in Appendix A.

2. METHANE (CH_4)

Atmospheric mole fractions of methane (CH_4) – the second most significant anthropogenic greenhouse gas – have been increasing since the beginning of the industrial era (1750). The globally averaged mole fraction of CH_4 was 1934±2 ppb in 2023, representing an increase of 11 ppb relative to the previous year and 265% of the pre-industrial level of 729.2 ppb. CH_4 is responsible for around 16% of radiative forcing (relative to the pre-industrial era) caused by all long-lived greenhouse gases (WMO, 2024).

CH_4 has a variety of natural and anthropogenic sources. Natural ones (about 40% of emissions) are predominantly wetlands and inland freshwater, with various other minor but significant sources including wild animals, termites, permafrost and geological sources. Emissions from ruminant livestock and rice paddies associated with agricultural activities are categorized as anthropogenic sources. Other sources are directly related to industrial activity, including gas and oil exploration, waste management and biomass burning. Many of CH_4 sources are very sensitive to climate change. In contrast to the variety of sources, sinks are predominantly attributed to the destruction of CH_4 via reaction with a hydroxyl (OH) radical, which is especially abundant over oceans at low latitudes since it forms from the exposure of water vapor to ultraviolet (UV) radiation. This reaction determines CH_4 lifetime in the atmosphere. There are several factors that determine OH abundance and that can impact the lifetime of CH_4 in the atmosphere (for examples, the levels of traditional air pollutants).

Globally averaged mole fractions

The blue dots in Fig. 2.1 show globally averaged monthly mean CH_4 mole fractions (top) and their growth rates (bottom) based on the WDCGG data analysis described in Appendix A. The red line in the top panel shows the residual component after removal of seasonal cycle from globally averaged monthly mean mole fractions (referred to here as the long-term trend).

The seasonal cycle of CH_4 mole fraction depicted in Fig. 2.4 is primarily driven by the destruction of CH_4 via reaction with OH radicals. More such radicals are generated in summer due to enhanced UV radiation, resulting in increased CH_4 destruction. Biogenic sources

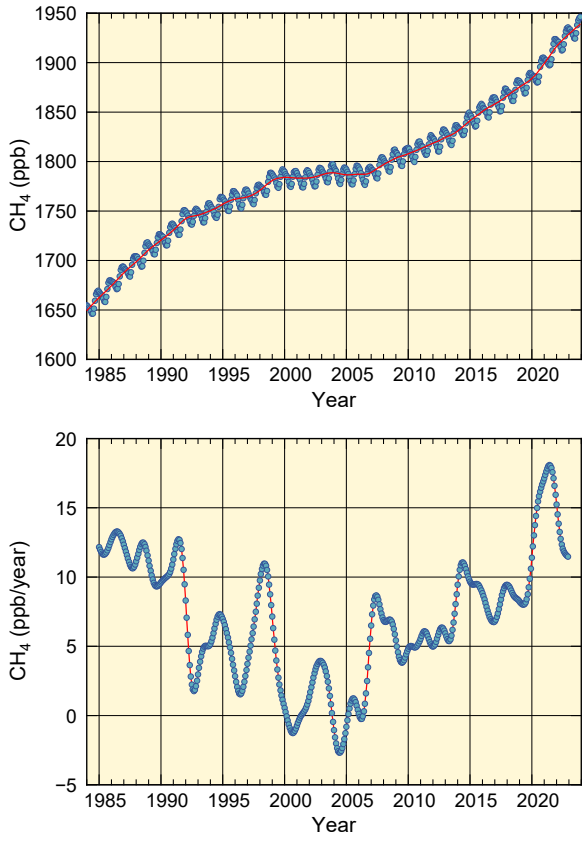

Fig. 2.1 Globally averaged monthly mean mole fraction of CH_4 from 1984 to 2023 (top) and its growth rate (bottom). Red line on the top panel presents the deseasonalized long-term trend.

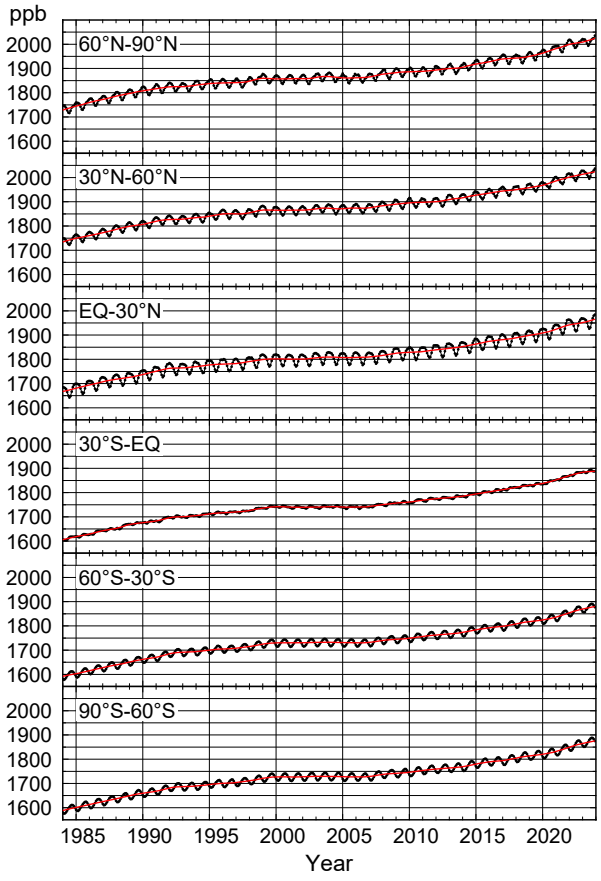

Fig. 2.2 Monthly mean mole fractions of CH_4 from 1984 to 2023 for each 30° latitudinal zone (black) and their deseasonalized long-term trends (red).

such as wetlands also have individual characteristics of seasonal variability, contributing to variations in observed CH_4 mole fractions.

The globally averaged CH_4 mole fraction shows a continuous increase throughout the period for which observational data are available. The mean annual total CH_4 emissions for the period 2010 – 2019 are 32 $TgCH_4$/yr larger than the estimates for 2000 – 2009 (Saunois *et al.*, 2025). Notably, the increase of the mole fraction almost stagnated from 1999 to 2006. As shown in the bottom panel, the growth rate actually began to decrease in the late 1990s (in fact approaching zero during this period) for reasons that remain under discussion (IPCC (2021) and references noted therein). By way of example, anthropogenic emissions from the oil and gas sectors declined by about 10 Tg/yr through the 1990s, and atmospheric CH_4 loss steadily increased (Dlugokencky *et al.*, 2003; Simpson *et al.*, 2012; Crippa *et al.*, 2020; Höglund-Isaksson *et al.*, 2020; Chandra *et al.*, 2021).

The situation changed in 2007 and mole fractions began increasing again. Recent studies (including work based on inverse modelling, CH_4 isotopic composition observation and inventory data) have suggested that concurrent emission changes from fossil fuels, agriculture, biomass burning and feedback from the natural sources have contributed to the resumed CH_4 growth rate observed since 2007, though there is still no consensus on this issue (Rice *et al.*, 2016; Nisbet *et al.*, 2016; Schwietzke *et al.*, 2016; Schaefer *et al.*, 2016; Worden *et al.*, 2017; Patra *et al.*, 2016; Thompson *et al.*, 2018; Lan *et al.*, 2019; Crippa *et al.*, 2020; Höglund-Isaksson *et al.*, 2020; Jackson *et al.*, 2020; Chandra *et al.*, 2021; Basu *et al.*, 2022; Oh *et al.*, 2022).

The average CH_4 growth rate from 2020 to 2022 exhibited the largest three-year increase since the 1980s. Observations and model simulations point to a significant increase in CH_4 emissions from natural wetlands in response to higher temperatures and markedly wetter land conditions during the 2020 – 2022 La Niña event (WMO, 2024). The increase is related to biogenic sources according to isotopic analysis, though the attribution to natural or anthropogenic processes remains unclear. Feng *et al.* (2023) attributed the change mostly to increased CH_4 emissions over the tropics. There are also suggestions in literature (Michel *et al.*, 2024; Zhang *et al.*, 2023; Feng *et al.*, 2022; Peng *et al.*, 2022) that the exceptional CH_4 growth may be associated with climate feedback given that 2022 was a third consecutive La Niña year.

Latitudinal dependence of mole fractions

The black lines in Fig. 2.2 show CH_4 mole fractions averaged over six 30° latitudinal zones. Long-term trends are shown by the red lines in each panel. These trends are summarized in the top panel of Figure 2.3. The bottom panel of this figure shows growth rates of CH_4 for the six latitudinal zones, and Figure 2.4 shows average seasonal cycles of CH_4 mole fraction for each zone.

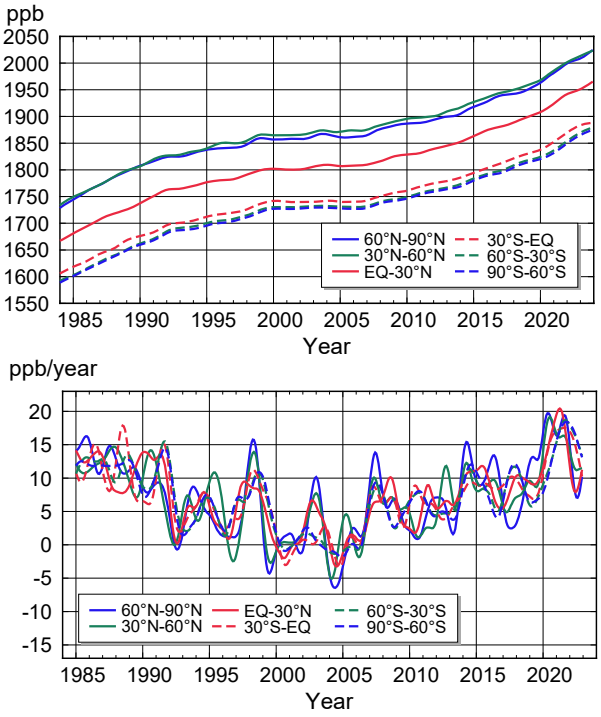

Fig. 2.3 Long-term trends of the CH_4 mole fractions for each 30° latitudinal zone (top) and their growth rates (bottom).

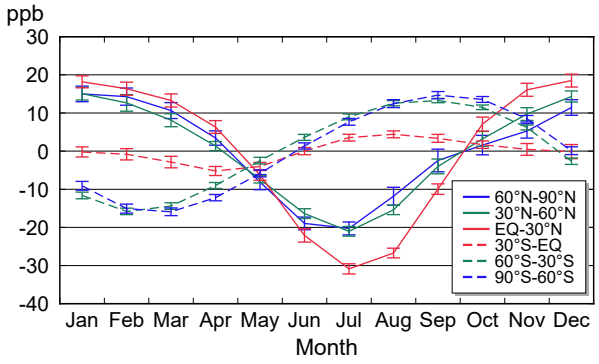

Fig. 2.4 Average seasonal cycles of CH_4 mole fractions for each 30° latitudinal zone obtained by subtracting long-term trends from the zonally averaged time series. Vertical error bars represent the range of ±1σ calculated for each month (period 1984 to 2023).

As shown in the top panel of Figure 2.3, the mole fraction gradient between the six long-term trends is the most pronounced between 30 – 60°N and EQ – 30°N and between EQ – 30°N and south hemispheric zones. These gradients are largely attributable to presence of major CH_4 sources in the Northern Hemisphere and to an abundance of OH radicals over oceanic regions extending southward.

The CH_4 growth rate exhibits similar but not identical characteristics in all latitudinal zones, as shown in the bottom panel of Figure 2.3. There are singular peaks and troughs, each of which has an individual complex origin, and collective explanation of two or more peaks is challenging. For example, the peaks observed in every

zone in 1998 are attributed to enhanced CH_4 emissions from tropical wetland areas in association with the major El Niño event observed the same year, and to forest/peat fires in Siberia and elsewhere (Dlugokencky *et al*., 2001).

Figure 2.4 shows clear seasonal cycles of CH_4 mole fraction in both hemispheres, while those of CO_2 mole fractions are only pronounced in the Northern Hemisphere (Fig. 1.5). This difference is related to the differences in the processes behind the seasonal cycles of the two species. CH_4 sinks are mainly driven by the availability of OH radicals produced over oceans, which peak during summer in both hemispheres and at the same time. In contrast, CO_2 sinks in summer are mainly driven by terrestrial biosphere activity, which is limited in the ocean-rich Southern Hemisphere and has pronounced difference in the month of the maximum uptake in different latitudes. The CH_4 cycles have a roughly opposite phase in each hemisphere because the seasons are opposite. The relatively low amplitude of seasonal cycles for CH_4 mole fraction in the low latitudes of the Southern Hemisphere indicates that the atmosphere in this region tends to be influenced by the mixing between the Northern Hemisphere and South Hemisphere air masses, and the cycles are partially offset. In the low latitudes of the Northern Hemisphere, mole fractions are significantly lower in summer because OH radicals are plentiful over ocean areas due to enhanced UV radiation.

3.

NITROUS OXIDE

(N_2O)

● : CONTINUOUS STATION

△ : FLASK STATION

□ : FLASK MOBILE (SHIP)*

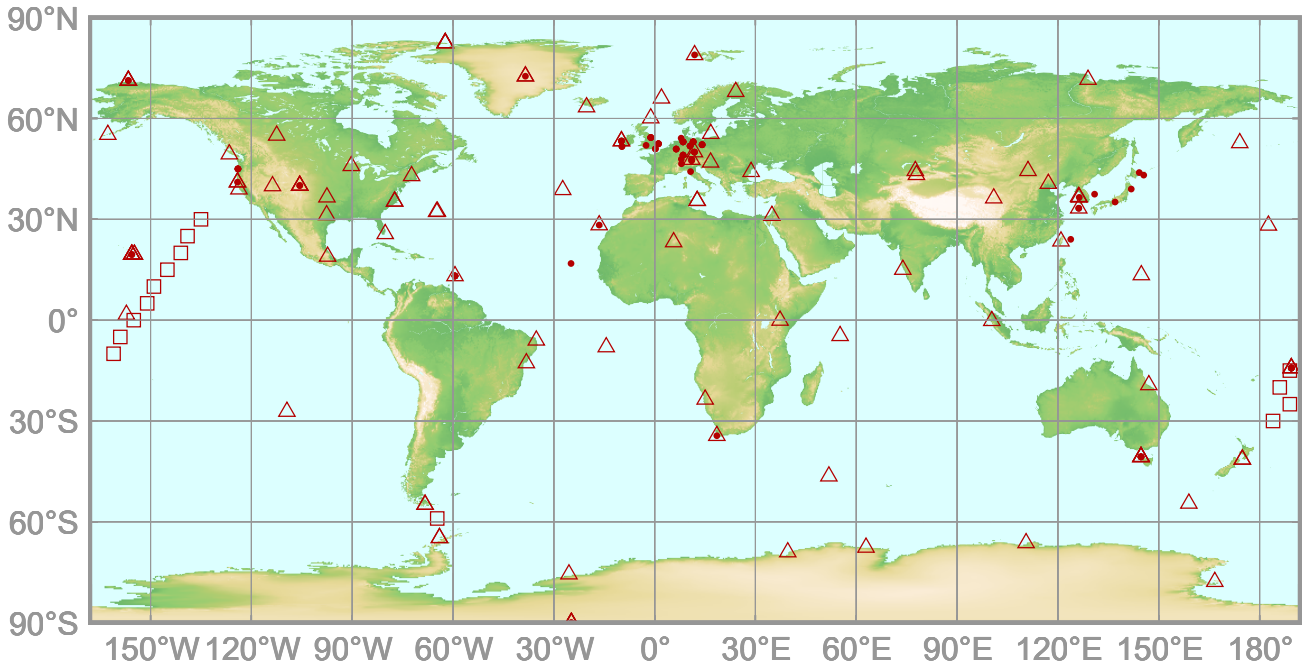

This map shows locations of the stations that have submitted data for monthly mean mole fractions.

* Only fixed point observations are shown in the figure. Other observational locations from mobile platform can be found at https://gaw.kishou.go.jp/search/mobile.

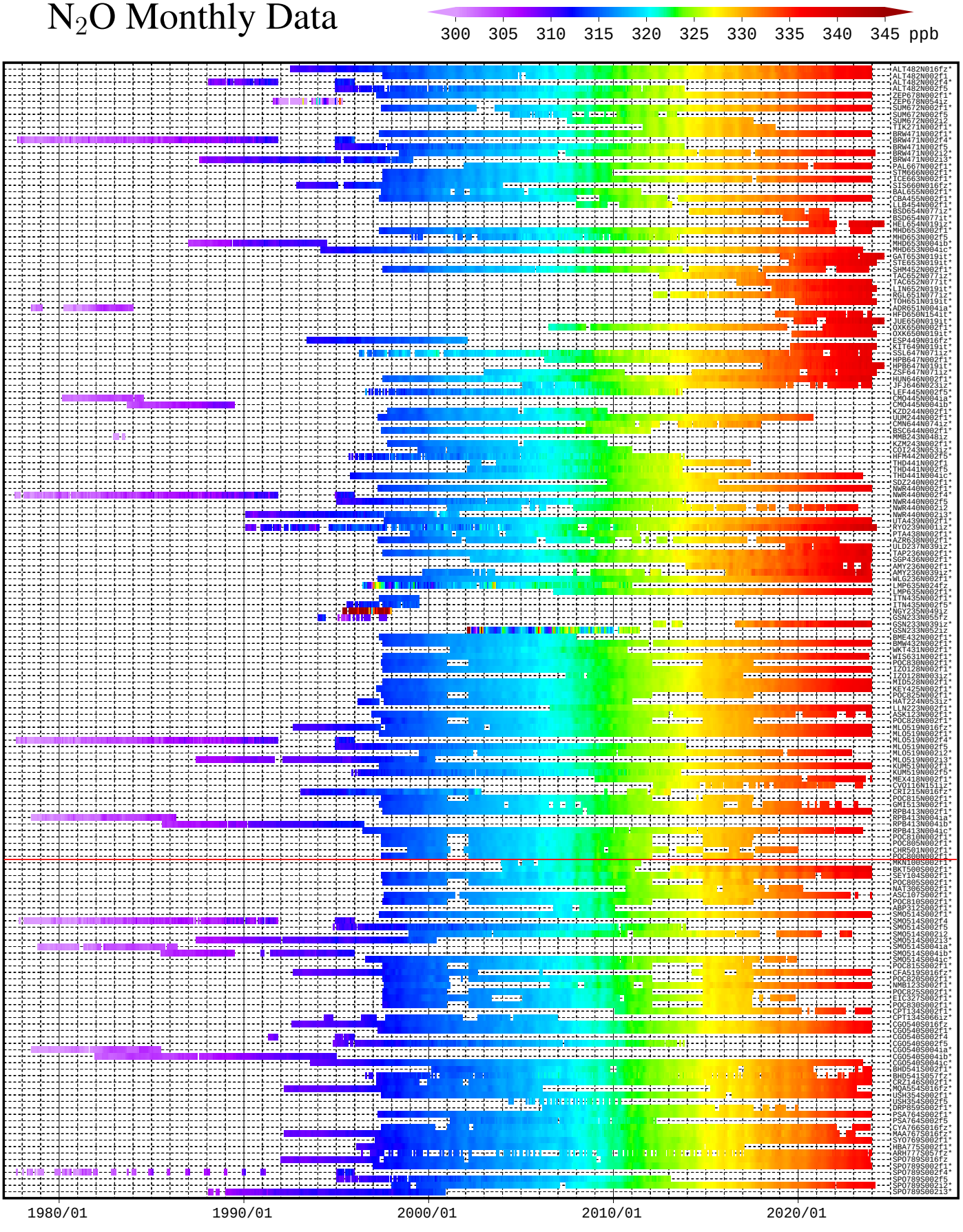

https://doi.org/10.50849/WDCGG_N2O_ALL_2024

Plate 3.1 Monthly mean N_2O mole fractions that have been reported to the WDCGG. The mole fractions are illustrated in different colors. The sites are listed in order from north to south. The red line indicates the equator. The data from the sites with an asterisk at the end of the station index were used for the analyses shown in Plate 3.2 (see Appendix A).

N_2O mole fraction

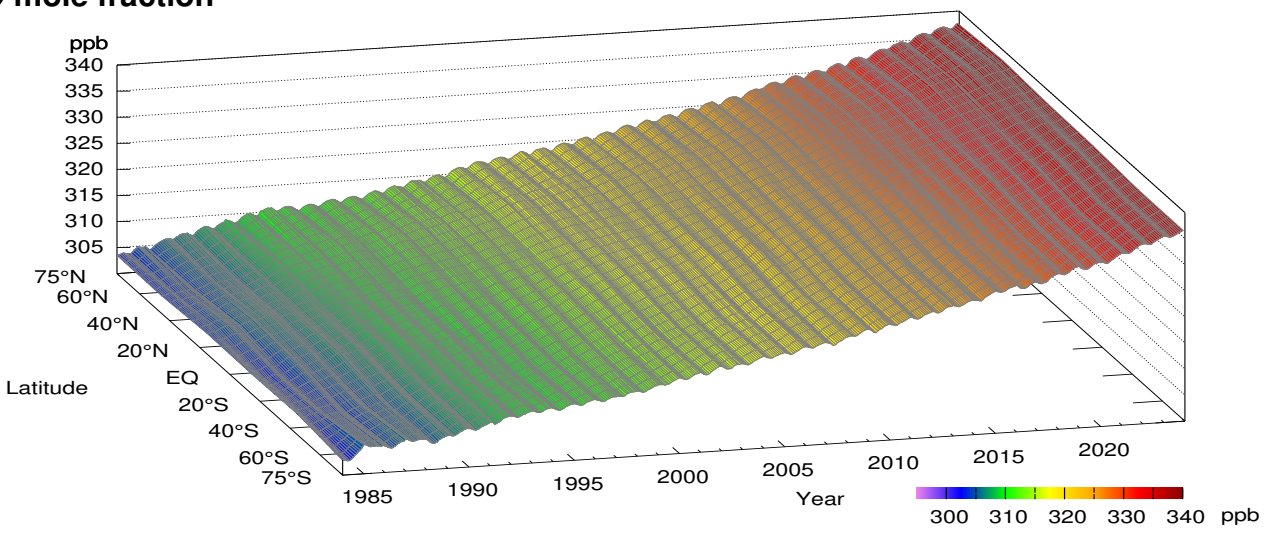

N_2O deseasonalized mole fraction

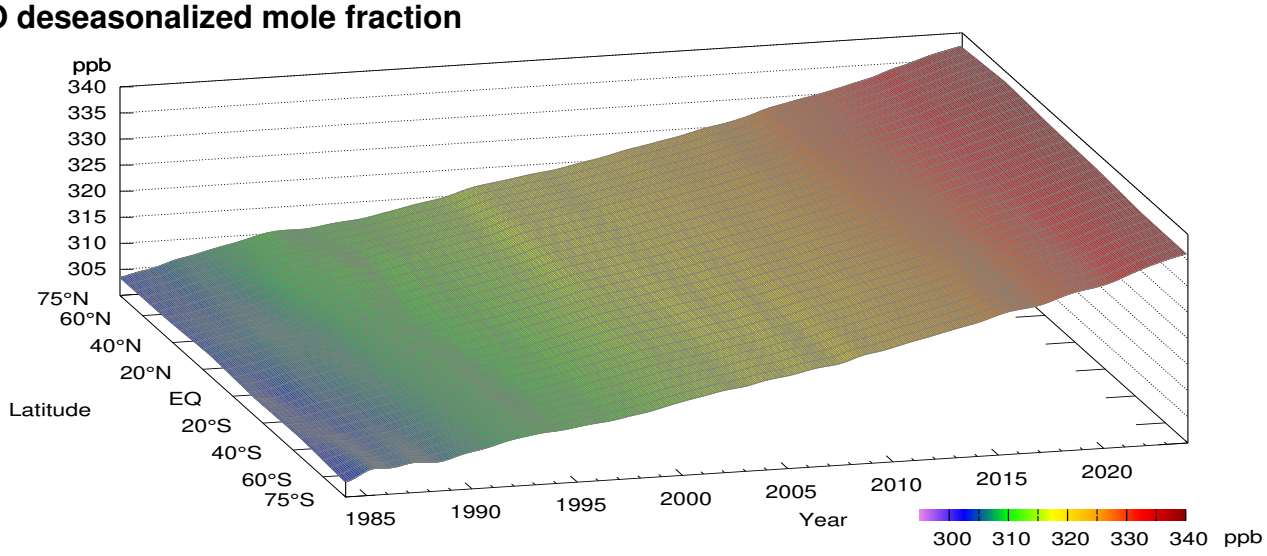

N_2O growth rate

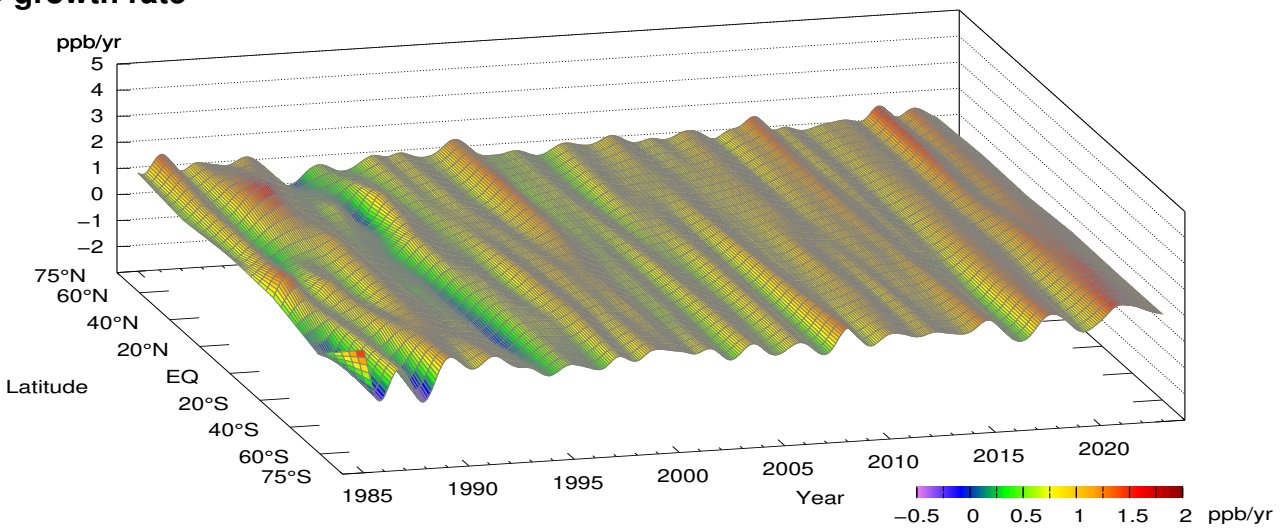

Plate 3.2 Variation of zonally averaged monthly mean N_2O mole fractions (top), deseasonalized long-term trends (middle), and growth rates (bottom). The zonally averaged mole fractions were calculated for each 30° zone. The deseasonalized trends and growth rates were derived as described in Appendix A.

3. NITROUS OXIDE (N_2O)

Atmospheric mole fractions of nitrous oxide (N_2O) – the third most important anthropogenic greenhouse gas – have been increasing since the beginning of the industrial era (1750). The globally averaged mole fraction of N_2O in 2023 was 336.9±0.1 ppb, representing an increase of 1.1 ppb relative to the previous year and 125% of the pre-industrial level of 270.1 ppb. N_2O is responsible for approximately 6% of total radiative forcing (relative to the pre-industrial era) from all long-lived greenhouse gases (WMO, 2024).

N_2O sources include microbial processes (nitrification and denitrification), emissions from oceans, nitrogen fertilizers generally used in agriculture and fossil fuel/biomass combustion. Global human-induced emissions, which are dominated by nitrogen additions to croplands, increased by 40% over the past four decades and are mainly responsible for the growth in the atmospheric burden (Tian *et al*., 2024). N_2O is relatively stable in the troposphere with a lifetime of about 110 years. Its mole fraction is relatively uniformly distributed in the troposphere and declines in the stratosphere, where it is destroyed via ultraviolet (UV) photo-decomposition. N_2O is also an important ozone-depleting substance in the stratosphere and its unmitigated emissions will further undermine the achievements of the Montreal protocol (Solomon *et al*., 2020).

Globally and hemispherically averaged mole fractions

Figure 3.1 shows globally averaged N_2O mole fraction and its growth rate. Details of the analysis are provided in Appendix A. Unlike CO_2 and CH_4, N_2O mole fractions exhibit low seasonal variability. Nevertheless, the same deseasonalization procedure was applied to N_2O datasets as to CO_2 and CH_4, and the residual is shown by the red line in the top panel. The difference between original and deseasonalized time series is very small. Figure 3.2 shows N_2O mole fractions averaged over the Northern Hemisphere (dark blue) and the Southern Hemisphere (light blue) in the top panel, with corresponding growth rates in the bottom panel.

Throughout the period for which observational data are available, N_2O mole fractions have steadily increased in both hemispheres, and therefore over the whole globe.

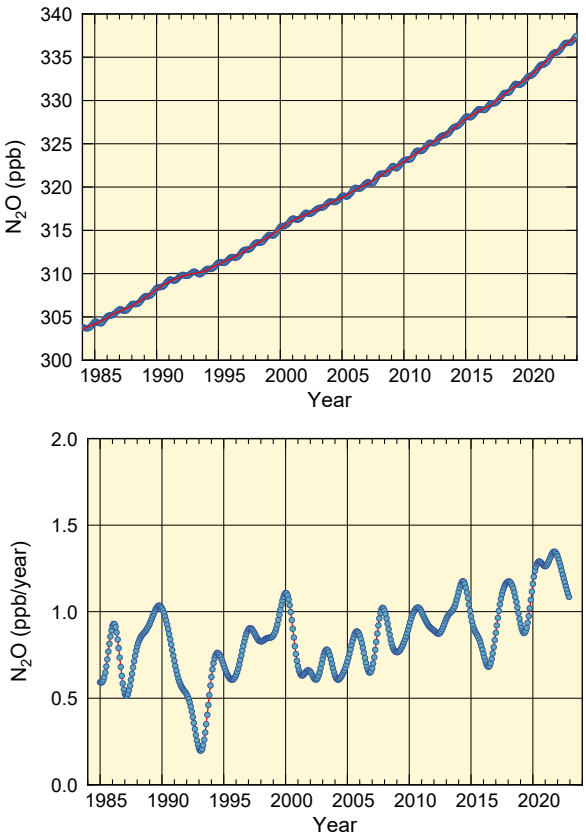

Fig. 3.1 Globally averaged monthly mean mole fraction of N_2O from 1984 to 2023 (top) and its growth rate (bottom). Red line on the top panel presents the deseasonalized long-term trend.

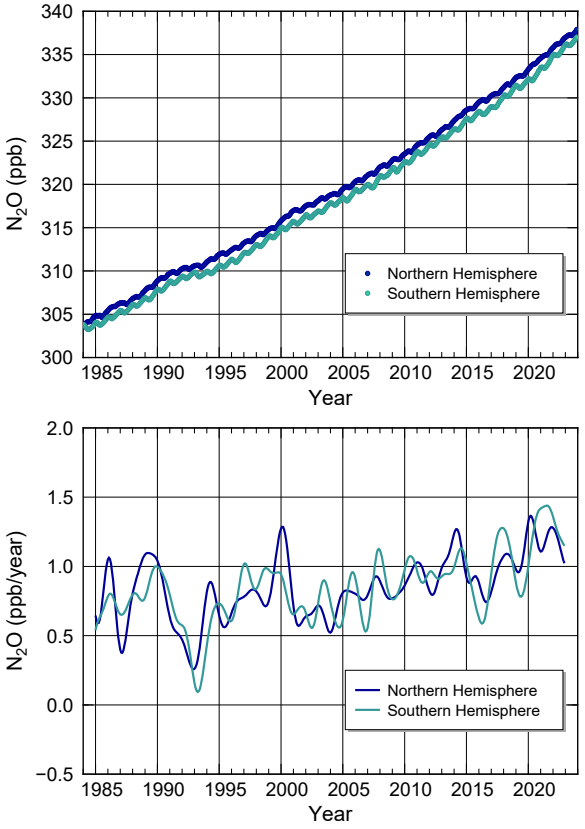

Fig. 3.2 Monthly mean mole fractions of N_2O from 1984 to 2023 (top) and their growth rates (bottom), averaged over the Northern and Southern Hemispheres.

Mole fractions are higher in the Northern Hemisphere, mainly due to high concentrations of anthropogenic and microbial sources in continental areas.

The growth rate of N_2O is positive over the period 1984 – 2023 as a whole, although significant inter-annual variations are observed. IPCC (2021) reports that the large inter-annual variations observed in the atmospheric N_2O growth rate over the tropics and sub-tropics are negatively correlated with the multivariate ENSO index (MEI) and associated anomalies in land and ocean fluxes (Ji *et al.*, 2019; Thompson *et al.*, 2019; Yang *et al.*, 2020). It is suggested that continued La Niña over the period 2020 – 2022 could have played a role in the higher N_2O growth rate in 2022 than 10 years average (WMO, 2023). However, quantitative verification of specific variability patterns is challenging due to the complexity of the processes related to nitrogen cycle and uncertainty over the intensities and locations of N_2O sources. Accordingly, further extension of the global observational network is needed for N_2O as well as for other greenhouse gases.

4.

HALOCARBONS AND OTHER HALOGENATED SPECIES

● : CONTINUOUS STATION

△ : FLASK STATION

□ : FLASK MOBILE (SHIP)*

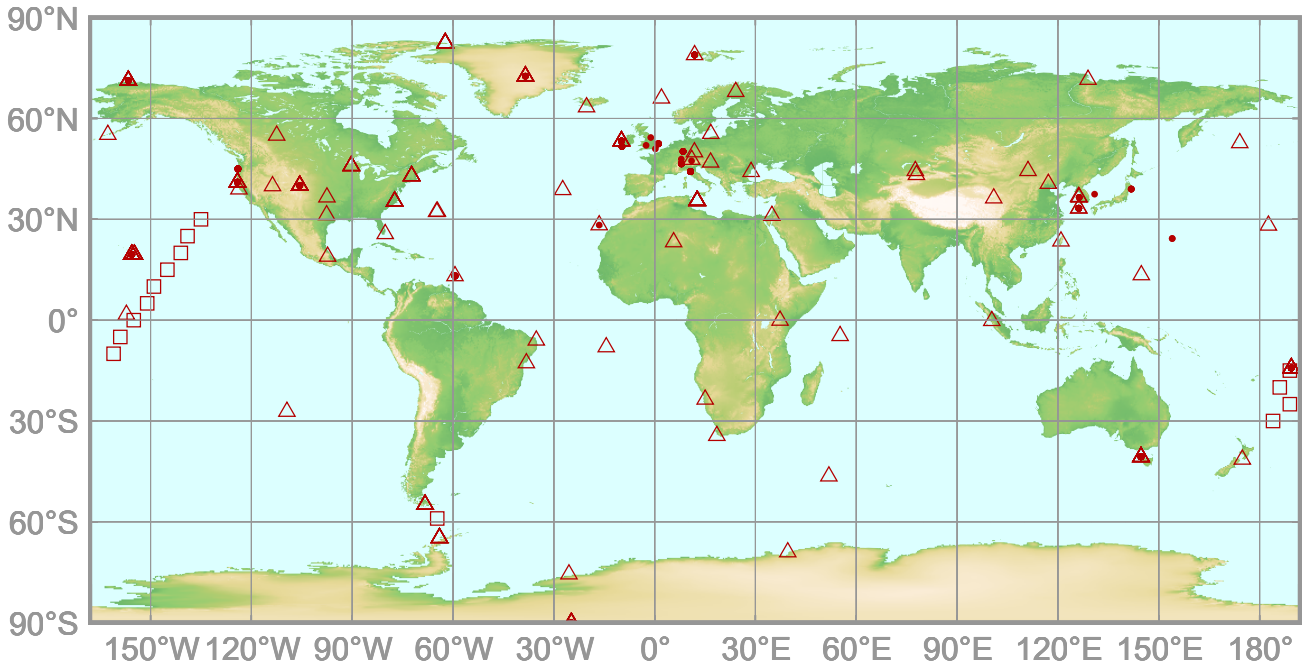

This map shows locations of the stations that have submitted data for monthly mean mole fractions.

* Only fixed point observations are shown in the figure. Other observational locations from mobile platform can be found at https://gaw.kishou.go.jp/search/mobile.

(a) CFC-11 Monthly Data

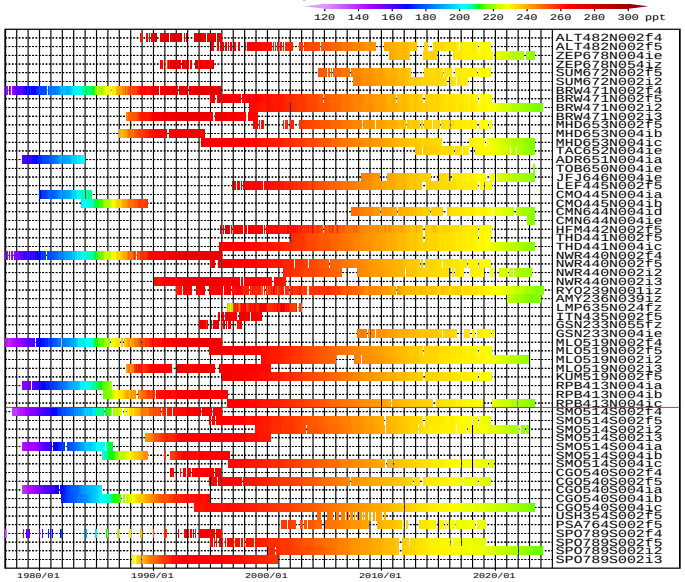

https://doi.org/10.50849/WDCGG_CFC11_ALL_2024

(b) CFC-12 Monthly Data

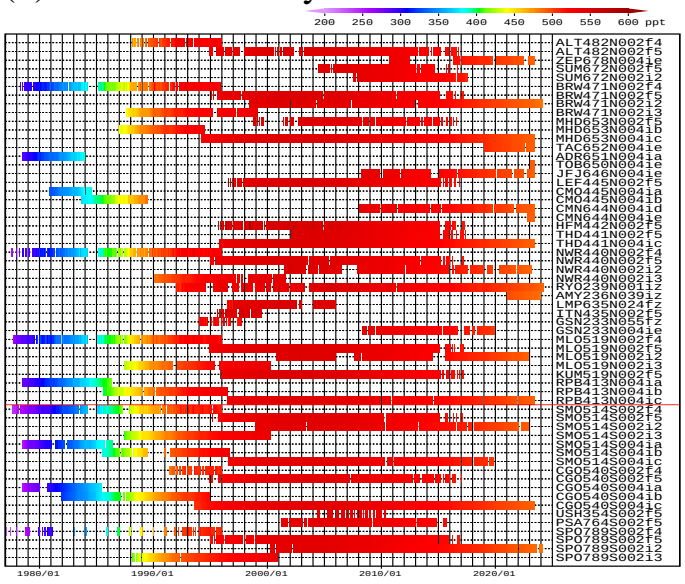

https://doi.org/10.50849/WDCGG_CFC12_ALL_2024

(c) CFC-113 Monthly Data

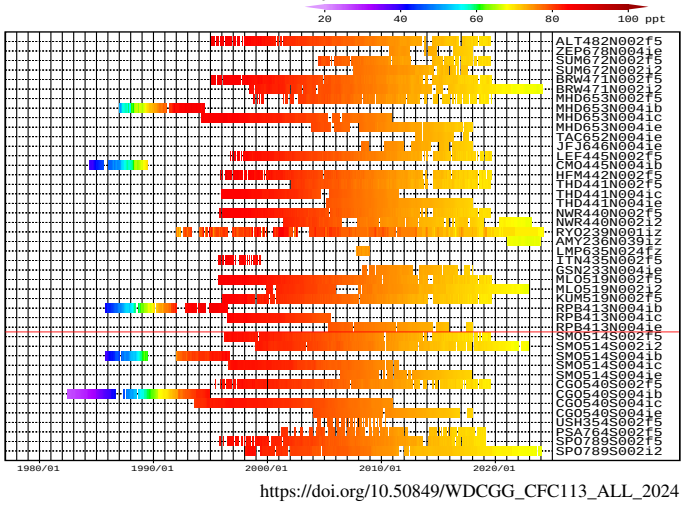

https://doi.org/10.50849/WDCGG_CFC113_ALL_2024

(d) CCl_4 Monthly Data

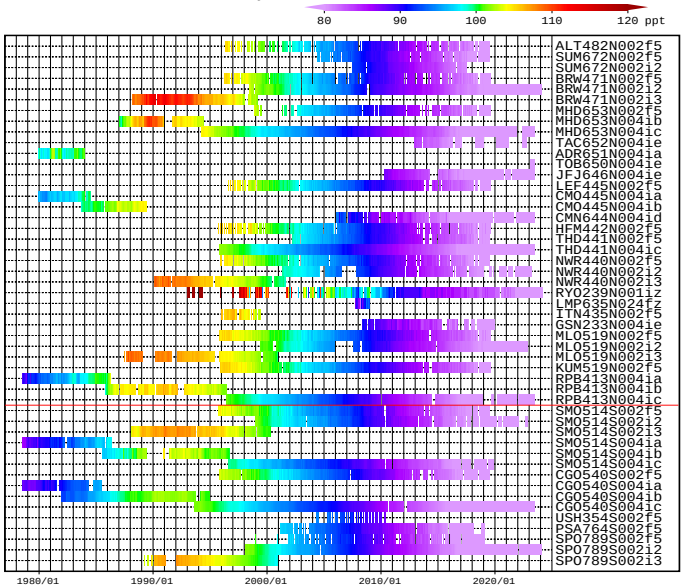

https://doi.org/10.50849/WDCGG_CCL4_ALL_2024

(e) CH_3CCl_3 Monthly Data

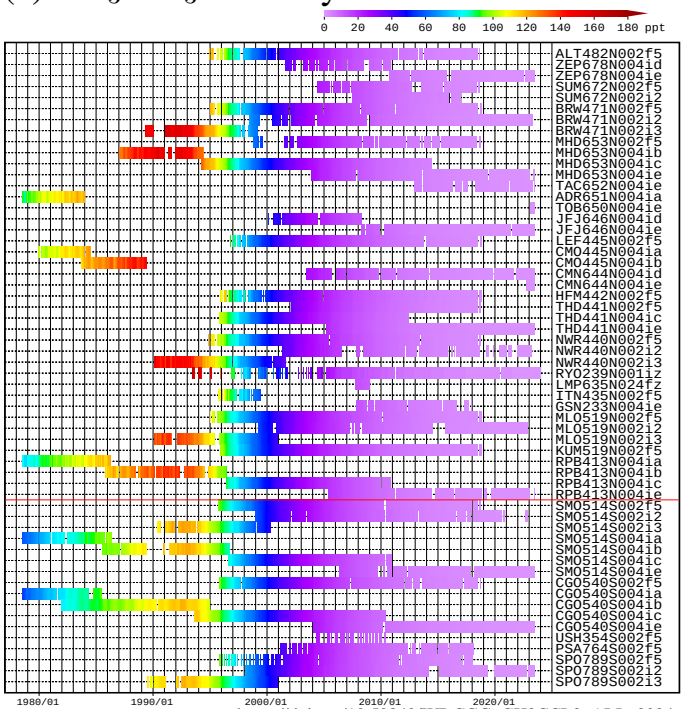

https://doi.org/10.50849/WDCGG_CH3CCL3_ALL_2024

(f) Halon-1211 Monthly Data

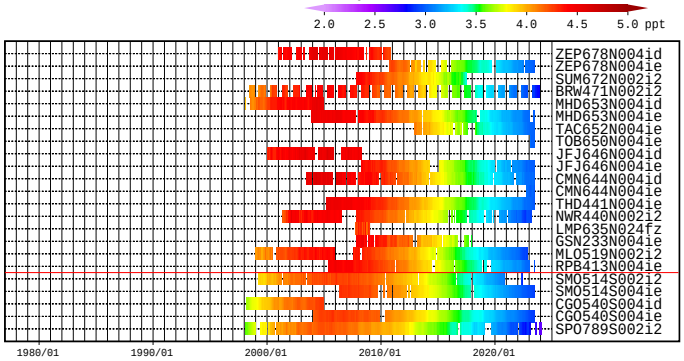

https://doi.org/10.50849/WDCGG_CBRCLF2_ALL_2024

Plate 4.1 Monthly mean (a) CFC-11, (b) CFC-12, (c) CFC-113, (d) CCl_4, (e) CH_3CCl_3, (f) Halon-1211 mole fractions that have been reported to the WDCGG. The mole fractions are illustrated in different colors. The sites are listed in order from north to south. The red line indicates the equator.

(a) Halon-1301 Monthly Data

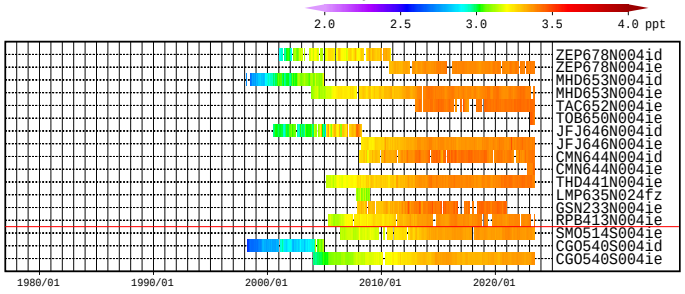

https://doi.org/10.50849/WDCGG_CBRF3_ALL_2024

(b) HCFC-22 Monthly Data

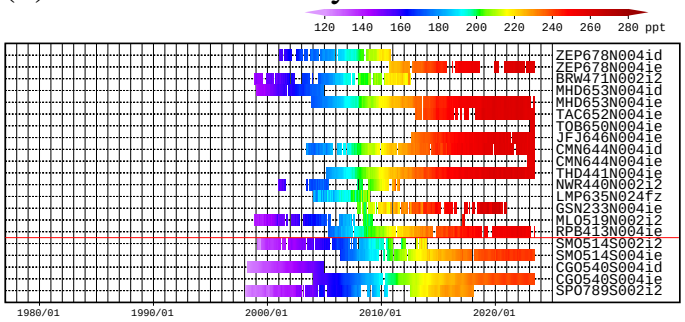

https://doi.org/10.50849/WDCGG_HCFC22_ALL_2024

(c) HCFC-141b Monthly Data

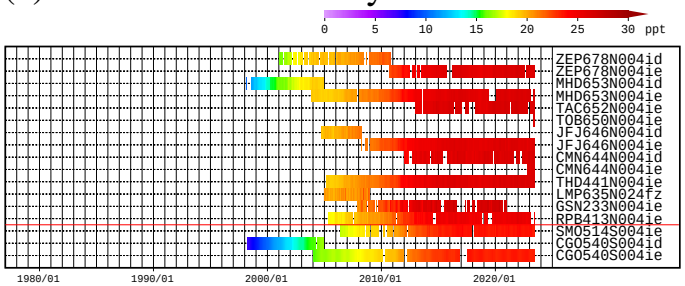

https://doi.org/10.50849/WDCGG_HCFC141B_ALL_2024

(d) HCFC-142b Monthly Data

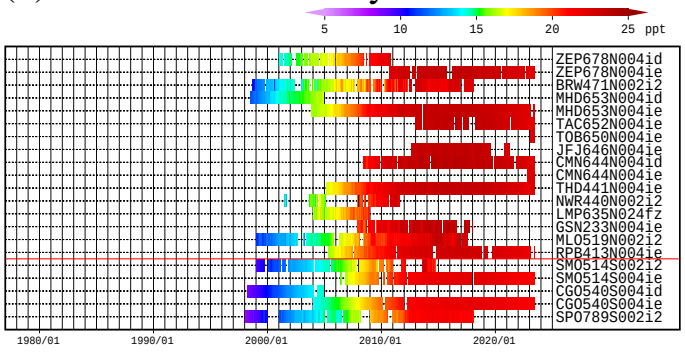

https://doi.org/10.50849/WDCGG_HCFC142B_ALL_2024

(e) HFC-134a Monthly Data

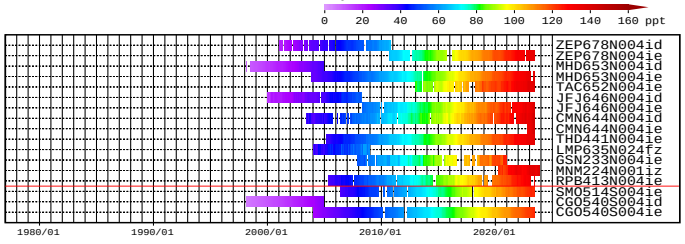

https://doi.org/10.50849/WDCGG_HFC134A_ALL_2024

(f) HFC-152a Monthly Data

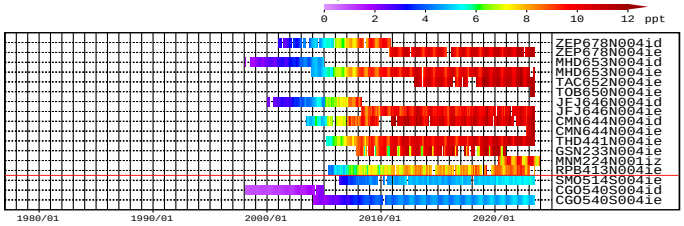

https://doi.org/10.50849/WDCGG_HFC152A_ALL_2024

(g) CH_3Cl Monthly Data

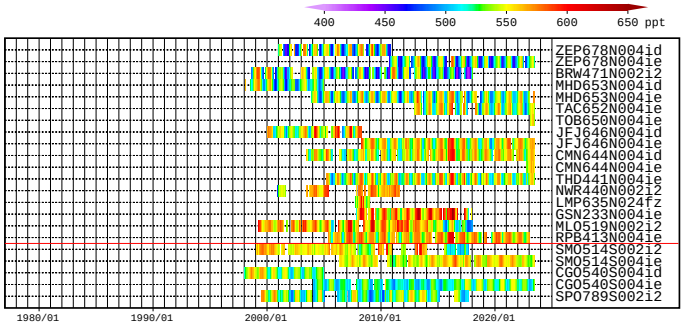

https://doi.org/10.50849/WDCGG_CH3CL_ALL_2024

(h) SF_6 Monthly Data

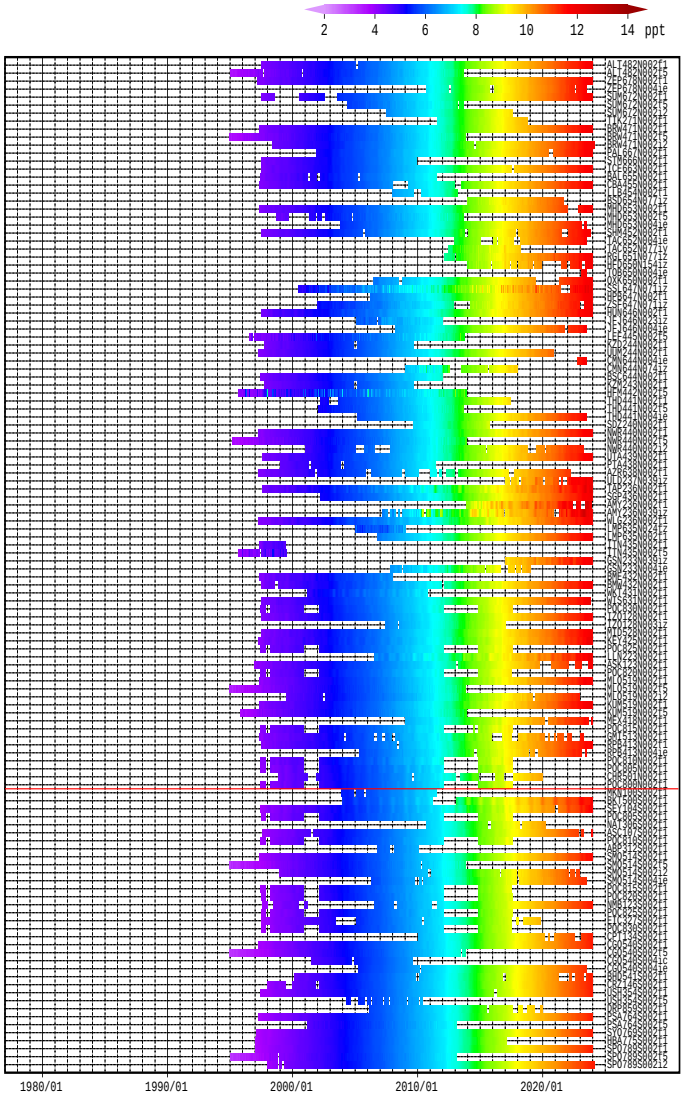

https://doi.org/10.50849/WDCGG_SF6_ALL_2024

Plate 4.2 Monthly mean (a) Halon-1301, (b) HCFC-22, (c) HCFC-141b, (d) HCFC-142b, (e) HFC-134a, (f) HFC-152a, (g) CH_3Cl, (h) SF_6 mole fractions that have been reported to the WDCGG. The mole fractions are illustrated in different colors. The sites are listed in order from north to south. The red line indicates the equator.

4. HALOCARBONS AND OTHER HALOGENATED SPECIES

Halocarbons are generally carbon compounds containing halogens. Most are artificially generated and have much lower atmospheric mole fractions than major greenhouse gases, but they contribute significantly to global warming. These gases together are responsible for around 12% of the total increase in radiative forcing since the pre-industrial era (1750) caused by all long-lived greenhouse gases (WMO, 2024).

Major examples include chlorofluorocarbons (CFCs; carbon compounds containing both fluorine and chlorine), with CFC-11, CFC-12 and CFC-113 having particularly significant impacts on global warming. CFCs used to be mass-produced as refrigerants, propellants, detergents and other functional substances until their connection with stratospheric ozone depletion became evident. After CFC production and consumption were internationally prohibited under the Montreal Protocol in 1989, mole fractions of CFC-11, CFC-12 and CFC-113 are slowly decreasing in the atmosphere. However, a slowing of the decrease in CFC-11 mole fractions was observed from 2013 to 2018 (Figures 4.1, 4.2). This is considered to be associated with CFC-11 emissions from renewed production in eastern Asia (Montzka *et al*., 2018). Since 2019, an accelerated decline in CFC-11 mole fractions has been observed (Montzka *et al*., 2021; WMO, 2021). Recent publications highlighted that other CFCs in the atmosphere are decreasing slower than anticipated similar to CFC-11 (Solomon *et al*., 2020).

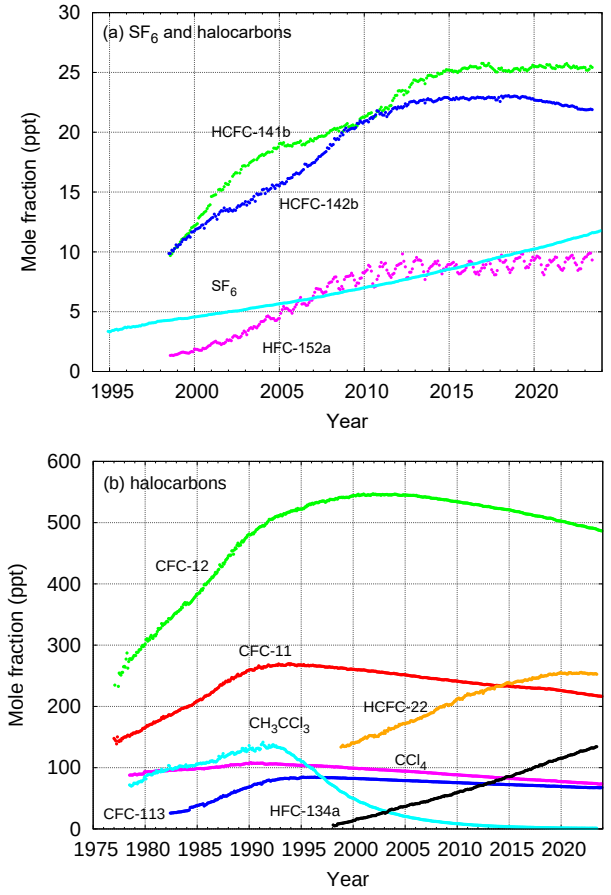

Fig. 4.1 Monthly mean mole fractions of SF_6 and the most important halocarbons: (a) SF_6 and halocarbons of lower mole fractions, and (b) halocarbons of higher mole fractions. The monthly mean for each compound is an arithmetic mean of monthly means at multiple stations without considering scale differences. The number of stations used for the analysis was as follows: SF_6 (91), CFC-11 (26), CFC-12 (28), CFC-113 (23), CCl_4 (24), CH_3CCl_3 (26), HCFC-141b (12), HCFC-142b (16), HCFC-22 (16), HFC-134a (12), HFC-152a (12).

Carbon tetrachloride (CCl_4), methyl chloroform (1,1,1-trichloroethane, CH_3CCl_3), halons and hydrochlorofluorocarbons (HCFCs) are also considered ozone-depleting substances, with related production and consumption regulated under the Montreal Protocol and associated amendments made in the 1990s. Halons are carbon compounds containing bromine, with Halon-1211 and Halon-1301 as typical species. HCFCs represent carbon compounds containing hydrogen, in addition to fluorine and chlorine, with HCFC-22, HCFC-141b and HCFC-142b as major examples. Mole fractions of CCl_4, CH_3CCl_3 and Halon-1211 are decreasing. Growth rates of Halon-1301, HCFC-141b and HCFC-142b have levelled off in recent years, and mole fractions of HCFC-22 are increasing slower than in the 2000s (Figure 4.1, 4.2).

Hydrofluorocarbons (HFCs; carbon compounds containing hydrogen and fluorine but no chlorine) are not ozone depletion substances, and were developed as substitutes for CFCs and HCFCs. However, due to their significant greenhouse effects, they are regulated under the Kigali amendment to the Montreal Protocol adopted in 2016 (effective as of 2019). Typical species include HFC-134a and HFC-152a. Mole fractions of HFC-134a are rapidly increasing, while the growth rate of HFC-152a has levelled off in recent years (Figure 4.1, 4.2).

Unlike other halocarbons that have only anthropogenic origin, methyl chloride (chloromethane, CH_3Cl) comes from natural sources such as ocean, microbial activity and biomass burning as well. Mole fractions of CH_3Cl show no significant long-term trend, although clear seasonal cycle is observed (see Figure 4.2). CH_3Cl is not regulated under the Montreal Protocol, but its status is monitored at many observational stations. Because CH_3Cl is one of the most abundant halocarbons in the remote atmosphere, it plays an important role as a carrier of ozone-depleting chlorine into the stratosphere (Laube *et al.*, 2022).

Although not technically a halocarbon, sulfur hexafluoride (SF_6) is often discussed together with halocarbons and other halogenated gases. SF_6 has very significant greenhouse effects (24300 times more

effective at trapping infrared radiation than an equivalent amount of CO_2 and stays in the atmosphere for 1000 years (IPCC, 2021)) despite its low abundance, and is targeted for reduction by the Kyoto Protocol. Mole fractions of SF_6 show a continuous increase (see Figure 4.1, 4.2). SF_6 is a substance which originates only from anthropogenic sources. It comes from the electricity and electronics supply industries, e.g. the semiconductor industry, where it is used as an electric insulator due to its inertness. Increasing demand for the electricity and power networks will continue leading to SF_6 increases in the atmosphere.

Figure 4.2 displays mole fractions of 14 gas species, with circles representing monthly mean values at individual stations (rather than values averaged over different stations). Solid and open circles correspond to stations in the Northern Hemisphere and Southern Hemisphere, respectively. Due to more intensive production of artificial halocarbons in the Northern Hemisphere, related mole fractions tend to be higher in this region, especially in their increasing phases.

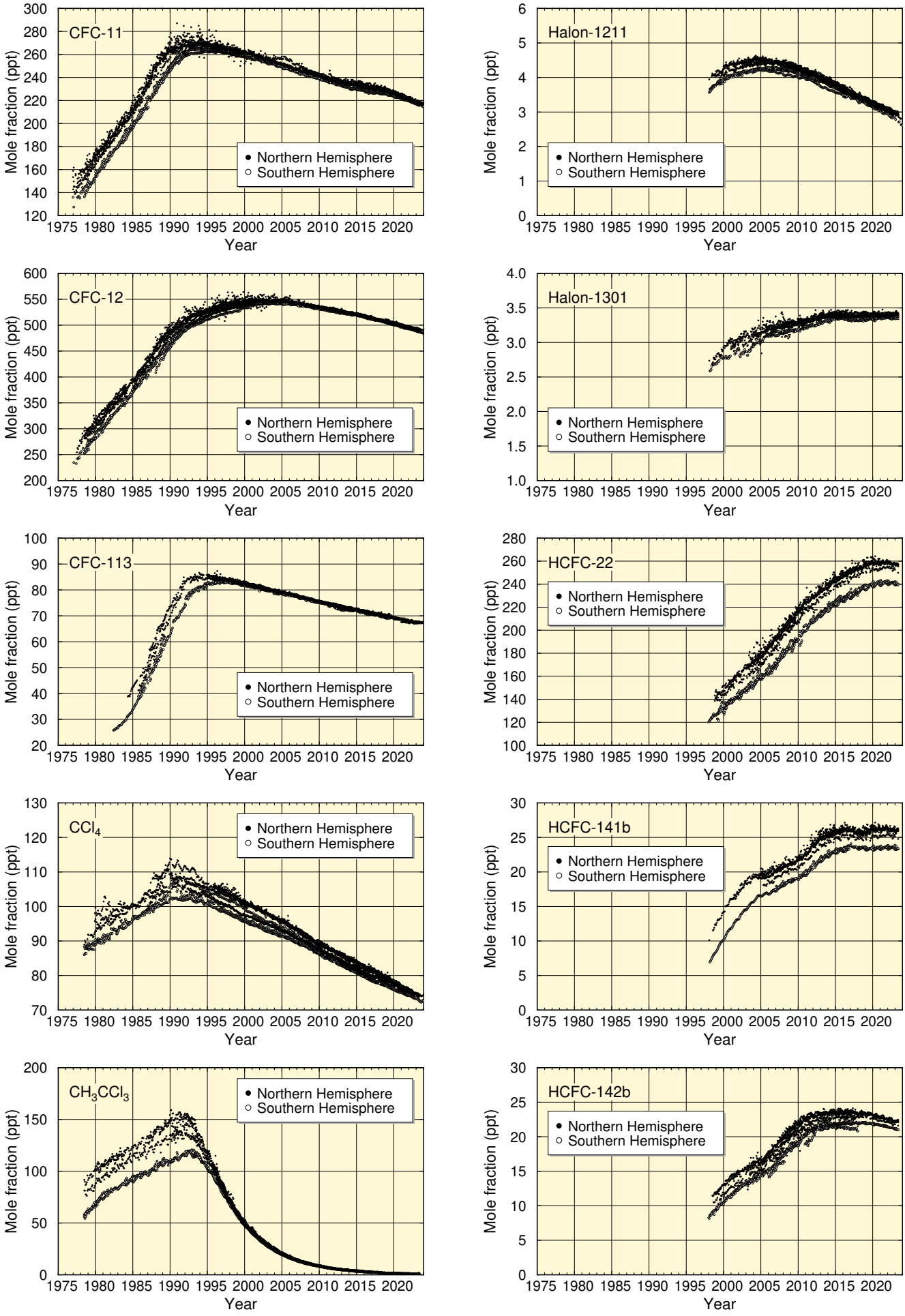

Fig. 4.2 Time series of the monthly mean mole fractions of halocarbons, other halogenated species and sulfur hexafluoride at individual stations. Solid circles show mole fractions in the Northern Hemisphere and open circles show those measured in the Southern Hemisphere. Monthly mean mole fractions from observations at individual stations are directly presented on the plots. Scale differences are not taken into account in this analysis.

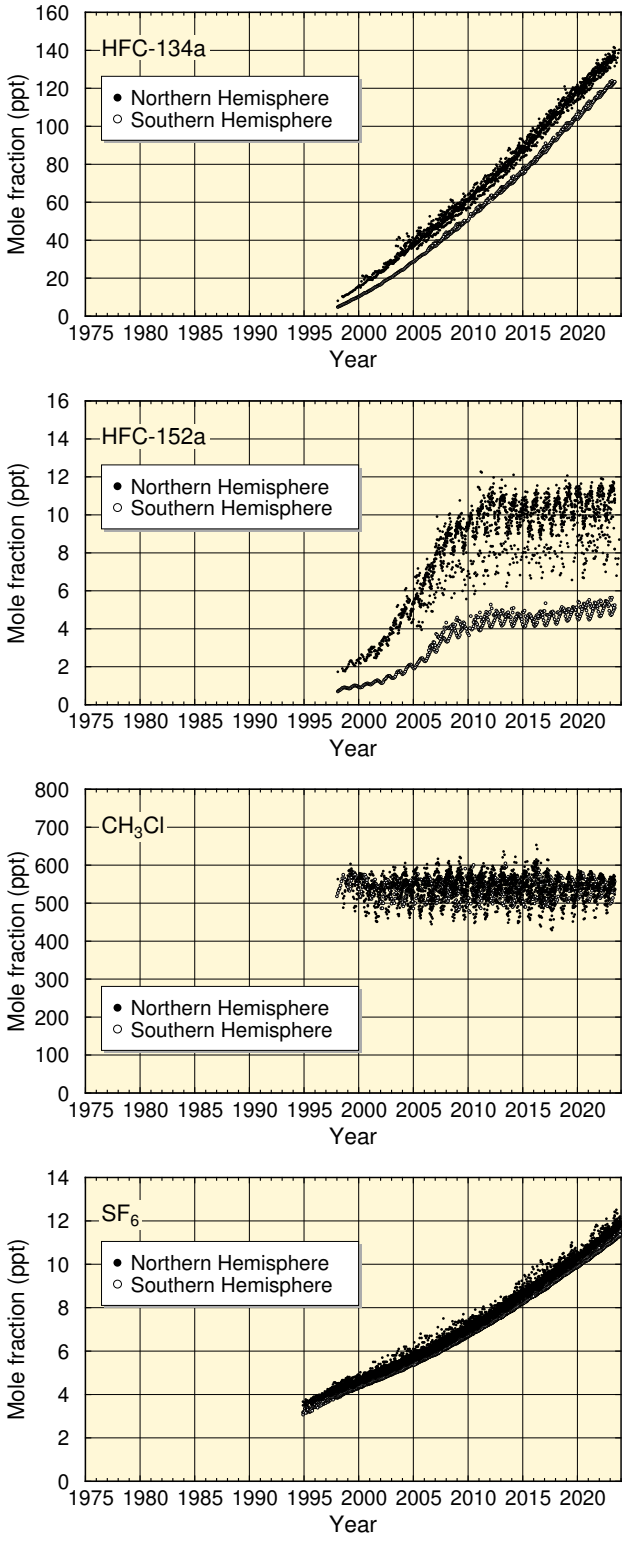

Fig. 4.2 (Continued)

5.

CARBON MONOXIDE

(CO)

● : CONTINUOUS STATION

△ : FLASK STATION

□ : FLASK MOBILE (SHIP)*

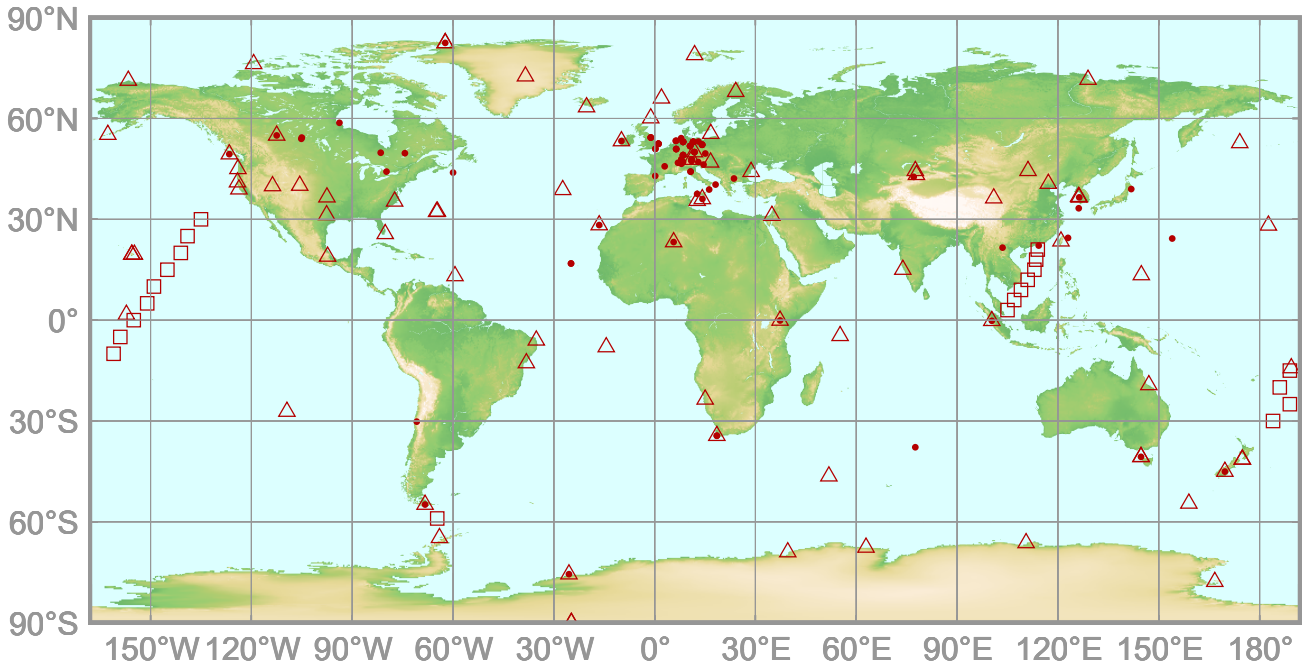

This map shows locations of the stations that have submitted data for monthly mean mole fractions.

* Only fixed point observations are shown in the figure. Other observational locations from mobile platform can be found at https://gaw.kishou.go.jp/search/mobile.

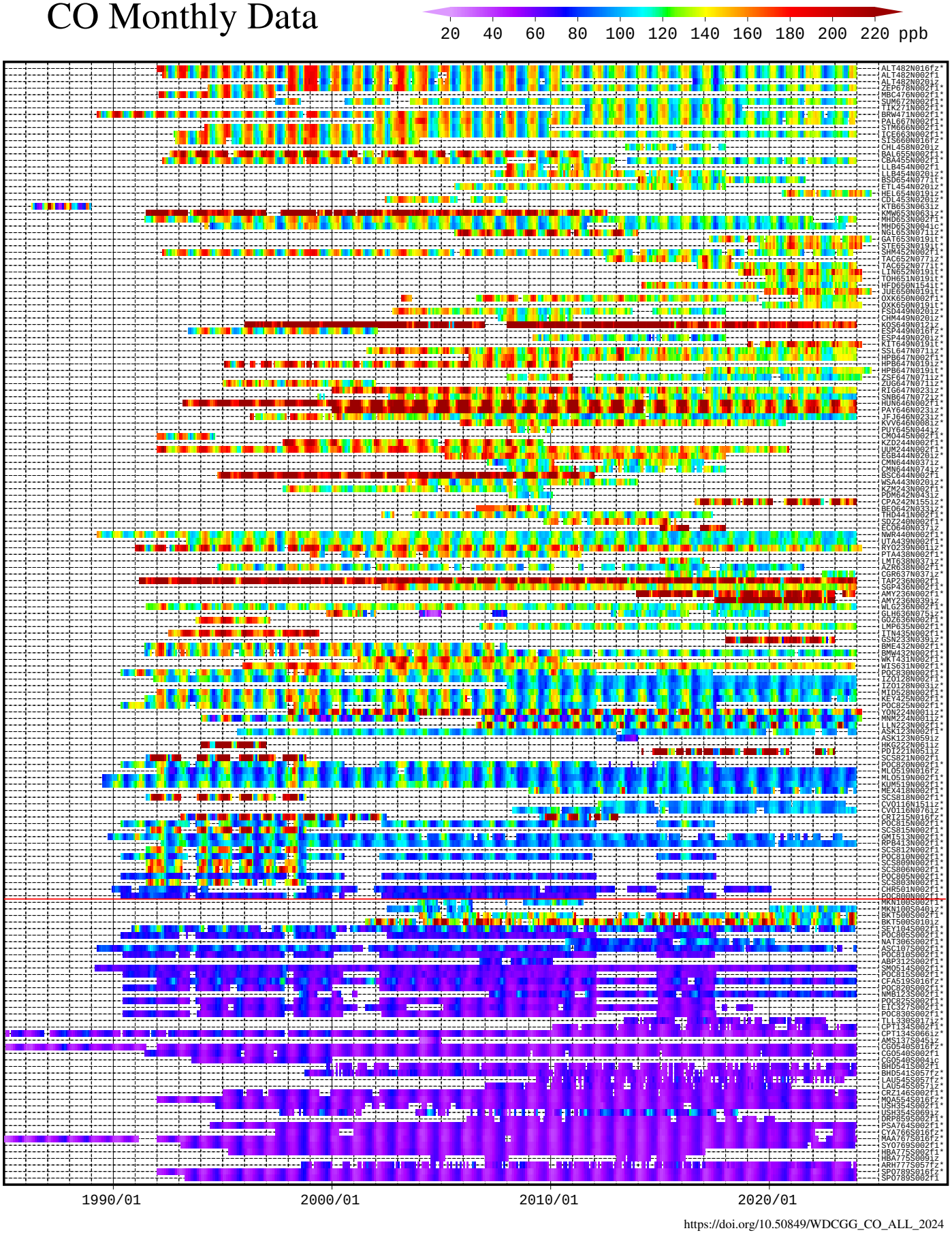

https://doi.org/10.50849/WDCGG_CO_ALL_2024

Plate 5.1 Monthly mean CO mole fractions that have been reported to the WDCGG. The mole fractions are illustrated in different colors. The sites are listed in order from north to south. The red line indicates the equator. The data from the sites with an asterisk at the end of the station index were used for the analyses shown in Plate 5.2 (see Appendix A).

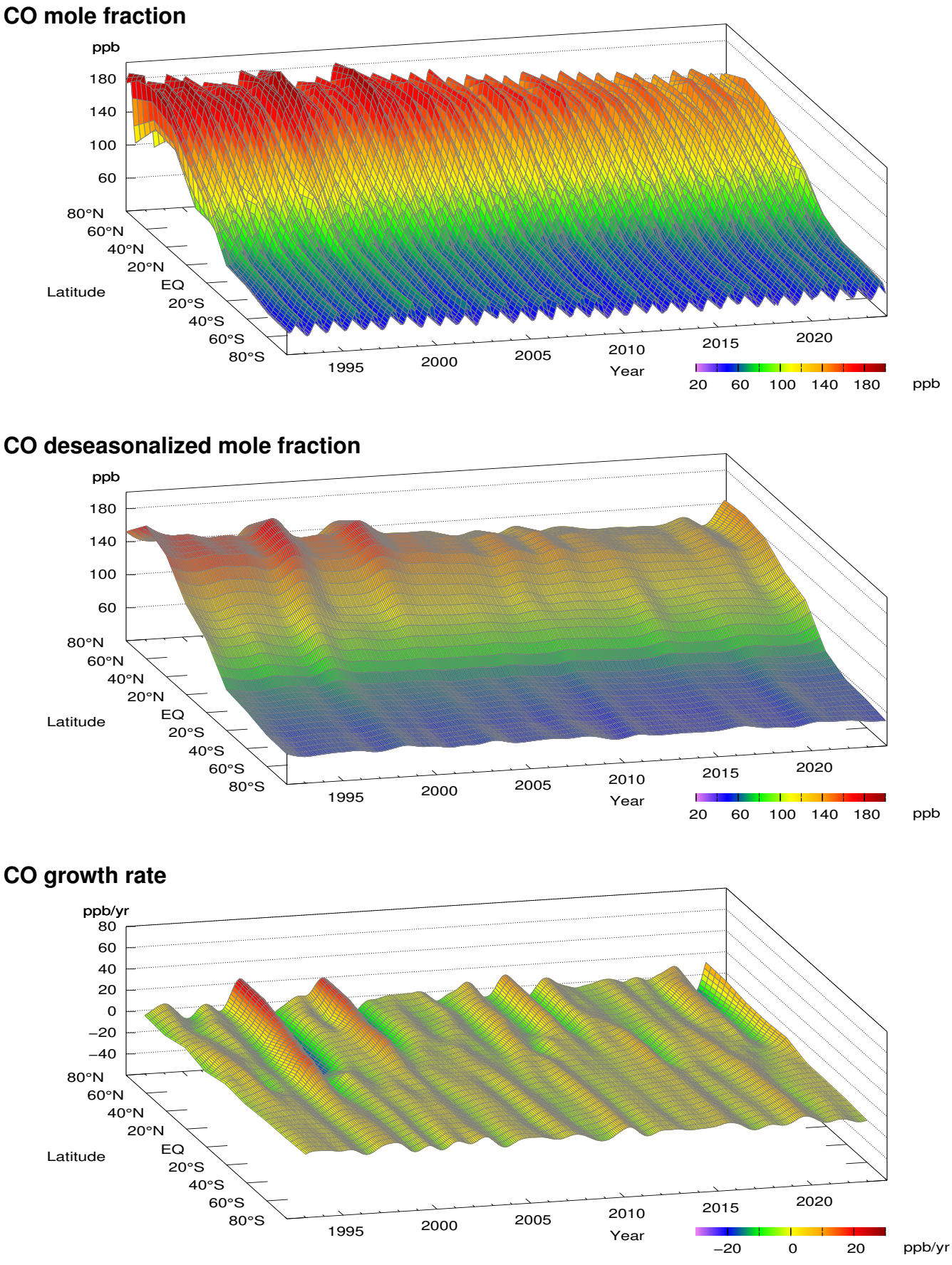

Plate 5.2 Variation of zonally averaged monthly mean CO mole fractions (top), deseasonalized long-term trends (middle), and growth rates (bottom). The zonally averaged mole fractions were calculated for each 20° zone. The deseasonalized trends and growth rates were derived as described in Appendix A.

5. CARBON MONOXIDE (CO)

Carbon monoxide (CO) is not categorized as a greenhouse gas because it absorbs hardly any infrared radiation from the earth. However, it influences major greenhouse gases, particularly through reaction with hydroxyl (OH) radical, and is therefore often addressed in the context of global warming. CO is also part of the global carbon cycle.

Analysis of the global tendencies of CO is complicated by the fact that observations of CO in different part of the world are performed not in a fully consistent way. In contrast to the situation with major greenhouse gases, CO calibration scales cannot be easily interlinked (see Appendix B). Global analysis performed irrespective of scale differences showed a globally averaged CO mole fraction of 95±2 ppb for 2023. Similarly, the analysis results presented in this chapter are based on observations performed on different scales.

CO is emitted into the atmosphere from fossil fuel/biomass burning among other sources, and is destroyed predominantly via reaction with OH radical. Due to its chemical reactivity, CO is characterized by a relatively short lifetime (in the range of several weeks, Zheng et al. 2019) and large spatial variations. Ice core measurements performed by Haan and Raynaud (1998) revealed that the CO mole fractions of approximately 90 ppb observed in Greenland around 1750 had increased to approximately 110 ppb by 1950, indicating an impact of human activity on CO levels. CO mole fractions have shown a gradual decline since around the beginning of the 21st century, particularly in the Northern Hemisphere (IPCC, 2021).

Globally averaged mole fractions

The blue dots in Fig. 5.1 show globally averaged monthly mean CO mole fraction (top) and its growth rate (bottom) based on the analysis described in Appendix A. Clear seasonal variability is observed, and the long-term trend was determined after subtraction of the seasonal component (shown by the red line in the top panel of Fig. 5.1). The globally averaged CO mole fraction exhibits a gradual but significant decrease, with the growth rate oscillating around zero. Mole fractions exhibit clear seasonal cycle, being lower in boreal summer and higher in winter. This is mainly because OH radicals, which react

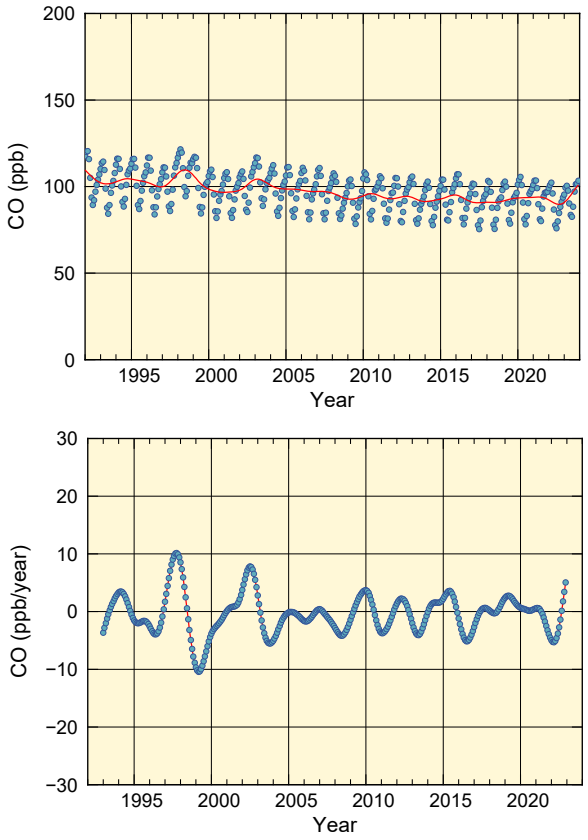

Fig. 5.1 Globally averaged monthly mean mole fraction of CO from 1992 to 2023 (top) and its growth rate (bottom). Red line on the top panel presents the deseasonalized long-term trend.

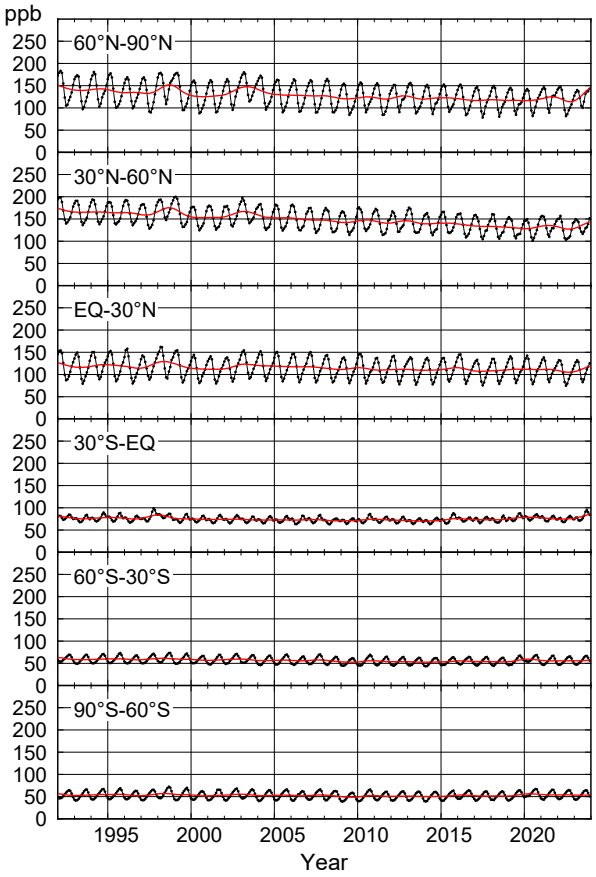

Fig. 5.2 Monthly mean mole fractions of CO from 1992 to 2023 for each 30° latitudinal zone (black) and their deseasonalized long-term trends (red).

with and destroy CO, become more abundant in summer due to enhanced ultraviolet (UV) radiation. Seasonally varying sources such as biomass burning, domestic combustion and traffic emissions also contribute to the formation of the seasonal cycle.

Latitudinal dependence of mole fractions

Fig. 5.2 shows CO mole fractions averaged over six 30° latitudinal zones as black lines, and the red lines show corresponding long-term trends. These trends are collectively shown in the top panel of Figure 5.3, and the corresponding growth rates are shown in the bottom panel. Average seasonal cycles of CO mole fractions for each latitudinal zone are shown in Figure 5.4.

As shown in Figure 5.3, northern hemispheric zones have higher mole fractions, indicating the presence of more CO sources such as fossil fuel/biomass combustion. CO mole fractions in the Northern Hemisphere have shown slight declines throughout the period for which global averaging is feasible, and have remained almost constant in the Southern Hemisphere. CO growth rates also exhibit significant spatial and temporal variability, and tend to be readily influenced by local events with limited time durations. By way of example, the large growth rate peak of 1997/1998 observed in the Northern Hemisphere and elsewhere may be considered attributable to forest fires in Siberia and tropical areas (Novelli *et al.*, 2003) during El Niño. CO mole fractions in the Northern Hemisphere and southern low latitudes increased in 2023. Large emissions from wildfires in Canada and Australia during the year may have contributed to this change (Byrne *et al.*, 2024; Blunden *et al.*, 2024).

The amplitude of seasonal cycle of CO mole fraction is larger in northern zones than in southern zones, as shown in Figure 5.4. In the Northern Hemisphere, CO emitted from fossil fuel combustion accumulates in the mid- and high latitudes during winter and early spring under low OH radical conditions. In addition, CO emissions from biomass burning in the low latitudes peak in early spring. In summer, most of the CO accumulated during winter is destroyed by OH radical. In the Southern Hemisphere, seasonal cycle of CO mole fraction is driven by emissions from biomass burning in the tropics and removal via reaction with OH radicals, resulting in a smaller seasonal-cycle amplitude (Novelli *et al.*, 1998). The phase of seasonal cycles of CO mole fraction in the two hemispheres is opposed due to the reversed seasons. Seasonal variability in the low latitudes of the Southern Hemisphere is slightly more complex due to impact of inter-hemispheric mixing.

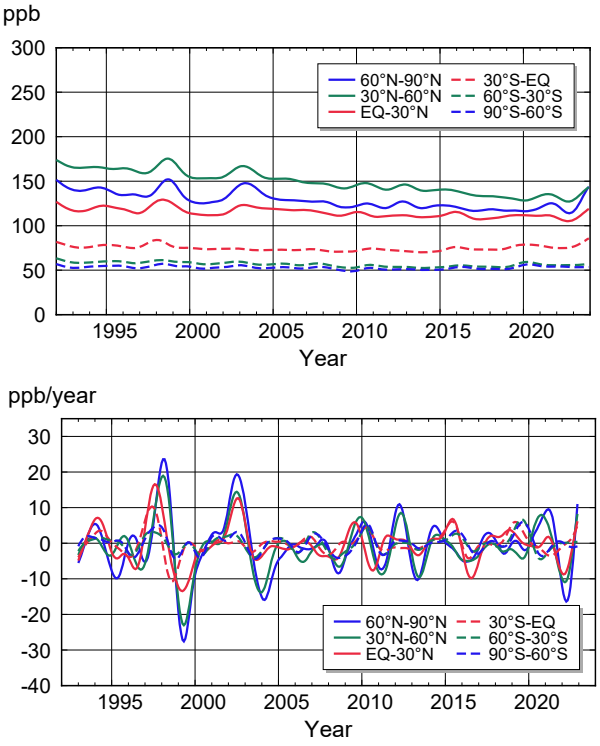

Fig. 5.3 Deseasonalized long-term trends of CO for each 30° latitudinal zone (top) and their growth rates (bottom).

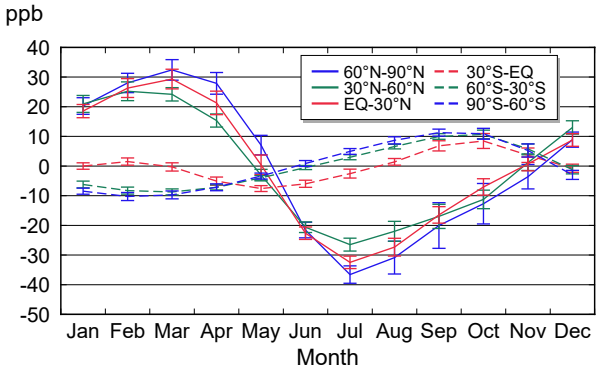

Fig. 5.4 Average seasonal cycles of CO mole fractions for each 30° latitudinal zone obtained by subtracting long-term trends from the zonally averaged time series. Error bars represent the range of ±1σ calculated for each month (period 1992 to 2023).

APPENDICES

APPENDIX A ANALYSIS

This appendix summarizes calculation of globally averaged mole fractions and related quantities of CO_2, CH_4, N_2O and CO as described by WMO (2009) and in Wu et al. (2024).

The analysis is applied to monthly mean mole fraction data reported to WDCGG by fixed stations and ships with fixed geographic observational points. Where no monthly data are reported, values are calculated from valid daily or hourly data using a simple arithmetic mean with the consent of data contributors. Data from mobile platforms such as ships without fixed observation points and aircraft are not used, but are considered in other analysis. Where data are reported for several different altitudes, those for the highest level are used due to their expected larger footprint.

In this data summary, mole fraction units are used following GGMT-2022. The mole fraction is defined as the number of molecules of a target gas species divided by the number of all molecules in dry air. Values are expressed as parts per million (ppm), parts per billion (ppb) and parts per trillion (ppt), corresponding to the SI units of μmol/mol, nmol/mol and pmol/mol, respectively.

(1) Site selection

All observation data are objectively examined for global analysis as described here.

Data on a standard scale traceable to the WMO Mole Fraction Scale (or a compatible standard for conversion) are first selected. CO data are an exception due to the lack of consistency in the implementation of the established WMO standard scales. There is no accurate conversion of the other CO scales to the WMO Scale possible.

For individual sites, annual mean mole fractions relative to those of the South Pole (averaged over the years for which data are available) are plotted to show latitudinal distribution and fitted to the LOESS model curve (Cleveland and Devlin, 1988). Outlier sites beyond the 3 sigma (residual standard deviation) of the fitted curve are excluded from further analysis, and the process is iterated until exclusion terminates. Exclusion is not applied to N_2O due to the scarcity of annual mean data from the 1980s.

The numbers of sites that fit for global analysis (before and after this selection procedure) are shown in Table A1.

(2) Extension of observation data to cover the entire analysis period

Time-series data from some sites may contain gaps or fail to cover the entire analysis period. To ensure the homogeneity of globally averaged values over analysis periods exceeding 30 years, shortfalls in data coverage are compensated for using interpolation and extrapolation as described below.

Gaps in time-series representations are first interpolated for each site. The longest period among continuous monthly mean mole fraction data is identified, and the seasonal cycle and long-term trend are determined as detailed in WMO (2009). In short, a time series of mole fractions is approximated based on the sum of a Fourier series up to the third harmonic of the annual cycle and a non-periodic component determined via a Lanczos filter (Duchon, 1979) with a cut-off frequency of 0.48 cycles per year; the former is a seasonal cycle, and the latter is a long-term trend. Mole fractions in gaps are then interpolated with a line connecting each end of the deseasonalized monthly values and superimposed with the seasonal cycle.

After interpolation, the data are extrapolated via a number of statistical procedures. First, a time series of mole fraction growth rates is calculated for each observation site by differentiating the long-term trend as determined from mole fractions with gaps interpolated as above. Next, for each of six 30° latitudinal zones (60 – 90°N, 30°S – EQ, etc.), an average time series of growth rates is calculated as an arithmetic mean over sites located within the zone. For individual sites, the long-term trend is then extended to cover the entire analysis period based on growth rates for the latitudinal zone where the site is located, and is finally superimposed with the seasonal cycle for the site determined after interpolation.

Table A1. Numbers of sites before/after the selection procedure outlined in Section (1) for CO_2, CH_4, N_2O and CO

	CO_2	CH_4	N_2O	CO
Pre-selection [(a)]	186	163	114	145
Post-selection [(b)]	146	153	112	133

(a) Figures are derived from the number of the first seven characters of the Filename Code (e.g., RYO239N) in Plate 1.1, 2.1, 3.1 and 5.1 (or Table B2 to B5), excluding duplicates.
(b) As per (a), but with Filename Codes marked with asterisks.

(3) Calculation of globally and hemispherically averaged mole fractions

With the extension procedure described above, all sites selected as described in Section (1) have a time series of mole fractions covering the entire analysis period with no data gaps. From these data, latitudinally averaged mole fractions are calculated for the six zones, and globally and hemispherically averaged mole fractions are then determined by averaging the mole fractions of six and three latitudinal zones, respectively, with weighting for surface area. The seasonal cycle, long-term trend and growth rate are then determined for every averaged time series. As long-term trend calculation is less precise at either end of mole fraction time-series representations (see WMO 2009 for details), growth rates originating from the related derivative function are characterized by larger uncertainty. Accordingly, growth rates for a year each from either end of the analysis period are not shown in the figures here.

(4) Uncertainty estimation

In this analysis, uncertainty in globally averaged mole fractions (at a 68% confidence level) is calculated using bootstrap analysis as described in Conway *et al*. (1994). From the dataset of mole fractions obtained after the site selection and data extension procedure described above, n sites are randomly selected, with duplication of the same sites allowed on condition that at least one site is selected from each of the six latitudinal zones, and a globally averaged mole fraction is calculated using the data from the n sites. The procedure is repeated m times to determine m different globally averaged mole fractions. Uncertainty is defined as the standard deviation of these mole fractions. In this analysis, the number of sites selected as described in Section (1) and 200 are chosen as n and m, respectively, for maximum stability in the standard deviation determination.

APPENDIX B CALIBRATION AND STANDARD SCALES

1. Calibration System in the GAW Programme

Under the Global Atmosphere Watch (GAW) Programme, the Central Calibration Laboratories (CCLs) are assigned to host a Primary (Reference) Standard/scale, while the World Calibration Centres (WCCs) and Regional Calibration Centres (RCC) are responsible for the scale propagation to the stations via distribution of calibration standards for certain compounds, conducting instrument calibrations, comparison campaigns, station audits and providing training to the station personnel. A Reference Standard/scale is designated for each variable to be used for all GAW measurements of that variable. Table B1 lists the organizations that serve as WCCs and CCLs for GAW (WMO, 2017). Empa has been confirmed as a WCC for N_2O. In that function Empa will perform stations audits.

Table B1. Overview of the GAW Central Calibration Laboratories (GAW-CCL, Reference Standard) and World Calibration Centres for greenhouse and other related gases. The World Calibration Centres have assumed global responsibilities, except where indicated (Am, Americas; E/A, Europe and Africa; A/O, Asia and the South-West Pacific)

Compounds	Central Calibration Laboratory (Host of Primary Standard)	World Calibration Centre
Carbon Dioxide (CO_2)	NOAA/GML	NOAA/GML (Round Robin) Empa (audits)
Carbon Dioxide (CO_2) isotopes	MPI-BGC	-
Methane (CH_4)	NOAA/GML	Empa (Am, E/A) JMA (A/O)
Nitrous Oxide (N_2O)	NOAA/GML	Empa（audits）
Chlorofluorocarbons (CFCs) Hydrochlorofluorocarbons (HCFCs) Hydrofluorocarbons (HFCs)	METAS[1]	-
Sulfur Hexafluoride (SF_6)	NOAA/GML	KMA
Molecular Hydrogen (H_2)	MPI-BGC	-
Carbon Monoxide (CO)	NOAA/GML	Empa

2. Carbon Dioxide (CO_2)

In 1995, the National Oceanic and Atmospheric Administration's Global Monitoring Laboratory (NOAA/GML; https://gml.noaa.gov/ccl/co2_scale.html, formerly the Earth System Research Laboratory (ESRL) and Climate Monitoring and Diagnostics Laboratory, or CMDL) in Boulder, Colorado, took over the CCL role from the Scripps Institution of Oceanography (SIO) in San Diego, California, and has since been responsible for maintenance of the GAW Primary Standard for CO_2. In this role, the laboratory maintains a high-precision manometric system for absolute calibration of CO_2 as reference for GAW monitoring worldwide (Zhao *et al.*, 1997), as well as carrying out round-robin operation in WCC functions. The standards of GAW monitoring laboratories should advisably be calibrated at least every three years at the CCL (WMO, 2020).

Under the WMO system there have been several calibration scales for CO_2, including the SIO-based X74, X85, X87, X93 and X2002 and the NOAA/GML-based WMO Mole Fraction Scale, partially based on previous SIO scales. The CCL adopted the WMO X2005 scale, reflecting historical manometric calibration of its set of cylinders and potential minor differences between SIO and NOAA/GML calibration. The latest WMO Mole Fraction Scale was the WMO X2019 version at the time of submission in 2021. Values on the former WMO X2007 scale can be converted to WMO X2019 values using [X2019 = 1.00079 * X2007 - 0.142] (Hall *et al.*, 2021).
To assess differences in standard scales among monitoring laboratories, NOAA/GML organizes intercomparisons

[1] Federal Institute of Metrology (METAS) in Switzerland serves as the CCL for certain halogenated compounds.

and round-robin experiments endorsed by WMO every three years or so. Numerous laboratories contributed to experiments conducted in 1991 – 1992, 1995 – 1997, 1999 – 2000, 2002 – 2006, 2009 – 2012 and 2014 – 2015 (https://gml.noaa.gov/ccgg/wmorr/wmorr_results.php).

Table B2 lists organizations and sites contributing to the present issue of the Data Summary with standard scales of reported data and histories of contribution to WMO intercomparison experiments. The calibration scales in the table are based on information from data contributors.

Table B2. Status of standard scales and calibration/intercomparison for CO_2.

Organi-zation	WDCGG Filename	Filename Code in Plate 1.1	Calib-ration Scale	WMO Inter-comparison
AEMET	co2_izo_surface-insitu_3_9999-9999_monthly.txt	IZO128N003iz*	WMO X1987 WMO X1993 WMO X2019	91/92, 96/97, 99/00, 09/12, 14/15
AICH	co2_mkw_surface-insitu_5_9999-9999_monthly.txt	MKW234N005iz	WMO	
AIST	co2_tky_tower-insitu_6_6028-9999_monthly.txt	TKY236N006it	Tohoku Univ. 2010	96/97, 99/00, 02/06, 09/12, 14/15
ATOMKI	co2_hun_tower-insitu_157_6116-9999_monthly.txt	HUN646N157it	WMO X2019	
BMKG	co2_bkt_surface-insitu_10_9999-9999_monthly.txt	BKT500S010iz	WMO X2007	
CMA	co2_wlg_surface-insitu_13_9999-9999_monthly.txt	WLG236N013iz*	WMO X2019	96/97, 99/00, 02/06, 09/12, 14/15
CSIRO	co2_alt_surface-flask_16_9999-9999_monthly.txt co2_cfa_surface-flask_16_9999-9999_monthly.txt co2_cgo_surface-flask_16_9999-9999_monthly.txt co2_cri_surface-flask_16_9999-9999_monthly.txt co2_cya_surface-flask_16_9999-9999_monthly.txt co2_esp_surface-flask_16_9999-9999_monthly.txt co2_maa_surface-flask_16_9999-9999_monthly.txt co2_mlo_surface-flask_16_9999-9999_monthly.txt co2_mqa_surface-flask_16_9999-9999_monthly.txt co2_sis_surface-flask_16_9999-9999_monthly.txt co2_spo_surface-flask_16_9999-9999_monthly.txt	ALT482N016fz CFA519S016fz* CGO540S016fz CRI215N016fz* CYA766S016fz* ESP449N016fz* MAA767S016fz* MLO519N016fz MQA554S016fz* SIS660N016fz* SPO789S016fz	WMO X2019	91/92, 96/97, 99/00, 02/06, 09/12, 14/15
	co2_cgo_surface-insitu_16_9997-9999_monthly.txt co2_cgo_surface-insitu_16_9998-9999_monthly.txt	CGO540S016ix* CGO540S016iy	WMO X1985	
	co2_cgo_surface-insitu_16_9999-9999_monthly.txt co2_mqa_surface-insitu_16_9999-9999_monthly.txt	CGO540S016iz MQA554S016iz*	WMO X2007	
DMC	co2_tll_surface-insitu_17_9999-9999_monthly.txt	TLL330S017iz*	WMO X2019	
DWD	co2_gat_tower-insitu_19_6342-9999_monthly.txt co2_hel_surface-insitu_19_9999-9999_monthly.txt co2_hpb_tower-insitu_19_6132-9999_monthly.txt co2_jue_tower-insitu_19_6121-9999_monthly.txt co2_kit_tower-insitu_19_6201-9999_monthly.txt co2_lin_tower-insitu_19_6099-9999_monthly.txt co2_oxk_tower-insitu_19_6164-9999_monthly.txt co2_ste_tower-insitu_19_6253-9999_monthly.txt co2_toh_tower-insitu_19_6148-9999_monthly.txt	GAT653N019it* HEL654N019iz* HPB647N019it JUE650N019it KIT649N019it LIN652N019it OXK650N019it* STE653N019it TOH651N019it*	WMO X2019	

ECCC	co2_alt_surface-insitu_20_9999-9999_monthly.txt co2_bck_surface-insitu_20_9999-9999_monthly.txt co2_bra_surface-insitu_20_9999-9999_monthly.txt co2_cby_surface-insitu_20_9999-9999_monthly.txt co2_cdl_surface-insitu_20_9999-9999_monthly.txt co2_chl_surface-insitu_20_9999-9999_monthly.txt co2_chm_surface-insitu_20_9999-9999_monthly.txt co2_cps_surface-insitu_20_9999-9999_monthly.txt co2_egb_surface-insitu_20_9999-9999_monthly.txt co2_esp_surface-insitu_20_9999-9999_monthly.txt co2_est_surface-insitu_20_9999-9999_monthly.txt co2_etl_surface-insitu_20_9999-9999_monthly.txt co2_fsd_surface-insitu_20_9999-9999_monthly.txt co2_inu_surface-insitu_20_9999-9999_monthly.txt co2_llb_surface-insitu_20_9999-9999_monthly.txt co2_wsa_surface-insitu_20_9999-9999_monthly.txt	ALT482N020iz* BCK462N020iz* BRA450N020iz* CBY469N020iz* CDL453N020iz* CHL458N020iz* CHM449N020iz* CPS449N020iz* EGB444N020iz* ESP449N020iz* EST451N020iz* ETL454N020iz* FSD449N020iz* INU468N020iz* LLB454N020iz* WSA443N020iz*	WMO X2019	91/92, 96/97, 99/00, 02/06, 09/12, 14/15
EMA	co2_cai_surface-insitu_22_9999-9999_monthly.txt co2_frf_surface-insitu_22_9999-9999_monthly.txt	CAI130N022iz FRF127N022iz		
Empa	co2_jfj_surface-insitu_23_9999-9999_monthly.txt	JFJ646N023iz*	WMO X2019	09/12, 14/15
ENEA	co2_lmp_surface-flask_24_9999-9999_monthly.txt co2_mdn_surface-flask_24_9999-9999_monthly.txt	LMP635N024fz* MDN637N024fz*	WMO X2019	91/92, 96/97, 99/00, 02/06, 09/12, 14/15
	co2_lmp_surface-insitu_24_9999-9999_monthly.txt	LMP635N024iz*	WMO X2007	
FMI	co2_pal_surface-insitu_25_9999-9999_monthly.txt co2_tik_surface-insitu_25_9999-9999_monthly.txt	PAL667N025iz* TIK271N025iz*	WMO X2019	02/06, 09/12 14/15
GERC	co2_gsn_surface-insitu_52_9999-9999_monthly.txt	GSN233N052iz*	WMO X2007	
HKO	co2_hkg_surface-insitu_27_9999-9999_monthly.txt	HKG222N027iz	WMO X2007 WMO X2019	
	co2_hko_surface-insitu_27_9999-9999_monthly.txt	HKO222N027iz	WMO X2007 WMO X2019 NIST	
HMS	co2_kps_surface-insitu_28_9999-9999_monthly.txt	KPS646N028iz*	WMO X2007	91/92, 96/97, 99/00, 02/06, 09/12, 14/15
IAA	co2_jbn_surface-insitu_18_9999-9999_monthly.txt	JBN762S018iz*	WMO X1993	
IAFMS	co2_cmn_surface-insitu_29_9999-9999_monthly.txt	CMN644N029iz*	WMO X1993 WMO X2019	91/92, 96/97, 02/06, 14/15
IGP	co2_hua_surface-insitu_30_9999-9999_monthly.txt	HUA312S030iz	WMO X1981	
IMKIFU	co2_wnk_surface-insitu_31_9999-9999_monthly.txt co2_zug_surface-insitu_31_9999-9999_monthly.txt	WNK647N031iz ZUG647N031iz	WMO X1974	99/00
INMH	co2_fdt_surface-insitu_58_9999-9999_monthly.txt	FDT645N058iz		
INRNE	co2_beo_surface-insitu_33_9999-9999_monthly.txt	BEO642N033iz	WMO	
IOEP	co2_dig_surface-insitu_35_9999-9999_monthly.txt	DIG654N035iz		

ISAC	co2_cgr_surface-insitu_37_9999-9999_monthly.txt	CGR637N037iz*	WMO X2019	
	co2_lmt_surface-insitu_37_9999-9999_monthly.txt	LMT638N037iz	WMO X2007	
	co2_eco_surface-insitu_37_9999-9999_monthly.txt	ECO640N037iz		
ITM	co2_zep_surface-insitu_38_9999-9999_monthly.txt	ZEP678N038iz	WMO X2007	96/97, 99/00, 09/12
JMA	co2_mnm_surface-insitu_1_9999-9999_monthly.txt co2_ryo_surface-insitu_1_9999-9999_monthly.txt co2_yon_surface-insitu_1_9999-9999_monthly.txt	MNM224N001iz* RYO239N001iz* YON224N001iz*	WMO X2019	91/92, 96/97, 99/00, 02/06, 09/12, 14/15
KMA	co2_gsn_surface-insitu_39_9999-9999_monthly.txt	GSN233N039iz*	WMO X2019	02/06, 09/12 14/15
	co2_uld_surface-insitu_39_9999-9999_monthly.txt	ULD237N039iz*		
	co2_ksg_surface-insitu_39_9999-9999_monthly.txt	KSG762S039iz	KRISS	
	co2_amy_surface-insitu_39_9999-9999_monthly.txt	AMY236N039iz	WMO X2019 KRISS	
KMD	co2_mkn_surface-insitu_40_9999-9999_monthly.txt	MKN100S040iz*	WMO X2019	
KSNU	co2_isk_surface-remote_41_9999-9999_monthly.txt	ISK242N041rz		
KUP	co2_jfj_surface-insitu_42_9999-9999_monthly.txt	JFJ646N042iz*	WMO X2019	09/12
Kyrgyzhydromet	co2_cpa_surface-insitu_155_9999-9999_monthly.txt	CPA242N155iz	WMO X2019	
LSCE	co2_ams_surface-insitu_45_9998-9999_monthly.txt	AMS137S045iy*	WMO X1993 WMO X2002	91/92, 96/97, 99/00, 02/06, 09/12, 14/15
	co2_bgu_surface-flask_45_9999-9999_monthly.txt co2_lpo_surface-flask_45_9999-9999_monthly.txt co2_pdm_surface-flask_45_9999-9999_monthly.txt	BGU641N045fz* LPO648N045fz PDM642N045fz*	WMO X2001	
	co2_mhd_surface-insitu_45_9999-9999_monthly.txt	MHD653N045iz	WMO X1993	
	co2_puy_surface-insitu_45_9999-9999_monthly.txt	PUY645N045iz*	WMO X2001 WMO X2007	
	co2_fkl_surface-flask_45_9999-9999_monthly.txt	FKL635N045fz		
METRI	co2_gsn_surface-flask_55_9999-9999_monthly.txt	GSN233N055fz*	WMO X1997	96/97
MGO	co2_ber_surface-flask_46_9999-9999_monthly.txt co2_kot_surface-flask_46_9999-9999_monthly.txt co2_kyz_surface-flask_46_9999-9999_monthly.txt co2_stc_surface-flask_46_9999-9999_monthly.txt	BER255N046fz* KOT276N046fz* KYZ240N046fz* STC654N046fz*	WMO X1987	14/15
	co2_ter_surface-flask_46_9999-9999_monthly.txt	TER669N046fz*	WMO X2019	
	co2_tik_surface-flask_46_9999-9999_monthly.txt	TIK271N046fz*	WMO X2007	
MMD	co2_dmv_surface-insitu_47_9999-9999_monthly.txt	DMV504N047iz	WMO	
MRI	co2_tkb_tower-insitu_48_6201-9999_monthly.txt	TKB236N048it	MRI-87	91/92, 96/97, 99/00, 02/06, 09/12, 14/15
NIES	co2_coi_surface-insitu_53_9999-9999_monthly.txt co2_hat_surface-insitu_53_9999-9999_monthly.txt	COI243N053iz* HAT224N053iz*	NIES 09**	96/97, 99/00, 02/06, 09/12,

				14/15
NILU	co2_zep_surface-insitu_54_9999-9999_monthly.txt	ZEP678N054iz*	WMO X2007 WMO X2019	
NIWA	co2_bhd_surface-insitu_57_9999-9999_monthly.txt	BHD541S057iz*	WMO X2019	91/92, 96/97, 99/00, 02/06, 09/12, 14/15
	co2_lau_surface-insitu_57_9999-9999_monthly.txt	LAU545S057iz*	WMO X2007	
NOAA	co2_abp_surface-flask_2_3001-9999_monthly.txt	ABP312S002f1*	WMO X2019	91/92, 96/97, 99/00, 02/06, 09/12, 14/15
	co2_alt_surface-flask_2_3001-9999_monthly.txt	ALT482N002f1*		
	co2_ams_surface-flask_2_3001-9999_monthly.txt	AMS137S002f1*		
	co2_amy_surface-flask_2_3001-9999_monthly.txt	AMY236N002f1		
	co2_asc_surface-flask_2_3001-9999_monthly.txt	ASC107S002f1*		
	co2_ask_surface-flask_2_3001-9999_monthly.txt	ASK123N002f1*		
	co2_avi_surface-flask_2_3001-9999_monthly.txt	AVI417N002f1*		
	co2_azr_surface-flask_2_3001-9999_monthly.txt	AZR638N002f1*		
	co2_bal_surface-flask_2_3001-9999_monthly.txt	BAL655N002f1*		
	co2_bhd_surface-flask_2_3001-9999_monthly.txt	BHD541S002f1*		
	co2_bkt_surface-flask_2_3001-9999_monthly.txt	BKT500S002f1		
	co2_bme_surface-flask_2_3001-9999_monthly.txt	BME432N002f1*		
	co2_bmw_surface-flask_2_3001-9999_monthly.txt	BMW432N002f1*		
	co2_brw_surface-flask_2_3001-9999_monthly.txt	BRW471N002f1		
	co2_brw_surface-insitu_2_3001-9999_monthly.txt	BRW471N002i1*		
	co2_bsc_surface-flask_2_3001-9999_monthly.txt	BSC644N002f1		
	co2_cba_surface-flask_2_3001-9999_monthly.txt	CBA455N002f1*		
	co2_cgo_surface-flask_2_3001-9999_monthly.txt	CGO540S002f1*		
	co2_chr_surface-flask_2_3001-9999_monthly.txt	CHR501N002f1*		
	co2_cmo_surface-flask_2_3001-9999_monthly.txt	CMO445N002f1*		
	co2_cpt_surface-flask_2_3001-9999_monthly.txt	CPT134S002f1		
	co2_crz_surface-flask_2_3001-9999_monthly.txt	CRZ146S002f1*		
	co2_drp_ship-flask_2_3001-9999_monthly.txt	DRP859S002f1*		
	co2_eic_surface-flask_2_3001-9999_monthly.txt	EIC327S002f1*		
	co2_gmi_surface-flask_2_3001-9999_monthly.txt	GMI513N002f1*		
	co2_goz_surface-flask_2_3001-9999_monthly.txt	GOZ636N002f1*		
	co2_hba_surface-flask_2_3001-9999_monthly.txt	HBA775S002f1*		
	co2_hpb_surface-flask_2_3001-9999_monthly.txt	HPB647N002f1*		
	co2_hun_surface-flask_2_3001-9999_monthly.txt	HUN646N002f1*		
	co2_ice_surface-flask_2_3001-9999_monthly.txt	ICE663N002f1*		
	co2_izo_surface-flask_2_3001-9999_monthly.txt	IZO128N002f1		
	co2_key_surface-flask_2_3001-9999_monthly.txt	KEY425N002f1*		
	co2_kum_surface-flask_2_3001-9999_monthly.txt	KUM519N002f1*		
	co2_kzd_surface-flask_2_3001-9999_monthly.txt	KZD244N002f1*		
	co2_kzm_surface-flask_2_3001-9999_monthly.txt	KZM243N002f1*		
	co2_llb_surface-flask_2_3001-9999_monthly.txt	LLB454N002f1		
	co2_lln_surface-flask_2_3001-9999_monthly.txt	LLN223N002f1*		
	co2_lmp_surface-flask_2_3001-9999_monthly.txt	LMP635N002f1*		
	co2_mbc_surface-flask_2_3001-9999_monthly.txt	MBC476N002f1*		
	co2_mex_surface-flask_2_3001-9999_monthly.txt	MEX418N002f1*		
	co2_mhd_surface-flask_2_3001-9999_monthly.txt	MHD653N002f1*		
	co2_mid_surface-flask_2_3001-9999_monthly.txt	MID528N002f1*		
	co2_mkn_surface-flask_2_3001-9999_monthly.txt	MKN100S002f1*		
	co2_mko_surface-insitu_2_3001-9999_monthly.txt	MKO519N002i1		
	co2_mlo_surface-flask_2_3001-9999_monthly.txt	MLO519N002f1*		
	co2_mlo_surface-insitu_2_3001-9999_monthly.txt	MLO519N002i1*		
	co2_nat_surface-flask_2_3001-9999_monthly.txt	NAT306S002f1*		

	co2_nmb_surface-flask_2_3001-9999_monthly.txt	NMB123S002f1*		
	co2_nwr_surface-flask_2_3001-9999_monthly.txt	NWR440N002f1*		
	co2_opw_surface-flask_2_3001-9999_monthly.txt	OPW448N002f1*		
	co2_oxk_surface-flask_2_3001-9999_monthly.txt	OXK650N002f1*		
	co2_pal_surface-flask_2_3001-9999_monthly.txt	PAL667N002f1		
	co2_poc_ship-flask_2_3001-3001_monthly.txt	POC800N002f1*		
	co2_poc_ship-flask_2_3001-3002_monthly.txt	POC805N002f1*		
	co2_poc_ship-flask_2_3001-3003_monthly.txt	POC810N002f1*		
	co2_poc_ship-flask_2_3001-3004_monthly.txt	POC815N002f1*		
	co2_poc_ship-flask_2_3001-3005_monthly.txt	POC820N002f1*		
	co2_poc_ship-flask_2_3001-3006_monthly.txt	POC825N002f1*		
	co2_poc_ship-flask_2_3001-3007_monthly.txt	POC830N002f1*		
	co2_poc_ship-flask_2_3001-3012_monthly.txt	POC805S002f1*		
	co2_poc_ship-flask_2_3001-3013_monthly.txt	POC810S002f1*		
	co2_poc_ship-flask_2_3001-3014_monthly.txt	POC815S002f1*		
	co2_poc_ship-flask_2_3001-3015_monthly.txt	POC820S002f1*		
	co2_poc_ship-flask_2_3001-3016_monthly.txt	POC825S002f1*		
	co2_poc_ship-flask_2_3001-3017_monthly.txt	POC830S002f1*		
	co2_poc_ship-flask_2_3001-3018_monthly.txt	POC835S002f1*		
	co2_psa_surface-flask_2_3001-9999_monthly.txt	PSA764S002f1*		
	co2_pta_surface-flask_2_3001-9999_monthly.txt	PTA438N002f1*		
	co2_rpb_surface-flask_2_3001-9999_monthly.txt	RPB413N002f1*		
	co2_scs_ship-flask_2_3001-3101_monthly.txt	SCS803N002f1*		
	co2_scs_ship-flask_2_3001-3102_monthly.txt	SCS806N002f1*		
	co2_scs_ship-flask_2_3001-3103_monthly.txt	SCS809N002f1*		
	co2_scs_ship-flask_2_3001-3104_monthly.txt	SCS812N002f1*		
	co2_scs_ship-flask_2_3001-3105_monthly.txt	SCS815N002f1*		
	co2_scs_ship-flask_2_3001-3106_monthly.txt	SCS818N002f1*		
	co2_scs_ship-flask_2_3001-3107_monthly.txt	SCS821N002f1*		
	co2_sdz_surface-flask_2_3001-9999_monthly.txt	SDZ240N002f1		
	co2_sey_surface-flask_2_3001-9999_monthly.txt	SEY104S002f1*		
	co2_sgp_surface-flask_2_3001-9999_monthly.txt	SGP436N002f1*		
	co2_shm_surface-flask_2_3001-9999_monthly.txt	SHM452N002f1*		
	co2_smo_surface-flask_2_3001-9999_monthly.txt	SMO514S002f1*		
	co2_smo_surface-insitu_2_3001-9999_monthly.txt	SMO514S002i1*		
	co2_spo_surface-flask_2_3001-9999_monthly.txt	SPO789S002f1		
	co2_spo_surface-insitu_2_3001-9999_monthly.txt	SPO789S002i1*		
	co2_stc_surface-flask_2_3001-9999_monthly.txt	STC654N002f1		
	co2_stm_surface-flask_2_3001-9999_monthly.txt	STM666N002f1*		
	co2_sum_surface-flask_2_3001-9999_monthly.txt	SUM672N002f1*		
	co2_syo_surface-flask_2_3001-9999_monthly.txt	SYO769S002f1*		
	co2_tap_surface-flask_2_3001-9999_monthly.txt	TAP236N002f1*		
	co2_thd_surface-flask_2_3001-9999_monthly.txt	THD441N002f1*		
	co2_tik_surface-flask_2_3001-9999_monthly.txt	TIK271N002f1*		
	co2_ush_surface-flask_2_3001-9999_monthly.txt	USH354S002f1*		
	co2_uta_surface-flask_2_3001-9999_monthly.txt	UTA439N002f1*		
	co2_uum_surface-flask_2_3001-9999_monthly.txt	UUM244N002f1*		
	co2_wis_surface-flask_2_3001-9999_monthly.txt	WIS631N002f1*		
	co2_wlg_surface-flask_2_3001-9999_monthly.txt	WLG236N002f1*		
	co2_zep_surface-flask_2_3001-9999_monthly.txt	ZEP678N002f1*		
NPL	co2_hfd_tower-insitu_154_6101-9999_monthly.txt	HFD650N154it*	WMO X2019	
OSAKAU	co2_sui_surface-insitu_60_9999-9999_monthly.txt	SUI234N060iz		
RIVM	co2_kmw_surface-insitu_63_9999-9999_monthly.txt	KMW653N063iz	NIST	

RSE	co2_prs_surface-insitu_64_9999-9999_monthly.txt	PRS645N064iz*	WMO X1993 WMO X2007 ICOS	99/00, 02/06 14/15
SAIPF	co2_ddr_surface-insitu_65_9999-9999_monthly.txt co2_kis_surface-insitu_65_9999-9999_monthly.txt co2_urw_surface-insitu_65_9999-9999_monthly.txt	DDR236N065iz* KIS236N065iz URW235N065iz	WMO X2007	
SAWS	co2_cpt_surface-insitu_66_9999-1001_monthly.txt	CPT134S066iz*	WMO X2019	99/00, 02/06, 09/12, 14/15
SHIZU	co2_hmm_surface-insitu_67_9999-9999_monthly.txt	HMM234N067iz		
TU	co2_syo_surface-insitu_70_9999-9999_monthly.txt	SYO769S070iz	Tohoku Univ. 2010	91/92, 96/97, 99/00, 02/06, 09/12
UBAA	co2_snb_surface-insitu_72_9999-9999_monthly.txt	SNB647N072iz*	WMO X2007	
UBAG	co2_brt_surface-insitu_71_9999-9999_monthly.txt co2_deu_surface-insitu_71_9999-9999_monthly.txt co2_ngl_surface-insitu_71_9999-9999_monthly.txt co2_wal_surface-insitu_71_9999-9999_monthly.txt co2_wes_surface-insitu_71_9999-9999_monthly.txt co2_zgt_surface-insitu_71_9999-9999_monthly.txt	BRT648N071iz* DEU649N071iz NGL653N071iz WAL652N071iz WES654N071iz* ZGT654N071iz	WMO	91/92, 96/97, 99/00, 02/06, 09/12, 14/15
	co2_ssl_surface-insitu_71_9998-9999_monthly.txt	SSL647N071iy	WMO X2007	
	co2_ssl_surface-insitu_71_9999-9999_monthly.txt co2_wes_surface-insitu_71_9998-9999_monthly.txt co2_zsf_surface-insitu_71_9999-9999_monthly.txt	SSL647N071iz* WES654N071iy* ZSF647N071iz*	WMO X2019	
	co2_zug_surface-insitu_71_9999-9999_monthly.txt	ZUG647N071iz*	WMO X1985	
UMLT	co2_glh_surface-insitu_75_9999-9999_monthly.txt	GLH636N075iz		
UNIVBRIS	co2_bsd_tower-insitu_77_6249-9999_monthly.txt co2_rgl_tower-insitu_77_6091-9999_monthly.txt co2_tac_tower-insitu_77_6186-9999_monthly.txt	BSD654N077it* RGL651N077it* TAC652N077it*	WMO X2019	
UoE	co2_cvo_surface-insitu_151_9999-9999_monthly.txt	CVO116N151iz*	WMO X2019	
UYRK	co2_cvo_surface-insitu_76_9999-9999_monthly.txt	CVO116N076iz*	WMO X2019	
VNMHA	co2_pdi_surface-insitu_51_9999-9999_monthly.txt	PDI221N051iz	WMO X2019	

* Stations marked with an asterisk are used for the calculation of globally averaged mole fractions and related quantities. The site selection procedure is described in Appendix A.
** The NIES 09 CO_2 scale is consistent with WMO X2007 CO_2 to within 0.1 ppm.

3. Methane (CH_4)

The GAW Programme has a CCL for CH_4 at NOAA/GML (Dlugokencky *et al.*, 2005; WMO, 2017). Two WCCs for CH_4 are also run by the Swiss Federal Laboratories for Materials Science and Technology (Empa; Dübendorf, Switzerland) and the Japan Meteorological Agency (JMA; Tokyo, Japan) (WMO, 2017).

The current WMO Mole Fraction Scale is X2004A, which consists of 16 existing standards covering the range of the previous WMO X2004 scale and 6 new standards to expand the range of the scale (https://gml.noaa.gov /ccl/ch4_scale.html). Table B3 summarizes the CH_4 standard scales used by stations contributing to the WDCGG. In this issue, the multiplying factor for conversion between X2004A and X2004 is taken as 1 because the related difference is minor.

Mole fractions on the WMO X2004 scale are 1.0124 times higher than those on the NOAA 1983 scale (Dlugokencky *et al.*, 2005). The value on the NOAA 1983 scale is 1.0151 times lower than that on the scale of the Atmospheric Environment Service (AES, now known as Environment and Climate Change Canada (ECCC))

(Worthy *et al.*, 1998). The multiplying conversion factor of 1.0124 / 1.0151 = 0.9973 is adopted for comparison of the ECCC scale with the WMO X2004 scale. Mole fractions of the WMO X2004A scale are higher than those on the Tohoku University 1987 scale by around 0.5 ppb (Fujita *et al*., 2018).

Table B3. Status of the standard scales of CH_4.

Organi-zation	WDCGG Filename	Filename Code in Plate 2.1	Calibration Scale
AEMET	ch4_izo_surface-insitu_3_9999-9999_monthly.txt	IZO128N003iz*	WMO X2004A
AGAGE	ch4_cgo_surface-insitu_4_2024-9999_monthly.txt ch4_rpb_surface-insitu_4_2024-9999_monthly.txt ch4_thd_surface-insitu_4_2024-9999_monthly.txt	CGO540S004if RPB413N004if THD441N004if*	WMO X2004A
	ch4_cgo_surface-insitu_4_2011-2016_monthly.txt ch4_cgo_surface-insitu_4_2021-9999_monthly.txt ch4_cmo_surface-insitu_4_2011-2016_monthly.txt ch4_mhd_surface-insitu_4_2011-2016_monthly.txt ch4_mhd_surface-insitu_4_2021-9999_monthly.txt ch4_rpb_surface-insitu_4_2021-9999_monthly.txt ch4_smo_surface-insitu_4_2011-2016_monthly.txt ch4_smo_surface-insitu_4_2021-9999_monthly.txt ch4_thd_surface-insitu_4_2021-9999_monthly.txt	CGO540S004ib CGO540S004ic* CMO445N004ib MHD653N004ib* MHD653N004ic* RPB413N004ic* SMO514S004ib SMO514S004ic* THD441N004ic*	TU-1987
ATOMKI	ch4_hun_tower-insitu_157_6116-9999_monthly.txt	HUN646N157it	WMO X2004
BMKG	ch4_bkt_surface-insitu_10_9999-9999_monthly.txt	BKT500S010iz	WMO X2004 WMO X2004A
CMA	ch4_wlg_surface-insitu_13_9999-9999_monthly.txt	WLG236N013iz	WMO X2004
CSIRO	ch4_alt_surface-flask_16_9999-9999_monthly.txt ch4_cfa_surface-flask_16_9999-9999_monthly.txt ch4_cgo_surface-flask_16_9999-9999_monthly.txt ch4_cri_surface-flask_16_9999-9999_monthly.txt ch4_cya_surface-flask_16_9999-9999_monthly.txt ch4_esp_surface-flask_16_9999-9999_monthly.txt ch4_maa_surface-flask_16_9999-9999_monthly.txt ch4_mlo_surface-flask_16_9999-9999_monthly.txt ch4_mqa_surface-flask_16_9999-9999_monthly.txt ch4_sis_surface-flask_16_9999-9999_monthly.txt ch4_spo_surface-flask_16_9999-9999_monthly.txt	ALT482N016fz CFA519S016fz* CGO540S016fz CRI215N016fz* CYA766S016fz* ESP449N016fz* MAA767S016fz* MLO519N016fz MQA554S016fz* SIS660N016fz* SPO789S016fz	WMO X2004A
DMC	ch4_tll_surface-insitu_17_9999-9999_monthly.txt	TLL330S017iz*	WMO X2004A
DWD	ch4_gat_tower-insitu_19_6342-9999_monthly.txt ch4_hel_surface-insitu_19_9999-9999_monthly.txt ch4_hpb_tower-insitu_19_6132-9999_monthly.txt ch4_jue_tower-insitu_19_6121-9999_monthly.txt ch4_kit_tower-insitu_19_6201-9999_monthly.txt ch4_lin_tower-insitu_19_6099-9999_monthly.txt ch4_oxk_tower-insitu_19_6164-9999_monthly.txt ch4_ste_tower-insitu_19_6253-9999_monthly.txt ch4_toh_tower-insitu_19_6148-9999_monthly.txt	GAT653N019it* HEL654N019iz* HPB647N019it JUE650N019it* KIT649N019it* LIN652N019it* OXK650N019it* STE653N019it* TOH651N019it*	WMO X2004A
ECCC	ch4_alt_surface-insitu_20_9999-9999_monthly.txt ch4_bck_surface-insitu_20_9999-9999_monthly.txt ch4_bra_surface-insitu_20_9999-9999_monthly.txt ch4_cby_surface-insitu_20_9999-9999_monthly.txt ch4_cdl_surface-insitu_20_9999-9999_monthly.txt ch4_chl_surface-insitu_20_9999-9999_monthly.txt	ALT482N020iz* BCK462N020iz* BRA450N020iz* CBY469N020iz* CDL453N020iz* CHL458N020iz*	WMO X2004A

	ch4_chm_surface-insitu_20_9999-9999_monthly.txt ch4_cps_surface-insitu_20_9999-9999_monthly.txt ch4_egb_surface-insitu_20_9999-9999_monthly.txt ch4_esp_surface-insitu_20_9999-9999_monthly.txt ch4_est_surface-insitu_20_9999-9999_monthly.txt ch4_etl_surface-insitu_20_9999-9999_monthly.txt ch4_fsd_surface-insitu_20_9999-9999_monthly.txt ch4_inu_surface-insitu_20_9999-9999_monthly.txt ch4_llb_surface-insitu_20_9999-9999_monthly.txt ch4_wsa_surface-insitu_20_9999-9999_monthly.txt	CHM449N020iz* CPS449N020iz* EGB444N020iz* ESP449N020iz* EST451N020iz* ETL454N020iz* FSD449N020iz* INU468N020iz* LLB454N020iz* WSA443N020iz*	
Empa	ch4_jfj_surface-insitu_23_9999-9999_monthly.txt	JFJ646N023iz*	WMO X2004A
ENEA	ch4_lmp_surface-flask_24_9999-9999_monthly.txt ch4_mdn_surface-flask_24_9999-9999_monthly.txt	LMP635N024fz* MDN637N024fz*	WMO X2004
FMI	ch4_pal_surface-insitu_25_9999-9999_monthly.txt ch4_tik_surface-insitu_25_9999-9999_monthly.txt	PAL667N025iz* TIK271N025iz*	WMO X2004A
GERC	ch4_gsn_surface-insitu_52_9999-9999_monthly.txt	GSN233N052iz*	WMO X2004
IAFMS	ch4_cmn_surface-insitu_29_9999-9999_monthly.txt	CMN644N029iz*	WMO X2004
INSTAAR	ch4_sum_surface-insitu_34_9999-9999_monthly.txt	SUM672N034iz	
ISAC	ch4_cgr_surface-insitu_37_9999-9999_monthly.txt ch4_lmt_surface-insitu_37_9999-9999_monthly.txt	CGR637N037iz* LMT638N037iz	WMO X2004A
	ch4_eco_surface-insitu_37_9999-9999_monthly.txt	ECO640N037iz	
JMA	ch4_mnm_surface-insitu_1_9999-9999_monthly.txt ch4_ryo_surface-insitu_1_9999-9999_monthly.txt ch4_yon_surface-insitu_1_9999-9999_monthly.txt	MNM224N001iz* RYO239N001iz* YON224N001iz*	WMO X2004A
KMA	ch4_amy_surface-insitu_39_9999-9999_monthly.txt	AMY236N039iz*	WMO X2004 WMO X2004A
	ch4_gsn_surface-insitu_39_9999-9999_monthly.txt ch4_uld_surface-insitu_39_9999-9999_monthly.txt	GSN233N039iz* ULD237N039iz*	WMO X2004A
KMD	ch4_mkn_surface-insitu_40_9999-9999_monthly.txt	MKN100S040iz*	WMO X2004A
KSNU	ch4_isk_surface-remote_41_9999-9999_monthly.txt	ISK242N041rz	
Kyrgyzhydromet	ch4_cpa_surface-insitu_155_9999-9999_monthly.txt	CPA242N155iz*	WMO X2004A
LSCE	ch4_ams_surface-flask_45_9999-9999_monthly.txt ch4_bgu_surface-flask_45_9999-9999_monthly.txt ch4_lpo_surface-flask_45_9999-9999_monthly.txt ch4_pdm_surface-flask_45_9999-9999_monthly.txt ch4_puy_surface-flask_45_9999-9999_monthly.txt	AMS137S045fz* BGU641N045fz* LPO648N045fz PDM642N045fz PUY645N045fz*	NOAA 1983
	ch4_fkl_surface-flask_45_9999-9999_monthly.txt ch4_mhd_surface-flask_45_9999-9999_monthly.txt	FKL635N045fz MHD653N045fz	
METRI	ch4_gsn_surface-flask_55_9999-9999_monthly.txt	GSN233N055fz	SIO-97
MGO	ch4_ter_surface-flask_46_9999-9999_monthly.txt ch4_tik_surface-flask_46_9999-9999_monthly.txt	TER669N046fz* TIK271N046fz*	WMO X2004A
MRI	ch4_tkb_surface-insitu_48_9999-9999_monthly.txt	TKB236N048iz*	MRI
NIES	ch4_coi_surface-insitu_53_9999-9999_monthly.txt ch4_hat_surface-insitu_53_9999-9999_monthly.txt	COI243N053iz* HAT224N053iz*	NIES 94**
NILU	ch4_zep_surface-insitu_54_9999-9999_monthly.txt	ZEP678N054iz*	WMO X2004
NIWA	ch4_arh_surface-flask_57_9999-9999_monthly.txt ch4_bhd_surface-flask_57_9999-9999_monthly.txt ch4_bhd_surface-insitu_57_9999-9999_monthly.txt ch4_lau_surface-flask_57_9999-9999_monthly.txt	ARH777S057fz* BHD541S057fz* BHD541S057iz* LAU545S057fz*	WMO X2004A

	ch4_lau_surface-insitu_57_9999-9999_monthly.txt	LAU545S057iz*	
NOAA	ch4_abp_surface-flask_2_3001-9999_monthly.txt	ABP312S002f1*	WMO X2004A
	ch4_alt_surface-flask_2_3001-9999_monthly.txt	ALT482N002f1*	
	ch4_ams_surface-flask_2_3001-9999_monthly.txt	AMS137S002f1*	
	ch4_amy_surface-flask_2_3001-9999_monthly.txt	AMY236N002f1*	
	ch4_asc_surface-flask_2_3001-9999_monthly.txt	ASC107S002f1*	
	ch4_ask_surface-flask_2_3001-9999_monthly.txt	ASK123N002f1*	
	ch4_avi_surface-flask_2_3001-9999_monthly.txt	AVI417N002f1*	
	ch4_azr_surface-flask_2_3001-9999_monthly.txt	AZR638N002f1*	
	ch4_bal_surface-flask_2_3001-9999_monthly.txt	BAL655N002f1*	
	ch4_bhd_surface-flask_2_3001-9999_monthly.txt	BHD541S002f1*	
	ch4_bkt_surface-flask_2_3001-9999_monthly.txt	BKT500S002f1	
	ch4_bme_surface-flask_2_3001-9999_monthly.txt	BME432N002f1*	
	ch4_bmw_surface-flask_2_3001-9999_monthly.txt	BMW432N002f1*	
	ch4_brw_surface-flask_2_3001-9999_monthly.txt	BRW471N002f1*	
	ch4_brw_surface-insitu_2_3001-9999_monthly.txt	BRW471N002i1*	
	ch4_bsc_surface-flask_2_3001-9999_monthly.txt	BSC644N002f1*	
	ch4_cba_surface-flask_2_3001-9999_monthly.txt	CBA455N002f1*	
	ch4_cgo_surface-flask_2_3001-9999_monthly.txt	CGO540S002f1*	
	ch4_chr_surface-flask_2_3001-9999_monthly.txt	CHR501N002f1*	
	ch4_cmo_surface-flask_2_3001-9999_monthly.txt	CMO445N002f1*	
	ch4_cpt_surface-flask_2_3001-9999_monthly.txt	CPT134S002f1*	
	ch4_crz_surface-flask_2_3001-9999_monthly.txt	CRZ146S002f1*	
	ch4_drp_ship-flask_2_3001-9999_monthly.txt	DRP859S002f1*	
	ch4_eic_surface-flask_2_3001-9999_monthly.txt	EIC327S002f1*	
	ch4_gmi_surface-flask_2_3001-9999_monthly.txt	GMI513N002f1*	
	ch4_goz_surface-flask_2_3001-9999_monthly.txt	GOZ636N002f1*	
	ch4_hba_surface-flask_2_3001-9999_monthly.txt	HBA775S002f1*	
	ch4_hpb_surface-flask_2_3001-9999_monthly.txt	HPB647N002f1*	
	ch4_hun_surface-flask_2_3001-9999_monthly.txt	HUN646N002f1*	
	ch4_ice_surface-flask_2_3001-9999_monthly.txt	ICE663N002f1*	
	ch4_itn_surface-flask_2_3001-9999_monthly.txt	ITN435N002f1*	
	ch4_izo_surface-flask_2_3001-9999_monthly.txt	IZO128N002f1*	
	ch4_key_surface-flask_2_3001-9999_monthly.txt	KEY425N002f1*	
	ch4_kum_surface-flask_2_3001-9999_monthly.txt	KUM519N002f1*	
	ch4_kzd_surface-flask_2_3001-9999_monthly.txt	KZD244N002f1*	
	ch4_kzm_surface-flask_2_3001-9999_monthly.txt	KZM243N002f1*	
	ch4_llb_surface-flask_2_3001-9999_monthly.txt	LLB454N002f1	
	ch4_lln_surface-flask_2_3001-9999_monthly.txt	LLN223N002f1*	
	ch4_lmp_surface-flask_2_3001-9999_monthly.txt	LMP635N002f1*	
	ch4_mbc_surface-flask_2_3001-9999_monthly.txt	MBC476N002f1*	
	ch4_mex_surface-flask_2_3001-9999_monthly.txt	MEX418N002f1*	
	ch4_mhd_surface-flask_2_3001-9999_monthly.txt	MHD653N002f1*	
	ch4_mid_surface-flask_2_3001-9999_monthly.txt	MID528N002f1*	
	ch4_mkn_surface-flask_2_3001-9999_monthly.txt	MKN100S002f1*	
	ch4_mko_surface-insitu_2_3001-9999_monthly.txt	MKO519N002i1	
	ch4_mlo_surface-flask_2_3001-9999_monthly.txt	MLO519N002f1*	
	ch4_mlo_surface-insitu_2_3001-9999_monthly.txt	MLO519N002i1*	
	ch4_nat_surface-flask_2_3001-9999_monthly.txt	NAT306S002f1*	
	ch4_nmb_surface-flask_2_3001-9999_monthly.txt	NMB123S002f1*	
	ch4_nwr_surface-flask_2_3001-9999_monthly.txt	NWR440N002f1*	
	ch4_opw_surface-flask_2_3001-9999_monthly.txt	OPW448N002f1*	
	ch4_oxk_surface-flask_2_3001-9999_monthly.txt	OXK650N002f1*	
	ch4_pal_surface-flask_2_3001-9999_monthly.txt	PAL667N002f1*	
	ch4_poc_ship-flask_2_3001-3001_monthly.txt	POC800N002f1*	
	ch4_poc_ship-flask_2_3001-3002_monthly.txt	POC805N002f1*	

	ch4_poc_ship-flask_2_3001-3003_monthly.txt ch4_poc_ship-flask_2_3001-3004_monthly.txt ch4_poc_ship-flask_2_3001-3005_monthly.txt ch4_poc_ship-flask_2_3001-3006_monthly.txt ch4_poc_ship-flask_2_3001-3007_monthly.txt ch4_poc_ship-flask_2_3001-3012_monthly.txt ch4_poc_ship-flask_2_3001-3013_monthly.txt ch4_poc_ship-flask_2_3001-3014_monthly.txt ch4_poc_ship-flask_2_3001-3015_monthly.txt ch4_poc_ship-flask_2_3001-3016_monthly.txt ch4_poc_ship-flask_2_3001-3017_monthly.txt ch4_poc_ship-flask_2_3001-3018_monthly.txt ch4_psa_surface-flask_2_3001-9999_monthly.txt ch4_pta_surface-flask_2_3001-9999_monthly.txt ch4_rpb_surface-flask_2_3001-9999_monthly.txt ch4_scs_ship-flask_2_3001-3101_monthly.txt ch4_scs_ship-flask_2_3001-3102_monthly.txt ch4_scs_ship-flask_2_3001-3103_monthly.txt ch4_scs_ship-flask_2_3001-3104_monthly.txt ch4_scs_ship-flask_2_3001-3105_monthly.txt ch4_scs_ship-flask_2_3001-3106_monthly.txt ch4_scs_ship-flask_2_3001-3107_monthly.txt ch4_sdz_surface-flask_2_3001-9999_monthly.txt ch4_sey_surface-flask_2_3001-9999_monthly.txt ch4_sgp_surface-flask_2_3001-9999_monthly.txt ch4_shm_surface-flask_2_3001-9999_monthly.txt ch4_smo_surface-flask_2_3001-9999_monthly.txt ch4_spo_surface-flask_2_3001-9999_monthly.txt ch4_stm_surface-flask_2_3001-9999_monthly.txt ch4_sum_surface-flask_2_3001-9999_monthly.txt ch4_syo_surface-flask_2_3001-9999_monthly.txt ch4_tap_surface-flask_2_3001-9999_monthly.txt ch4_thd_surface-flask_2_3001-9999_monthly.txt ch4_tik_surface-flask_2_3001-9999_monthly.txt ch4_ush_surface-flask_2_3001-9999_monthly.txt ch4_uta_surface-flask_2_3001-9999_monthly.txt ch4_uum_surface-flask_2_3001-9999_monthly.txt ch4_wis_surface-flask_2_3001-9999_monthly.txt ch4_wkt_surface-flask_2_3001-9999_monthly.txt ch4_wlg_surface-flask_2_3001-9999_monthly.txt ch4_zep_surface-flask_2_3001-9999_monthly.txt	POC810N002f1* POC815N002f1* POC820N002f1* POC825N002f1* POC830N002f1* POC805S002f1* POC810S002f1* POC815S002f1* POC820S002f1* POC825S002f1* POC830S002f1* POC835S002f1* PSA764S002f1* PTA438N002f1* RPB413N002f1* SCS803N002f1* SCS806N002f1* SCS809N002f1* SCS812N002f1* SCS815N002f1* SCS818N002f1* SCS821N002f1* SDZ240N002f1* SEY104S002f1* SGP436N002f1* SHM452N002f1* SMO514S002f1* SPO789S002f1* STM666N002f1* SUM672N002f1* SYO769S002f1* TAP236N002f1* THD441N002f1 TIK271N002f1* USH354S002f1* UTA439N002f1* UUM244N002f1* WIS631N002f1* WKT431N002f1* WLG236N002f1* ZEP678N002f1*	
NPL	ch4_hfd_tower-insitu_154_6101-9999_monthly.txt	HFD650N154it*	WMO X2004A
RIVM	ch4_kmw_surface-insitu_63_9999-9999_monthly.txt	KMW653N063iz	NIST
RSE	ch4_prs_surface-insitu_64_9999-9999_monthly.txt	PRS645N064iz*	WMO X2004 ICOS
SAWS	ch4_cpt_surface-insitu_66_9999-1001_monthly.txt	CPT134S066iz*	WMO X2004 WMO X2004A
TU	ch4_syo_surface-insitu_70_9999-9999_monthly.txt	SYO769S070iz*	TU-1987
UBAA	ch4_snb_surface-insitu_72_9999-9999_monthly.txt	SNB647N072iz*	WMO X2004
UBAG	ch4_deu_surface-insitu_71_9999-9999_monthly.txt ch4_ngl_surface-insitu_71_9999-9999_monthly.txt ch4_zgt_surface-insitu_71_9999-9999_monthly.txt	DEU649N071iz* NGL653N071iz* ZGT654N071iz*	WMO X2004

	ch4_ssl_surface-insitu_71_9999-9999_monthly.txt ch4_wes_surface-insitu_71_9999-9999_monthly.txt ch4_zsf_surface-insitu_71_9999-9999_monthly.txt ch4_zug_surface-insitu_71_9999-9999_monthly.txt	SSL647N071iz* WES654N071iz* ZSF647N071iz* ZUG647N071iz*	WMO X2004A
UMLT	ch4_glh_surface-insitu_75_9999-9999_monthly.txt	GLH636N075iz	
UNIURB	ch4_cmn_surface-insitu_74_9999-9999_monthly.txt	CMN644N074iz*	WMO X2004A
UNIVBRIS	ch4_bsd_tower-insitu_77_6249-9999_monthly.txt ch4_rgl_tower-insitu_77_6091-9999_monthly.txt ch4_tac_tower-insitu_77_6186-9999_monthly.txt	BSD654N077it* RGL651N077it* TAC652N077it*	WMO X2004A
UoE	ch4_cvo_surface-insitu_151_9999-9999_monthly.txt	CVO116N151iz*	WMO X2004A
UYRK	ch4_cvo_surface-insitu_76_9999-9999_monthly.txt	CVO116N076iz*	WMO X2004A
VNMHA	ch4_pdi_surface-insitu_51_9999-9999_monthly.txt	PDI221N051iz*	WMO X2004A

* Stations with an asterisk are used for the calculation of the globally averaged mole fractions and related quantities. The site selection procedure is described in Appendix A.
** The NIES 94 CH_4 scale is approximately 5 ppb higher than WMO X2004A CH_4.

4. Nitrous Oxide (N_2O)

The Halocarbons and Other Atmospheric Trace Species (HATS) Group of NOAA/GML maintains a set of standards for N_2O (Hall *et al.*, 2001) and serves as a CCL for N_2O. The WMO X2006 scale (Hall *et al.*, 2007) was revised and updated to WMO X2006A in 2011 to deal with drifting in secondary standards, and is now designated as the primary scale for the GAW Programme. CCL compares its standards with those of other laboratories, including ECCC and the Australian Commonwealth Scientific and Industrial Research Organisation (CSIRO). The Karlsruhe Institute of Technology under the Institute for Meteorology and Climate Research (KIT/IMK-IFU) in Germany used to serve as the GAW WCC for N_2O until 2022.

The SIO-98 scale is approximately equivalent to the WMO X2006 scale, with an average difference of 0.01% over the range of 299 – 319 ppb. SIO-16 scale values can be converted to WMO X2006A via multiplication by a factor of 0.9983 (Prinn *et al.*, 2018). The WMO X2000 scale can be converted to WMO X2006 values using a multiplication factor of 0.999402 (Hall *et al.*, 2007).

Table B4. Status of the standard scales of N_2O.

Organi-zation	WDCGG Filename	Filename Code in Plate 3.1	Calibration Scale
AEMET	n2o_izo_surface-insitu_3_9999-9999_monthly.txt	IZO128N003iz*	WMO X2006A
AGAGE	n2o_cgo_surface-insitu_4_2021-9999_monthly.txt n2o_mhd_surface-insitu_4_2021-9999_monthly.txt n2o_rpb_surface-insitu_4_2021-9999_monthly.txt n2o_smo_surface-insitu_4_2021-9999_monthly.txt n2o_thd_surface-insitu_4_2021-9999_monthly.txt	CGO540S004ic* MHD653N004ic* RPB413N004ic* SMO514S004ic* THD441N004ic*	SIO-16
	n2o_adr_surface-insitu_4_2001-2004_monthly.txt n2o_cgo_surface-insitu_4_2001-2004_monthly.txt n2o_cgo_surface-insitu_4_2011-2015_monthly.txt n2o_cmo_surface-insitu_4_2001-2004_monthly.txt n2o_cmo_surface-insitu_4_2011-2015_monthly.txt n2o_mhd_surface-insitu_4_2011-2015_monthly.txt n2o_rpb_surface-insitu_4_2001-2004_monthly.txt n2o_rpb_surface-insitu_4_2011-2015_monthly.txt n2o_smo_surface-insitu_4_2001-2004_monthly.txt n2o_smo_surface-insitu_4_2011-2015_monthly.txt	ADR651N004ia* CGO540S004ia* CGO540S004ib* CMO445N004ia* CMO445N004ib* MHD653N004ib* RPB413N004ia* RPB413N004ib* SMO514S004ia* SMO514S004ib*	SIO-98

CSIRO	n2o_alt_surface-flask_16_9999-9999_monthly.txt n2o_cfa_surface-flask_16_9999-9999_monthly.txt n2o_cgo_surface-flask_16_9999-9999_monthly.txt n2o_cri_surface-flask_16_9999-9999_monthly.txt n2o_cya_surface-flask_16_9999-9999_monthly.txt n2o_esp_surface-flask_16_9999-9999_monthly.txt n2o_maa_surface-flask_16_9999-9999_monthly.txt n2o_mlo_surface-flask_16_9999-9999_monthly.txt n2o_mqa_surface-flask_16_9999-9999_monthly.txt n2o_sis_surface-flask_16_9999-9999_monthly.txt n2o_spo_surface-flask_16_9999-9999_monthly.txt	ALT482N016fz* CFA519S016fz* CGO540S016fz CRI215N016fz* CYA766S016fz* ESP449N016fz* MAA767S016fz* MLO519N016fz* MQA554S016fz* SIS660N016fz* SPO789S016fz	WMO X2006A
DWD	n2o_gat_tower-insitu_19_6342-9999_monthly.txt n2o_hel_surface-insitu_19_9999-9999_monthly.txt n2o_hpb_tower-insitu_19_6132-9999_monthly.txt n2o_jue_tower-insitu_19_6121-9999_monthly.txt n2o_kit_tower-insitu_19_6201-9999_monthly.txt n2o_lin_tower-insitu_19_6099-9999_monthly.txt n2o_oxk_tower-insitu_19_6164-9999_monthly.txt n2o_ste_tower-insitu_19_6253-9999_monthly.txt n2o_toh_tower-insitu_19_6148-9999_monthly.txt	GAT653N019it* HEL654N019iz* HPB647N019it* JUE650N019it* KIT649N019it* LIN652N019it* OXK650N019it* STE653N019it* TOH651N019it*	WMO X2006A
Empa	n2o_jfj_surface-insitu_23_9999-9999_monthly.txt	JFJ646N023iz*	WMO X2006A SIO-98
ENEA	n2o_lmp_surface-flask_24_9999-9999_monthly.txt	LMP635N024fz	WMO X2006
GERC	n2o_gsn_surface-insitu_52_9999-9999_monthly.txt	GSN233N052iz	WMO X2006
JMA	n2o_ryo_surface-insitu_1_9999-9999_monthly.txt	RYO239N001iz*	WMO X2006A
KMA	n2o_amy_surface-insitu_39_9999-9999_monthly.txt n2o_gsn_surface-insitu_39_9999-9999_monthly.txt	AMY236N039iz* GSN233N039iz*	WMO X2006A KRISS
	n2o_uld_surface-insitu_39_9999-9999_monthly.txt	ULD237N039iz*	WMO X2006A
METRI	n2o_gsn_surface-flask_55_9999-9999_monthly.txt	GSN233N055fz	WMO X1997
MRI	n2o_mmb_surface-insitu_48_9999-9999_monthly.txt	MMB243N048iz	
NAGOU	n2o_ngy_surface-insitu_49_9999-9999_monthly.txt	NGY235N049iz	
NIES	n2o_coi_surface-insitu_53_9999-9999_monthly.txt n2o_hat_surface-insitu_53_9999-9999_monthly.txt	COI243N053iz* HAT224N053iz*	NIES 96**
NILU	n2o_zep_surface-insitu_54_9999-9999_monthly.txt	ZEP678N054iz	
NIWA	n2o_arh_surface-flask_57_9999-9999_monthly.txt n2o_bhd_surface-flask_57_9999-9999_monthly.txt	ARH777S057fz* BHD541S057fz*	WMO X2006A
NOAA	n2o_brw_surface-insitu_2_3003-9999_monthly.txt n2o_mlo_surface-insitu_2_3003-9999_monthly.txt n2o_nwr_surface-insitu_2_3003-9999_monthly.txt n2o_smo_surface-insitu_2_3003-9999_monthly.txt n2o_spo_surface-insitu_2_3003-9999_monthly.txt	BRW471N002i3* MLO519N002i3* NWR440N002i3* SMO514S002i3* SPO789S002i3*	WMO X2006
	n2o_abp_surface-flask_2_3001-9999_monthly.txt n2o_alt_surface-flask_2_3001-9999_monthly.txt n2o_alt_surface-flask_2_3004-9999_monthly.txt n2o_alt_surface-flask_2_3005-9999_monthly.txt n2o_amy_surface-flask_2_3001-9999_monthly.txt n2o_asc_surface-flask_2_3001-9999_monthly.txt	ABP312S002f1* ALT482N002f1 ALT482N002f4* ALT482N002f5 AMY236N002f1* ASC107S002f1*	WMO X2006A

	n2o_ask_surface-flask_2_3001-9999_monthly.txt	ASK123N002f1*	
	n2o_azr_surface-flask_2_3001-9999_monthly.txt	AZR638N002f1*	
	n2o_bal_surface-flask_2_3001-9999_monthly.txt	BAL655N002f1*	
	n2o_bhd_surface-flask_2_3001-9999_monthly.txt	BHD541S002f1*	
	n2o_bkt_surface-flask_2_3001-9999_monthly.txt	BKT500S002f1*	
	n2o_bme_surface-flask_2_3001-9999_monthly.txt	BME432N002f1*	
	n2o_bmw_surface-flask_2_3001-9999_monthly.txt	BMW432N002f1*	
	n2o_brw_surface-flask_2_3001-9999_monthly.txt	BRW471N002f1*	
	n2o_brw_surface-flask_2_3004-9999_monthly.txt	BRW471N002f4*	
	n2o_brw_surface-flask_2_3005-9999_monthly.txt	BRW471N002f5	
	n2o_brw_surface-insitu_2_3002-9999_monthly.txt	BRW471N002i2*	
	n2o_bsc_surface-flask_2_3001-9999_monthly.txt	BSC644N002f1*	
	n2o_cba_surface-flask_2_3001-9999_monthly.txt	CBA455N002f1*	
	n2o_cgo_surface-flask_2_3001-9999_monthly.txt	CGO540S002f1*	
	n2o_cgo_surface-flask_2_3004-9999_monthly.txt	CGO540S002f4	
	n2o_cgo_surface-flask_2_3005-9999_monthly.txt	CGO540S002f5	
	n2o_chr_surface-flask_2_3001-9999_monthly.txt	CHR501N002f1*	
	n2o_cpt_surface-flask_2_3001-9999_monthly.txt	CPT134S002f1*	
	n2o_crz_surface-flask_2_3001-9999_monthly.txt	CRZ146S002f1*	
	n2o_drp_ship-flask_2_3001-9999_monthly.txt	DRP859S002f1*	
	n2o_eic_surface-flask_2_3001-9999_monthly.txt	EIC327S002f1*	
	n2o_gmi_surface-flask_2_3001-9999_monthly.txt	GMI513N002f1*	
	n2o_hba_surface-flask_2_3001-9999_monthly.txt	HBA775S002f1*	
	n2o_hfm_surface-flask_2_3005-9999_monthly.txt	HFM442N002f5*	
	n2o_hpb_surface-flask_2_3001-9999_monthly.txt	HPB647N002f1*	
	n2o_hun_surface-flask_2_3001-9999_monthly.txt	HUN646N002f1*	
	n2o_ice_surface-flask_2_3001-9999_monthly.txt	ICE663N002f1*	
	n2o_itn_surface-flask_2_3001-9999_monthly.txt	ITN435N002f1*	
	n2o_itn_surface-flask_2_3005-9999_monthly.txt	ITN435N002f5*	
	n2o_izo_surface-flask_2_3001-9999_monthly.txt	IZO128N002f1*	
	n2o_key_surface-flask_2_3001-9999_monthly.txt	KEY425N002f1*	
	n2o_kum_surface-flask_2_3001-9999_monthly.txt	KUM519N002f1*	
	n2o_kum_surface-flask_2_3005-9999_monthly.txt	KUM519N002f5*	
	n2o_kzd_surface-flask_2_3001-9999_monthly.txt	KZD244N002f1*	
	n2o_kzm_surface-flask_2_3001-9999_monthly.txt	KZM243N002f1*	
	n2o_lef_surface-flask_2_3005-9999_monthly.txt	LEF445N002f5*	
	n2o_llb_surface-flask_2_3001-9999_monthly.txt	LLB454N002f1*	
	n2o_lln_surface-flask_2_3001-9999_monthly.txt	LLN223N002f1*	
	n2o_lmp_surface-flask_2_3001-9999_monthly.txt	LMP635N002f1*	
	n2o_mex_surface-flask_2_3001-9999_monthly.txt	MEX418N002f1*	
	n2o_mhd_surface-flask_2_3001-9999_monthly.txt	MHD653N002f1*	
	n2o_mhd_surface-flask_2_3005-9999_monthly.txt	MHD653N002f5	
	n2o_mid_surface-flask_2_3001-9999_monthly.txt	MID528N002f1*	
	n2o_mkn_surface-flask_2_3001-9999_monthly.txt	MKN100S002f1*	
	n2o_mlo_surface-flask_2_3001-9999_monthly.txt	MLO519N002f1*	
	n2o_mlo_surface-flask_2_3004-9999_monthly.txt	MLO519N002f4*	
	n2o_mlo_surface-flask_2_3005-9999_monthly.txt	MLO519N002f5	
	n2o_mlo_surface-insitu_2_3002-9999_monthly.txt	MLO519N002i2*	
	n2o_nat_surface-flask_2_3001-9999_monthly.txt	NAT306S002f1*	
	n2o_nmb_surface-flask_2_3001-9999_monthly.txt	NMB123S002f1*	
	n2o_nwr_surface-flask_2_3001-9999_monthly.txt	NWR440N002f1*	
	n2o_nwr_surface-flask_2_3004-9999_monthly.txt	NWR440N002f4*	
	n2o_nwr_surface-flask_2_3005-9999_monthly.txt	NWR440N002f5	
	n2o_nwr_surface-insitu_2_3002-9999_monthly.txt	NWR440N002i2	
	n2o_oxk_surface-flask_2_3001-9999_monthly.txt	OXK650N002f1*	
	n2o_pal_surface-flask_2_3001-9999_monthly.txt	PAL667N002f1*	

	n2o_poc_ship-flask_2_3001-3001_monthly.txt	POC800N002f1*	
	n2o_poc_ship-flask_2_3001-3002_monthly.txt	POC805N002f1*	
	n2o_poc_ship-flask_2_3001-3003_monthly.txt	POC810N002f1*	
	n2o_poc_ship-flask_2_3001-3004_monthly.txt	POC815N002f1*	
	n2o_poc_ship-flask_2_3001-3005_monthly.txt	POC820N002f1*	
	n2o_poc_ship-flask_2_3001-3006_monthly.txt	POC825N002f1*	
	n2o_poc_ship-flask_2_3001-3007_monthly.txt	POC830N002f1*	
	n2o_poc_ship-flask_2_3001-3012_monthly.txt	POC805S002f1*	
	n2o_poc_ship-flask_2_3001-3013_monthly.txt	POC810S002f1*	
	n2o_poc_ship-flask_2_3001-3014_monthly.txt	POC815S002f1*	
	n2o_poc_ship-flask_2_3001-3015_monthly.txt	POC820S002f1*	
	n2o_poc_ship-flask_2_3001-3016_monthly.txt	POC825S002f1*	
	n2o_poc_ship-flask_2_3001-3017_monthly.txt	POC830S002f1*	
	n2o_psa_surface-flask_2_3001-9999_monthly.txt	PSA764S002f1*	
	n2o_psa_surface-flask_2_3005-9999_monthly.txt	PSA764S002f5	
	n2o_pta_surface-flask_2_3001-9999_monthly.txt	PTA438N002f1*	
	n2o_rpb_surface-flask_2_3001-9999_monthly.txt	RPB413N002f1*	
	n2o_sdz_surface-flask_2_3001-9999_monthly.txt	SDZ240N002f1*	
	n2o_sey_surface-flask_2_3001-9999_monthly.txt	SEY104S002f1*	
	n2o_sgp_surface-flask_2_3001-9999_monthly.txt	SGP436N002f1*	
	n2o_shm_surface-flask_2_3001-9999_monthly.txt	SHM452N002f1*	
	n2o_smo_surface-flask_2_3001-9999_monthly.txt	SMO514S002f1*	
	n2o_smo_surface-flask_2_3004-9999_monthly.txt	SMO514S002f4	
	n2o_smo_surface-flask_2_3005-9999_monthly.txt	SMO514S002f5	
	n2o_smo_surface-insitu_2_3002-9999_monthly.txt	SMO514S002i2	
	n2o_spo_surface-flask_2_3001-9999_monthly.txt	SPO789S002f1*	
	n2o_spo_surface-flask_2_3004-9999_monthly.txt	SPO789S002f4*	
	n2o_spo_surface-flask_2_3005-9999_monthly.txt	SPO789S002f5	
	n2o_spo_surface-insitu_2_3002-9999_monthly.txt	SPO789S002i2*	
	n2o_stm_surface-flask_2_3001-9999_monthly.txt	STM666N002f1*	
	n2o_sum_surface-flask_2_3001-9999_monthly.txt	SUM672N002f1*	
	n2o_sum_surface-flask_2_3005-9999_monthly.txt	SUM672N002f5	
	n2o_sum_surface-insitu_2_3002-9999_monthly.txt	SUM672N002i2	
	n2o_syo_surface-flask_2_3001-9999_monthly.txt	SYO769S002f1*	
	n2o_tap_surface-flask_2_3001-9999_monthly.txt	TAP236N002f1*	
	n2o_thd_surface-flask_2_3001-9999_monthly.txt	THD441N002f1	
	n2o_thd_surface-flask_2_3005-9999_monthly.txt	THD441N002f5	
	n2o_tik_surface-flask_2_3001-9999_monthly.txt	TIK271N002f1*	
	n2o_ush_surface-flask_2_3001-9999_monthly.txt	USH354S002f1*	
	n2o_ush_surface-flask_2_3005-9999_monthly.txt	USH354S002f5	
	n2o_uta_surface-flask_2_3001-9999_monthly.txt	UTA439N002f1*	
	n2o_uum_surface-flask_2_3001-9999_monthly.txt	UUM244N002f1*	
	n2o_wis_surface-flask_2_3001-9999_monthly.txt	WIS631N002f1*	
	n2o_wkt_surface-flask_2_3001-9999_monthly.txt	WKT431N002f1*	
	n2o_wlg_surface-flask_2_3001-9999_monthly.txt	WLG236N002f1*	
	n2o_zep_surface-flask_2_3001-9999_monthly.txt	ZEP678N002f1*	
NPL	n2o_hfd_tower-insitu_154_6101-9999_monthly.txt	HFD650N154it*	WMO X2006A
SAWS	n2o_cpt_surface-insitu_66_9999-1001_monthly.txt	CPT134S066iz*	NOAA
UBAG	n2o_ssl_surface-insitu_71_9999-9999_monthly.txt n2o_zsf_surface-insitu_71_9999-9999_monthly.txt	SSL647N071iz* ZSF647N071iz*	WMO X2006A
UNIURB	n2o_cmn_surface-insitu_74_9999-9999_monthly.txt	CMN644N074iz*	WMO X2006A
UNIVBRIS	n2o_bsd_tower-insitu_77_6249-9999_monthly.txt n2o_tac_tower-insitu_77_6186-9999_monthly.txt	BSD654N077it* TAC652N077it*	WMO X2006A

	n2o_bsd_surface-insitu_77_9999-9999_monthly.txt n2o_rgl_surface-insitu_77_9999-9999_monthly.txt n2o_tac_surface-insitu_77_9999-9999_monthly.txt	BSD654N077iz* RGL651N077iz* TAC652N077iz*	SIO-16
UoE	n2o_cvo_surface-insitu_151_9999-9999_monthly.txt	CVO116N151iz*	WMO X2006A

* Stations with an asterisk are used for the calculation of the globally averaged mole fractions and related quantities. The site selection procedure is described in Appendix A.

** NIES 96 N_2O scale is approximately 0.7 ppb lower than that of WMO X2006A in the range 325 to 326 ppb. (https://gml.noaa.gov/ccgg/wmorr/wmorr_results.php?rr=rr6&param=n2o)

5. Carbon Monoxide (CO)

NOAA/GML is the WMO/GAW CCL for carbon monoxide. Due to lack of stability of CO in high pressure cylinders, the CO scale has historically been defined by repeated sets of gravimetric standards made in 1996/1997, 1999/2000, 2006 and 2011. The CCL makes revisions in the CO scale whenever new gravimetric standard sets indicate a significant drift in the scale. Scale revisions are indicated with date codes (WMO X2000, WMO X2004, WMO X2014) with the most recent made in December 2015 being WMO X2014A (WMO, 2020).

Empa serves as the WCC under GAW based on its secondary standards calibrated against the standard at NOAA/GML designated as the Primary Standard for GAW. Empa, as WCC for CO, has developed an audit system for CO measurements at GAW stations.

A small fraction of the data is reported in units of $\mu g/m^3$ or mg/m^3. In WDCGG analysis, these units are converted to ppb using the following formulas:

$$X_p\,[\text{ppb}] = (R \times T / M / P_0) \times 10 \times X_g\,[\mu g/m^3]$$

and

$$X_p\,[\text{ppb}] = (R \times T / M / P_0) \times 10^4 \times X_g\,[mg/m^3],$$

where

R is the molar gas constant (8.31451 [J/K/mol]),

T is the reported temperature for conversion (293.15 [K] or 298.15 [K]),

M is the molecular weight of CO (28.0101) and

P_0 is the standard pressure (1013.25 [hPa]).

It is highly desirable to report CO concentration data in mole fractions (mostly in ppb) traceable to the WMO Mole Fraction Scale.

Table B5. Status of CO standard scales.

Organi-zation	WDCGG Filename	Filename Code in Plate 5.1	Calibration Scale / Units except for using ppb	Audit Empa-WCC
AEMET	co_izo_surface-insitu_3_9999-9999_monthly.txt	IZO128N003iz*	WMO X2014A	00, 04, 09, 13, 19, 23
AGAGE	co_mhd_surface-insitu_4_2021-9999_monthly.txt	MHD653N004ic*	WMO X2014A	
	co_cgo_surface-insitu_4_2021-9999_monthly.txt	CGO540S004ic	CSIRO-2020	
ARSO	co_kvv_surface-insitu_8_9999-9999_monthly.txt	KVV646N008iz*		
BAS	co_hba_surface-insitu_9_9999-9999_monthly.txt	HBA775S009iz	WMO X2014A	
BMKG	co_bkt_surface-insitu_10_9999-9999_monthly.txt	BKT500S010iz	WMO X2000 WMO X2014A	01, 04, 07, 08, 11, 14, 19
CHMI	co_kos_surface-insitu_12_9999-9999_monthly.txt	KOS649N012iz	$\mu g/m^3$-20°C	
CSIRO	co_alt_surface-flask_16_9999-9999_monthly.txt co_cfa_surface-flask_16_9999-9999_monthly.txt co_cgo_surface-flask_16_9999-9999_monthly.txt co_cri_surface-flask_16_9999-9999_monthly.txt co_cya_surface-flask_16_9999-9999_monthly.txt co_esp_surface-flask_16_9999-9999_monthly.txt co_maa_surface-flask_16_9999-9999_monthly.txt	ALT482N016fz* CFA519S016fz* CGO540S016fz* CRI215N016fz* CYA766S016fz* ESP449N016fz* MAA767S016fz*	CSIRO-2020	Cape Grim: 02, 16, 23

	co_mlo_surface-flask_16_9999-9999_monthly.txt co_mqa_surface-flask_16_9999-9999_monthly.txt co_sis_surface-flask_16_9999-9999_monthly.txt co_spo_surface-flask_16_9999-9999_monthly.txt	MLO519N016fz MQA554S016fz* SIS660N016fz* SPO789S016fz*		
DMC	co_tll_surface-insitu_17_9999-9999_monthly.txt	TLL330S017iz*	WMO X2014A	
DWD	co_hpb_surface-insitu_19_9999-9999_monthly.txt	HPB647N019iz*	WMO X2004	97, 06, 11, 20
	co_gat_tower-insitu_19_6342-9999_monthly.txt co_hel_surface-insitu_19_9999-9999_monthly.txt co_hpb_tower-insitu_19_6132-9999_monthly.txt co_jue_tower-insitu_19_6121-9999_monthly.txt co_kit_tower-insitu_19_6201-9999_monthly.txt co_lin_tower-insitu_19_6099-9999_monthly.txt co_oxk_tower-insitu_19_6164-9999_monthly.txt co_ste_tower-insitu_19_6253-9999_monthly.txt co_toh_tower-insitu_19_6148-9999_monthly.txt	GAT653N019it* HEL654N019iz* HPB647N019it* JUE650N019it* KIT649N019it* LIN652N019it* OXK650N019it* STE653N019it* TOH651N019it*	WMO X2014A	
ECCC	co_alt_surface-insitu_20_9999-9999_monthly.txt co_cdl_surface-insitu_20_9999-9999_monthly.txt co_chl_surface-insitu_20_9999-9999_monthly.txt co_chm_surface-insitu_20_9999-9999_monthly.txt co_egb_surface-insitu_20_9999-9999_monthly.txt co_esp_surface-insitu_20_9999-9999_monthly.txt co_etl_surface-insitu_20_9999-9999_monthly.txt co_fsd_surface-insitu_20_9999-9999_monthly.txt co_llb_surface-insitu_20_9999-9999_monthly.txt co_wsa_surface-insitu_20_9999-9999_monthly.txt	ALT482N020iz CDL453N020iz* CHL458N020iz CHM449N020iz* EGB444N020iz* ESP449N020iz* ETL454N020iz* FSD449N020iz* LLB454N020iz* WSA443N020iz*	WMO X2014A	Alert: 04
Empa	co_jfj_surface-insitu_23_9999-9999_monthly.txt	JFJ646N023iz*	NIST SRM 1677c NMI PRM AC11 NIST SRM 2612a NPL PRGM in synth. Air WMO X2000 WMO X2004 WMO X2014A	99, 06, 15, 21
	co_pay_surface-insitu_23_9999-9999_monthly.txt co_rig_surface-insitu_23_9999-9999_monthly.txt	PAY646N023iz* RIG647N023iz*	NMI PRM AC11 NIST SRM 1677c NIST SRM 2612a NPL PRGM 221708SG in synth. Air NPL PRGM NG677 in synth. Air NPL PRGM 2851 in synth. Air	
INRNE	co_beo_surface-insitu_33_9999-9999_monthly.txt	BEO642N033iz*		
ISAC	co_cmn_surface-insitu_37_9999-9999_monthly.txt	CMN644N037iz	WMO X2004 WMO X2014A	12, 18, 23

	co_cgr_surface-insitu_37_9999-9999_monthly.txt co_lmt_surface-insitu_37_9999-9999_monthly.txt	CGR637N037iz* LMT638N037iz*	WMO X2014A	
	co_eco_surface-insitu_37_9999-9999_monthly.txt	ECO640N037iz		
JMA	co_mnm_surface-insitu_1_9999-9999_monthly.txt co_ryo_surface-insitu_1_9999-9999_monthly.txt co_yon_surface-insitu_1_9999-9999_monthly.txt	MNM224N001iz* RYO239N001iz* YON224N001iz*	WMO X2014A	Ryori: 05
KMA	co_amy_surface-insitu_39_9999-9999_monthly.txt	AMY236N039iz	KRISS	17, 22
	co_gsn_surface-insitu_39_9999-9999_monthly.txt	GSN233N039iz*	WMO X2014A KRISS	17, 22
KMD	co_mkn_surface-insitu_40_9999-9999_monthly.txt	MKN100S040iz*	WMO X2000 WMO X2014A	05, 06, 08, 10, 15, 19, 21
Kyrgyzhydromet	co_cpa_surface-insitu_155_9999-9999_monthly.txt	CPA242N155iz*	WMO X2014A	23
LA	co_pdm_surface-insitu_43_9999-9999_monthly.txt	PDM642N043iz		
LAMP	co_puy_surface-insitu_44_9999-9999_monthly.txt	PUY645N044iz		16
LSCE	co_ams_surface-insitu_45_9999-9999_monthly.txt	AMS137S045iz		08
NIWA	co_arh_surface-flask_57_9999-9999_monthly.txt co_bhd_surface-flask_57_9999-9999_monthly.txt co_lau_surface-flask_57_9999-9999_monthly.txt co_lau_surface-insitu_57_9999-9999_monthly.txt	ARH777S057fz* BHD541S057fz* LAU545S057fz* LAU545S057iz*	WMO X2014A	10, 16
NOAA	co_abp_surface-flask_2_3001-9999_monthly.txt co_alt_surface-flask_2_3001-9999_monthly.txt co_amy_surface-flask_2_3001-9999_monthly.txt co_asc_surface-flask_2_3001-9999_monthly.txt co_ask_surface-flask_2_3001-9999_monthly.txt co_azr_surface-flask_2_3001-9999_monthly.txt co_bal_surface-flask_2_3001-9999_monthly.txt co_bhd_surface-flask_2_3001-9999_monthly.txt co_bkt_surface-flask_2_3001-9999_monthly.txt co_bme_surface-flask_2_3001-9999_monthly.txt co_bmw_surface-flask_2_3001-9999_monthly.txt co_brw_surface-flask_2_3001-9999_monthly.txt co_bsc_surface-flask_2_3001-9999_monthly.txt co_cba_surface-flask_2_3001-9999_monthly.txt co_cgo_surface-flask_2_3001-9999_monthly.txt co_chr_surface-flask_2_3001-9999_monthly.txt co_cmo_surface-flask_2_3001-9999_monthly.txt co_cpt_surface-flask_2_3001-9999_monthly.txt co_crz_surface-flask_2_3001-9999_monthly.txt co_drp_ship-flask_2_3001-9999_monthly.txt co_eic_surface-flask_2_3001-9999_monthly.txt co_gmi_surface-flask_2_3001-9999_monthly.txt co_goz_surface-flask_2_3001-9999_monthly.txt co_hba_surface-flask_2_3001-9999_monthly.txt co_hpb_surface-flask_2_3001-9999_monthly.txt co_hun_surface-flask_2_3001-9999_monthly.txt co_ice_surface-flask_2_3001-9999_monthly.txt co_itn_surface-flask_2_3001-9999_monthly.txt co_izo_surface-flask_2_3001-9999_monthly.txt co_key_surface-flask_2_3001-9999_monthly.txt co_kum_surface-flask_2_3001-9999_monthly.txt	ABP312S002f1* ALT482N002f1 AMY236N002f1* ASC107S002f1* ASK123N002f1* AZR638N002f1* BAL655N002f1* BHD541S002f1 BKT500S002f1* BME432N002f1* BMW432N002f1* BRW471N002f1* BSC644N002f1 CBA455N002f1* CGO540S002f1 CHR501N002f1* CMO445N002f1* CPT134S002f1* CRZ146S002f1* DRP859S002f1* EIC327S002f1* GMI513N002f1* GOZ636N002f1* HBA775S002f1* HPB647N002f1* HUN646N002f1* ICE663N002f1* ITN435N002f1* IZO128N002f1* KEY425N002f1* KUM519N002f1*	WMO X2014A	

	co_kzd_surface-flask_2_3001-9999_monthly.txt	KZD244N002f1*		
	co_kzm_surface-flask_2_3001-9999_monthly.txt	KZM243N002f1*		
	co_llb_surface-flask_2_3001-9999_monthly.txt	LLB454N002f1		
	co_lln_surface-flask_2_3001-9999_monthly.txt	LLN223N002f1*		
	co_lmp_surface-flask_2_3001-9999_monthly.txt	LMP635N002f1*		
	co_mbc_surface-flask_2_3001-9999_monthly.txt	MBC476N002f1*		
	co_mex_surface-flask_2_3001-9999_monthly.txt	MEX418N002f1*		
	co_mhd_surface-flask_2_3001-9999_monthly.txt	MHD653N002f1*		
	co_mid_surface-flask_2_3001-9999_monthly.txt	MID528N002f1*		
	co_mkn_surface-flask_2_3001-9999_monthly.txt	MKN100S002f1*		
	co_mlo_surface-flask_2_3001-9999_monthly.txt	MLO519N002f1*		
	co_nat_surface-flask_2_3001-9999_monthly.txt	NAT306S002f1*		
	co_nmb_surface-flask_2_3001-9999_monthly.txt	NMB123S002f1*		
	co_nwr_surface-flask_2_3001-9999_monthly.txt	NWR440N002f1*		
	co_oxk_surface-flask_2_3001-9999_monthly.txt	OXK650N002f1*		
	co_pal_surface-flask_2_3001-9999_monthly.txt	PAL667N002f1*		
	co_poc_ship-flask_2_3001-3001_monthly.txt	POC800N002f1*		
	co_poc_ship-flask_2_3001-3002_monthly.txt	POC805N002f1*		
	co_poc_ship-flask_2_3001-3003_monthly.txt	POC810N002f1*		
	co_poc_ship-flask_2_3001-3004_monthly.txt	POC815N002f1*		
	co_poc_ship-flask_2_3001-3005_monthly.txt	POC820N002f1*		
	co_poc_ship-flask_2_3001-3006_monthly.txt	POC825N002f1*		
	co_poc_ship-flask_2_3001-3007_monthly.txt	POC830N002f1*		
	co_poc_ship-flask_2_3001-3012_monthly.txt	POC805S002f1*		
	co_poc_ship-flask_2_3001-3013_monthly.txt	POC810S002f1*		
	co_poc_ship-flask_2_3001-3014_monthly.txt	POC815S002f1*		
	co_poc_ship-flask_2_3001-3015_monthly.txt	POC820S002f1*		
	co_poc_ship-flask_2_3001-3016_monthly.txt	POC825S002f1*		
	co_poc_ship-flask_2_3001-3017_monthly.txt	POC830S002f1*		
	co_psa_surface-flask_2_3001-9999_monthly.txt	PSA764S002f1*		
	co_pta_surface-flask_2_3001-9999_monthly.txt	PTA438N002f1*		
	co_rpb_surface-flask_2_3001-9999_monthly.txt	RPB413N002f1*		
	co_scs_ship-flask_2_3001-3101_monthly.txt	SCS803N002f1*		
	co_scs_ship-flask_2_3001-3102_monthly.txt	SCS806N002f1*		
	co_scs_ship-flask_2_3001-3103_monthly.txt	SCS809N002f1*		
	co_scs_ship-flask_2_3001-3104_monthly.txt	SCS812N002f1*		
	co_scs_ship-flask_2_3001-3105_monthly.txt	SCS815N002f1*		
	co_scs_ship-flask_2_3001-3106_monthly.txt	SCS818N002f1*		
	co_scs_ship-flask_2_3001-3107_monthly.txt	SCS821N002f1		
	co_sdz_surface-flask_2_3001-9999_monthly.txt	SDZ240N002f1*		
	co_sey_surface-flask_2_3001-9999_monthly.txt	SEY104S002f1*		
	co_sgp_surface-flask_2_3001-9999_monthly.txt	SGP436N002f1*		
	co_shm_surface-flask_2_3001-9999_monthly.txt	SHM452N002f1*		
	co_smo_surface-flask_2_3001-9999_monthly.txt	SMO514S002f1*		
	co_spo_surface-flask_2_3001-9999_monthly.txt	SPO789S002f1		
	co_stm_surface-flask_2_3001-9999_monthly.txt	STM666N002f1*		
	co_sum_surface-flask_2_3001-9999_monthly.txt	SUM672N002f1*		
	co_syo_surface-flask_2_3001-9999_monthly.txt	SYO769S002f1*		
	co_tap_surface-flask_2_3001-9999_monthly.txt	TAP236N002f1		
	co_thd_surface-flask_2_3001-9999_monthly.txt	THD441N002f1*		
	co_tik_surface-flask_2_3001-9999_monthly.txt	TIK271N002f1*		
	co_ush_surface-flask_2_3001-9999_monthly.txt	USH354S002f1*		
	co_uta_surface-flask_2_3001-9999_monthly.txt	UTA439N002f1*		
	co_uum_surface-flask_2_3001-9999_monthly.txt	UUM244N002f1*		
	co_wis_surface-flask_2_3001-9999_monthly.txt	WIS631N002f1*		
	co_wkt_surface-flask_2_3001-9999_monthly.txt	WKT431N002f1*		

	co_wlg_surface-flask_2_3001-9999_monthly.txt co_zep_surface-flask_2_3001-9999_monthly.txt	WLG236N002f1* ZEP678N002f1*		
NPL	co_hfd_tower-insitu_154_6101-9999_monthly.txt	HFD650N154it*	WMO X2014A	
ONM	co_ask_surface-insitu_59_9999-9999_monthly.txt	ASK123N059iz		07, 15
PolyU	co_hkg_surface-insitu_61_9999-9999_monthly.txt	HKG222N061iz		
RIVM	co_kmw_surface-insitu_63_9999-9999_monthly.txt	KMW653N063iz*		
	co_ktb_surface-insitu_63_9999-9999_monthly.txt	KTB653N063iz	μg/m^3-25°C	
SAWS	co_cpt_surface-insitu_66_9999-1001_monthly.txt	CPT134S066iz*	WMO X2004 WMO X2014A CPT	98, 02, 06, 11, 15, 21
SMNA	co_ush_surface-insitu_69_9999-9999_monthly.txt	USH354S069iz	WMO X1988 WMO X2000	98, 03, 08, 16, 19
UBAA	co_snb_surface-insitu_72_9999-9999_monthly.txt	SNB647N072iz*	NIST	98, 20
UBAG	co_zsf_surface-insitu_71_9999-9999_monthly.txt	ZSF647N071iz*	WMO X2000 WMO X2004 WMO X2014 WMO X2014A	01, 06, 11, 20
	co_ssl_surface-insitu_71_9999-9999_monthly.txt	SSL647N071iz*	WMO X2014	
	co_ngl_surface-insitu_71_9999-9999_monthly.txt	NGL653N071iz*		
	co_zug_surface-insitu_71_9999-9999_monthly.txt	ZUG647N071iz*	mg/m^3-25°C	97, 01
UMLT	co_glh_surface-insitu_75_9999-9999_monthly.txt	GLH636N075iz*		
UNIURB	co_cmn_surface-insitu_74_9999-9999_monthly.txt	CMN644N074iz*	WMO X2014	12, 18, 23
UNIVBRIS	co_bsd_tower-insitu_77_6249-9999_monthly.txt co_tac_surface-insitu_77_9999-9999_monthly.txt co_tac_tower-insitu_77_6186-9999_monthly.txt	BSD654N077iz* TAC652N077iz* TAC652N077it*	WMO X2014A	
UoE	co_cvo_surface-insitu_151_9999-9999_monthly.txt	CVO116N151iz*	WMO X2014A	
UYRK	co_cvo_surface-insitu_76_9999-9999_monthly.txt	CVO116N076iz*	WMO X2014A	12
VNMHA	co_pdi_surface-insitu_51_9999-9999_monthly.txt	PDI221N051iz	WMO X2014A	22

* Stations with an asterisk are used for the calculation of the globally averaged mole fractions and related quantities. The site selection procedure is described in Appendix A.

6. Sulfur Hexafluoride (SF_6)

NOAA/GML is the WMO/GAW CCL for sulfur hexafluoride. The most current WMO Mole Fraction Scale is the WMO X2014 version defined using 17 primary standards over the 2 – 20 ppt range, with calibration performed using GC-ECD (Hall *et al.*, 2011). The Korea Meteorological Administration (KMA), assisted by the Korea Research Institute of Standards and Science (KRISS), serves as a WCC for SF_6. The first SF_6 intercomparison experiment was implemented by KMA WCC-SF_6 from 2016 to 2017 (Lee *et al.*, 2017; WMO, 2018).

SIO has developed and maintained a suite of standards for halogenated compounds at ppt levels since the 1990s (Weiss *et al.*, 1981; Prinn *et al.*, 2000). The SF_6 conversion factor between the WMO X2014 and SIO-05 calibration scales is reported as WMO X2014/SIO-05 = 1.0049 ± 0.0029 (Prinn *et al.*, 2018).

Table B6 summarizes the SF_6 standard scales used by stations contributing to the WDCGG.

Table B6. Status of SF_6 standard scales.

Organi-zation	WDCGG Filename	Filename Code in Plate 4.2	Calibration Scale
AEMET	sf6_izo_surface-insitu_3_9999-9999_monthly.txt	IZO128N003iz	WMO X2014
AGAGE	sf6_cgo_surface-insitu_4_2021-9999_monthly.txt sf6_cgo_surface-insitu_4_2023-9999_monthly.txt sf6_cmn_surface-insitu_4_2023-9999_monthly.txt sf6_gsn_surface-insitu_4_2023-9999_monthly.txt sf6_jfj_surface-insitu_4_2023-9999_monthly.txt sf6_mhd_surface-insitu_4_2023-9999_monthly.txt sf6_rpb_surface-insitu_4_2023-9999_monthly.txt sf6_smo_surface-insitu_4_2023-9999_monthly.txt sf6_tac_surface-insitu_4_2023-9999_monthly.txt sf6_thd_surface-insitu_4_2023-9999_monthly.txt sf6_tob_surface-insitu_4_2023-9999_monthly.txt sf6_zep_surface-insitu_4_2023-9999_monthly.txt	CGO540S004ic CGO540S004ie CMN644N004ie GSN233N004ie JFJ646N004ie MHD653N004ie RPB413N004ie SMO514S004ie TAC652N004ie THD441N004ie TOB650N004ie ZEP678N004ie	SIO-05
Empa	sf6_jfj_surface-insitu_23_9999-9999_monthly.txt	JFJ646N023iz	SIO-05
ENEA	sf6_lmp_surface-flask_24_9999-9999_monthly.txt	LMP635N024fz	
KMA	sf6_amy_surface-insitu_39_9999-9999_monthly.txt sf6_gsn_surface-insitu_39_9999-9999_monthly.txt sf6_uld_surface-insitu_39_9999-9999_monthly.txt	AMY236N039iz GSN233N039iz ULD237N039iz	WMO X2014
NOAA	sf6_abp_surface-flask_2_3001-9999_monthly.txt sf6_alt_surface-flask_2_3001-9999_monthly.txt sf6_alt_surface-flask_2_3005-9999_monthly.txt sf6_amy_surface-flask_2_3001-9999_monthly.txt sf6_asc_surface-flask_2_3001-9999_monthly.txt sf6_ask_surface-flask_2_3001-9999_monthly.txt sf6_azr_surface-flask_2_3001-9999_monthly.txt sf6_bal_surface-flask_2_3001-9999_monthly.txt sf6_bhd_surface-flask_2_3001-9999_monthly.txt sf6_bkt_surface-flask_2_3001-9999_monthly.txt sf6_bme_surface-flask_2_3001-9999_monthly.txt sf6_bmw_surface-flask_2_3001-9999_monthly.txt sf6_brw_surface-flask_2_3001-9999_monthly.txt sf6_brw_surface-flask_2_3005-9999_monthly.txt sf6_brw_surface-insitu_2_3002-9999_monthly.txt sf6_bsc_surface-flask_2_3001-9999_monthly.txt sf6_cba_surface-flask_2_3001-9999_monthly.txt sf6_cgo_surface-flask_2_3001-9999_monthly.txt sf6_cgo_surface-flask_2_3005-9999_monthly.txt sf6_chr_surface-flask_2_3001-9999_monthly.txt sf6_cpt_surface-flask_2_3001-9999_monthly.txt sf6_crz_surface-flask_2_3001-9999_monthly.txt sf6_drp_ship-flask_2_3001-9999_monthly.txt sf6_eic_surface-flask_2_3001-9999_monthly.txt sf6_gmi_surface-flask_2_3001-9999_monthly.txt sf6_hba_surface-flask_2_3001-9999_monthly.txt sf6_hfm_surface-flask_2_3005-9999_monthly.txt sf6_hpb_surface-flask_2_3001-9999_monthly.txt sf6_hun_surface-flask_2_3001-9999_monthly.txt sf6_ice_surface-flask_2_3001-9999_monthly.txt sf6_itn_surface-flask_2_3001-9999_monthly.txt sf6_itn_surface-flask_2_3005-9999_monthly.txt sf6_izo_surface-flask_2_3001-9999_monthly.txt sf6_key_surface-flask_2_3001-9999_monthly.txt	ABP312S002f1 ALT482N002f1 ALT482N002f5 AMY236N002f1 ASC107S002f1 ASK123N002f1 AZR638N002f1 BAL655N002f1 BHD541S002f1 BKT500S002f1 BME432N002f1 BMW432N002f1 BRW471N002f1 BRW471N002f5 BRW471N002i2 BSC644N002f1 CBA455N002f1 CGO540S002f1 CGO540S002f5 CHR501N002f1 CPT134S002f1 CRZ146S002f1 DRP859S002f1 EIC327S002f1 GMI513N002f1 HBA775S002f1 HFM442N002f5 HPB647N002f1 HUN646N002f1 ICE663N002f1 ITN435N002f1 ITN435N002f5 IZO128N002f1 KEY425N002f1	WMO X2014

	sf6_kum_surface-flask_2_3001-9999_monthly.txt	KUM519N002f1	
	sf6_kum_surface-flask_2_3005-9999_monthly.txt	KUM519N002f5	
	sf6_kzd_surface-flask_2_3001-9999_monthly.txt	KZD244N002f1	
	sf6_kzm_surface-flask_2_3001-9999_monthly.txt	KZM243N002f1	
	sf6_lef_surface-flask_2_3005-9999_monthly.txt	LEF445N002f5	
	sf6_llb_surface-flask_2_3001-9999_monthly.txt	LLB454N002f1	
	sf6_lln_surface-flask_2_3001-9999_monthly.txt	LLN223N002f1	
	sf6_lmp_surface-flask_2_3001-9999_monthly.txt	LMP635N002f1	
	sf6_mex_surface-flask_2_3001-9999_monthly.txt	MEX418N002f1	
	sf6_mhd_surface-flask_2_3001-9999_monthly.txt	MHD653N002f1	
	sf6_mhd_surface-flask_2_3005-9999_monthly.txt	MHD653N002f5	
	sf6_mid_surface-flask_2_3001-9999_monthly.txt	MID528N002f1	
	sf6_mkn_surface-flask_2_3001-9999_monthly.txt	MKN100S002f1	
	sf6_mlo_surface-flask_2_3001-9999_monthly.txt	MLO519N002f1	
	sf6_mlo_surface-flask_2_3005-9999_monthly.txt	MLO519N002f5	
	sf6_mlo_surface-insitu_2_3002-9999_monthly.txt	MLO519N002i2	
	sf6_nat_surface-flask_2_3001-9999_monthly.txt	NAT306S002f1	
	sf6_nmb_surface-flask_2_3001-9999_monthly.txt	NMB123S002f1	
	sf6_nwr_surface-flask_2_3001-9999_monthly.txt	NWR440N002f1	
	sf6_nwr_surface-flask_2_3005-9999_monthly.txt	NWR440N002f5	
	sf6_nwr_surface-insitu_2_3002-9999_monthly.txt	NWR440N002i2	
	sf6_oxk_surface-flask_2_3001-9999_monthly.txt	OXK650N002f1	
	sf6_pal_surface-flask_2_3001-9999_monthly.txt	PAL667N002f1	
	sf6_poc_ship-flask_2_3001-3001_monthly.txt	POC800N002f1	
	sf6_poc_ship-flask_2_3001-3002_monthly.txt	POC805N002f1	
	sf6_poc_ship-flask_2_3001-3003_monthly.txt	POC810N002f1	
	sf6_poc_ship-flask_2_3001-3004_monthly.txt	POC815N002f1	
	sf6_poc_ship-flask_2_3001-3005_monthly.txt	POC820N002f1	
	sf6_poc_ship-flask_2_3001-3006_monthly.txt	POC825N002f1	
	sf6_poc_ship-flask_2_3001-3007_monthly.txt	POC830N002f1	
	sf6_poc_ship-flask_2_3001-3012_monthly.txt	POC805S002f1	
	sf6_poc_ship-flask_2_3001-3013_monthly.txt	POC810S002f1	
	sf6_poc_ship-flask_2_3001-3014_monthly.txt	POC815S002f1	
	sf6_poc_ship-flask_2_3001-3015_monthly.txt	POC820S002f1	
	sf6_poc_ship-flask_2_3001-3016_monthly.txt	POC825S002f1	
	sf6_poc_ship-flask_2_3001-3017_monthly.txt	POC830S002f1	
	sf6_psa_surface-flask_2_3001-9999_monthly.txt	PSA764S002f1	
	sf6_psa_surface-flask_2_3005-9999_monthly.txt	PSA764S002f5	
	sf6_pta_surface-flask_2_3001-9999_monthly.txt	PTA438N002f1	
	sf6_rpb_surface-flask_2_3001-9999_monthly.txt	RPB413N002f1	
	sf6_sdz_surface-flask_2_3001-9999_monthly.txt	SDZ240N002f1	
	sf6_sey_surface-flask_2_3001-9999_monthly.txt	SEY104S002f1	
	sf6_sgp_surface-flask_2_3001-9999_monthly.txt	SGP436N002f1	
	sf6_shm_surface-flask_2_3001-9999_monthly.txt	SHM452N002f1	
	sf6_smo_surface-flask_2_3001-9999_monthly.txt	SMO514S002f1	
	sf6_smo_surface-flask_2_3005-9999_monthly.txt	SMO514S002f5	
	sf6_smo_surface-insitu_2_3002-9999_monthly.txt	SMO514S002i2	
	sf6_spo_surface-flask_2_3001-9999_monthly.txt	SPO789S002f1	
	sf6_spo_surface-flask_2_3005-9999_monthly.txt	SPO789S002f5	
	sf6_spo_surface-insitu_2_3002-9999_monthly.txt	SPO789S002i2	
	sf6_stm_surface-flask_2_3001-9999_monthly.txt	STM666N002f1	
	sf6_sum_surface-flask_2_3001-9999_monthly.txt	SUM672N002f1	
	sf6_sum_surface-flask_2_3005-9999_monthly.txt	SUM672N002f5	
	sf6_sum_surface-insitu_2_3002-9999_monthly.txt	SUM672N002i2	
	sf6_syo_surface-flask_2_3001-9999_monthly.txt	SYO769S002f1	
	sf6_tap_surface-flask_2_3001-9999_monthly.txt	TAP236N002f1	

	sf6_thd_surface-flask_2_3001-9999_monthly.txt sf6_thd_surface-flask_2_3005-9999_monthly.txt sf6_tik_surface-flask_2_3001-9999_monthly.txt sf6_ush_surface-flask_2_3001-9999_monthly.txt sf6_ush_surface-flask_2_3005-9999_monthly.txt sf6_uta_surface-flask_2_3001-9999_monthly.txt sf6_uum_surface-flask_2_3001-9999_monthly.txt sf6_wis_surface-flask_2_3001-9999_monthly.txt sf6_wkt_surface-flask_2_3001-9999_monthly.txt sf6_wlg_surface-flask_2_3001-9999_monthly.txt sf6_zep_surface-flask_2_3001-9999_monthly.txt	THD441N002f1 THD441N002f5 TIK271N002f1 USH354S002f1 USH354S002f5 UTA439N002f1 UUM244N002f1 WIS631N002f1 WKT431N002f1 WLG236N002f1 ZEP678N002f1	
NPL	sf6_hfd_surface-insitu_154_9999-9999_monthly.txt	HFD650N154iz	SIO-05
UBAG	sf6_ssl_surface-insitu_71_9999-9999_monthly.txt sf6_zsf_surface-insitu_71_9999-9999_monthly.txt	SSL647N071iz ZSF647N071iz	WMO X2014
UNIURB	sf6_cmn_surface-insitu_74_9999-9999_monthly.txt	CMN644N074iz	WMO X2014
UNIVBRIS	sf6_bsd_surface-insitu_77_9999-9999_monthly.txt sf6_rgl_surface-insitu_77_9999-9999_monthly.txt sf6_tac_surface-insitu_77_9998-9999_monthly.txt	BSD654N077iz RGL651N077iz TAC652N077iy	SIO-05

APPENDIX C LIST OF OBSERVATIONAL STATIONS

Station	Country/ Territory	GAW ID	WIGOS ID	WDCGG ID	Organization	Location Latitude (°)	Location Longitude (°)	Elevation (m)	Parameter
REGION I (Africa)									
Amsterdam Island	France	AMS	0-20008-0-AMS	AMS1010	NOAA	37.80 S	77.54 E	70	CO_2, CH_4
Amsterdam Island	France	AMS	0-20008-0-AMS	AMS1010	LSCE	37.80 S	77.54 E	70	CO_2, CH_4, CO
Ascension Island	United Kingdom of Great Britain and Northern Ireland	ASC	0-20008-0-ASC	ASC1007	NOAA	7.97 S	14.40 W	91	CO_2, CH_4, N_2O, SF_6, $^{13}CH_4$, $^{13}CO_2$, $C^{18}O_2$, CO, H_2
Assekrem	Algeria	ASK	0-20008-0-ASK	ASK1003	NOAA	23.26 N	5.63 E	2710	CO_2, CH_4, N_2O, SF_6, $^{13}CO_2$, $C^{18}O_2$, CO, H_2
Assekrem	Algeria	ASK	0-20008-0-ASK	ASK1003	ONM	23.26 N	5.63 E	2710	CO
CAIRO	Egypt	CAI	0-20008-0-CAI	CAI1001	EMA	30.08 N	31.28 E	35	CO_2
Cape Point	South Africa	CPT	0-20008-0-CPT	CPT1009	NOAA	34.35 S	18.49 E	230	CO_2, CH_4, N_2O, SF_6, $^{13}CO_2$, $C^{18}O_2$, CO, H_2
Cape Point	South Africa	CPT	0-20008-0-CPT	CPT1009	ANSTO	34.35 S	18.49 E	230	^{222}Rn
Cape Point	South Africa	CPT	0-20008-0-CPT	CPT1009	SAWS	34.35 S	18.49 E	230	CO_2, CH_4, N_2O, CO
Cape Verde Atmospheric Observatory	Cabo Verde	CVO	0-20008-0-CVO	CVO1004	UYRK	16.86 N	24.87 W	10	CO_2, CH_4, CO
Cape Verde Atmospheric Observatory	Cabo Verde	CVO	0-20008-0-CVO	CVO1004	UoE	16.86 N	24.87 W	10	CO_2, CH_4, N_2O, CO
Crozet	France	CRZ	0-20008-0-CRZ	CRZ1011	NOAA	46.43 S	51.83 E	120	CO_2, CH_4, N_2O, SF_6, $^{13}CO_2$, $C^{18}O_2$, CO, H_2
Farafra	Egypt	FRF	0-20008-0-FRF	FRF1012	EMA	27.06 N	27.99 E	92	CO_2
Gobabeb	Namibia	NMB	0-20008-0-NMB	NMB1008	NOAA	23.57 S	15.03 E	408	CO_2, CH_4, N_2O, SF_6, $^{13}CO_2$, $C^{18}O_2$, CO, H_2
Izaña (Tenerife)	Spain	IZO	0-20008-0-IZO	IZO1002	NOAA	28.31 N	16.50 W	2373	CO_2, CH_4, N_2O, SF_6, $^{13}CO_2$, $C^{18}O_2$, CO, H_2
Izaña (Tenerife)	Spain	IZO	0-20008-0-IZO	IZO1002	AEMET	28.31 N	16.50 W	2373	CO_2, CH_4, N_2O, SF_6, CO
Mahé	Seychelles	SEY	0-20008-0-SEY	SEY1006	NOAA	4.67 S	55.17 E	3	CO_2, CH_4, N_2O, SF_6, $^{13}CO_2$, $C^{18}O_2$, CO, H_2
Mt. Kenya	Kenya	MKN	0-20008-0-MKN	MKN1005	NOAA	0.06 S	37.30 E	3678	CO_2, CH_4, N_2O, SF_6, $^{13}CO_2$, $C^{18}O_2$, CO, H_2
Mt. Kenya	Kenya	MKN	0-20008-0-MKN	MKN1005	KMD	0.06 S	37.30 E	3678	CO_2, CH_4, CO
REGION II (Asia)									
Anmyeon-do	Republic of Korea	AMY	0-20008-0-AMY	AMY2014	NOAA	36.54 N	126.33 E	42	CO_2, CH_4, N_2O, SF_6, $^{13}CH_4$, HFCs, $CBrF_3$, CO, H_2
Anmyeon-do	Republic of Korea	AMY	0-20008-0-AMY	AMY2014	KMA	36.54 N	126.33 E	42	CO_2, CH_4, N_2O, SF_6, CFCs, CO
Bering Island	Russian Federation	BER	0-20008-0-BER	BER2003	MGO	55.20 N	165.98 E	13	CO_2
CHICHIJIMA	Japan	CCJ	0-20000-0-47971	CCJ2158	MRI	27.09 N	142.19 E	2.7	^{222}Rn
Cape Ochiishi	Japan	COI	0-20008-0-COI	COI2008	NIES	43.16 N	145.50 E	42.4	CO_2, CH_4, N_2O, SF_6, CFCs, HCFCs, HFCs
Cape Rama	India	CRI	0-20008-0-CRI	CRI2036	CSIRO	15.08 N	73.83 E	60	CO_2, CH_4, N_2O, $^{13}CO_2$, CO, H_2
Cholpon-Ata	Kyrgyzstan	CPA	0-417-0-CPA	CPA2157	Kyrgyzhydromet	42.64 N	77.07 E	1613	CO_2, CH_4, CO
Gosan	Republic of Korea	GSN	0-20008-0-GSN	GSN2025	AGAGE	33.29 N	126.16 E	71.39	SF_6, SO_2F_2, CCl_4, CH_3CCl_3, CFCs, HCFCs, HFCs, PFCs, $CBrClF_2$, $CBrF_3$, $C_2Br_2F_4$, $CHCl_3$, CH_3Cl, CH_2Cl_2, CH_3Br
Gosan	Republic of Korea	GSN	0-20008-0-GSN	GSN2025	KMA	33.29 N	126.16 E	71.39	CO_2, CH_4, N_2O, SF_6, CO
Gosan	Republic of Korea	GSN	0-20008-0-GSN	GSN2025	GERC	33.29 N	126.16 E	71.39	CO_2, CH_4, N_2O
Gosan	Republic of Korea	GSN	0-20008-0-GSN	GSN2025	METRI	33.29 N	126.16 E	71.39	CO_2, CH_4, N_2O, CFCs
Hamamatsu	Japan	HMM	0-20008-0-HMM	HMM2024	SHIZU	34.72 N	137.72 E	29	CO_2
Hateruma Island	Japan	HAT	0-20008-0-HAT	HAT2031	NIES	24.06 N	123.81 E	10	CO_2, CH_4, N_2O, SF_6, CFCs, HCFCs, HFCs

LIST OF OBSERVATIONAL STATIONS (continued)

Station	Country/ Territory	GAW ID	WIGOS ID	WDCGG ID	Organization	Location Latitude (°)	Location Longitude (°)	Elevation (m)	Parameter
Hok Tsui / Cape d Aguilar	Hong Kong, China	HKG	0-20008-0-HKG	HKG2034	HKO	22.21 N	114.25 E	53	CO_2
Hok Tsui / Cape d Aguilar	Hong Kong, China	HKG	0-20008-0-HKG	HKG2034	PolyU	22.21 N	114.25 E	53	CO
Issyk-Kul	Kyrgyzstan	ISK	0-20008-0-ISK	ISK2009	KSNU	42.62 N	76.98 E	1640	CO_2, CH_4
Kaashidhoo (Male Atoll)	Maldives	KCO	0-20008-0-KCO	KCO2037	NOAA	4.97 N	73.47 E	1	CO_2, CH_4, N_2O, SF_6, CO
King's Park	Hong Kong, China	HKO	0-20008-0-HKO	HKO2033	HKO	22.31 N	114.17 E	65	CO_2
Kisai	Japan	KIS	0-20008-0-KIS	KIS2017	SAIPF	36.08 N	139.56 E	14	CO_2
Kotelnyj Island	Russian Federation	KOT	0-20008-0-KOT	KOT2001	MGO	76.00 N	137.87 E	5	CO_2
Kyzylcha	Uzbekistan	KYZ	0-20008-0-KYZ	KYZ2010	MGO	40.87 N	66.15 E	340	CO_2
Lulin	Taiwan, province of China	LLN	0-20008-0-LLN	LLN2032	NOAA	23.47 N	120.87 E	2862	CO_2, CH_4, N_2O, SF_6, $^{13}CO_2$, $C^{18}O_2$, CO, H_2
Memanbetsu	Japan	MMB	0-20008-0-MMB	MMB2006	MRI	43.92 N	144.20 E	33	N_2O
Mikawa-Ichinomiya	Japan	MKW	0-20008-0-MKW	MKW2022	AICH	34.85 N	137.43 E	50	CO_2
Minamitorishima	Japan	MNM	0-20008-0-MNM	MNM2029	JMA	24.29 N	153.98 E	7.1	CO_2, CH_4, HFCs, CO
Minamitorishima	Japan	MNM	0-20008-0-MNM	MNM2029	MRI	24.29 N	153.98 E	7.1	^{222}Rn
Mt. Dodaira	Japan	DDR	0-20008-0-DDR	DDR2019	SAIPF	36.00 N	139.19 E	832	CO_2
Mt. Waliguan	China	WLG	0-20008-0-WLG	WLG2015	NOAA	36.29 N	100.90 E	3810	CO_2, CH_4, N_2O, SF_6, $^{13}CH_4$, $^{13}CO_2$, $C^{18}O_2$, CO, H_2
Mt. Waliguan	China	WLG	0-20008-0-WLG	WLG2015	CMA	36.29 N	100.90 E	3810	CO_2, CH_4
Nagoya	Japan	NGY	0-20008-0-NGY	NGY2021	NAGOU	35.15 N	136.97 E	35	N_2O
Nepal Climate Observatory - Pyramid	Nepal	PYR	0-20008-0-PYR	PYR2026	UNIURB	27.96 N	86.81 E	5079	SO_2F_2, COS, CCl_4, CH_3CCl_3, CFCs, HCFCs, HFCs, PFCs, $CBrClF_2$, $CBrF_3$, $CHCl_3$, CH_3Cl, CH_2Cl_2, CH_3I, CH_3Br, CH_2Br_2, C_2HCl_3, C_2Cl_4, $CHBr_3$
Pha Din	Viet Nam	PDI	0-20008-0-PDI	PDI2035	VNMHA	21.57 N	103.52 E	1466	CO_2, CH_4, CO
Plateau Assy	Kazakhstan	KZM	0-20008-0-KZM	KZM2007	NOAA	43.25 N	77.88 E	2519	CO_2, CH_4, N_2O, SF_6, $^{13}CO_2$, $C^{18}O_2$, CO
Ryori	Japan	RYO	0-20008-0-RYO	RYO2012	JMA	39.03 N	141.82 E	260	CO_2, CH_4, N_2O, CCl_4, CH_3CCl_3, CFCs, CO
Ryori	Japan	RYO	0-20008-0-RYO	RYO2012	AIST	39.03 N	141.82 E	260	CO_2, O_2/N_2 ratio
Ryori	Japan	RYO	0-20008-0-RYO	RYO2012	MRI	39.03 N	141.82 E	260	^{222}Rn
Sary Taukum	Kazakhstan	KZD	0-20008-0-KZD	KZD2005	NOAA	44.45 N	77.57 E	412	CO_2, CH_4, N_2O, SF_6, $^{13}CO_2$, $C^{18}O_2$, CO
Shangdianzi	China	SDZ	0-20008-0-SDZ	SDZ2011	NOAA	40.65 N	117.12 E	287	CO_2, CH_4, N_2O, SF_6, $^{13}CO_2$, $C^{18}O_2$, CO, H_2
Suita	Japan	SUI	0-20008-0-SUI	SUI2023	OSAKAU	34.82 N	135.52 E	63	CO_2
Tae-ahn Peninsula	Republic of Korea	TAP	0-20008-0-TAP	TAP2013	NOAA	36.73 N	126.13 E	20	CO_2, CH_4, N_2O, SF_6, $^{13}CH_4$, $^{13}CO_2$, $C^{18}O_2$, CO, H_2
Takayama	Japan	TKY	0-20008-0-TKY	TKY2016	AIST	36.15 N	137.42 E	1420	CO_2
Tateno (Tsukuba)	Japan	TKB	0-20008-0-TKB	TKB2018	MRI	36.06 N	140.13 E	25.2	CO_2, CH_4
Tiksi	Russian Federation	TIK	0-20008-0-TIK	TIK2002	NOAA	71.59 N	128.92 E	8	CO_2, CH_4, N_2O, SF_6, $^{13}CO_2$, $C^{18}O_2$, CO, H_2
Tiksi	Russian Federation	TIK	0-20008-0-TIK	TIK2002	FMI	71.59 N	128.92 E	8	CO_2, CH_4
Tiksi	Russian Federation	TIK	0-20008-0-TIK	TIK2002	MGO	71.59 N	128.92 E	8	CO_2, CH_4
Ulaan Uul	Mongolia	UUM	0-20008-0-UUM	UUM2004	NOAA	44.44 N	111.09 E	992	CO_2, CH_4, N_2O, SF_6, $^{13}CO_2$, $C^{18}O_2$, CO, H_2
Ulleungdo	Republic of Korea	ULD	0-410-0-ULD	ULD2159	KMA	37.48 N	130.90 E	220.9	CO_2, CH_4, N_2O, SF_6
Urawa	Japan	URW	0-20008-0-URW	URW2020	SAIPF	35.87 N	139.61 E	8	CO_2
Yonagunijima	Japan	YON	0-20008-0-YON	YON2028	JMA	24.47 N	123.01 E	30	CO_2, CH_4, CO
Yonagunijima	Japan	YON	0-20008-0-YON	YON2028	MRI	24.47 N	123.01 E	30	^{222}Rn
REGION III (South America)									
Arembepe	Brazil	ABP	0-20008-0-ABP	ABP3003	NOAA	12.77 S	38.17 W	0	CO_2, CH_4, N_2O, SF_6, $^{13}CO_2$, $C^{18}O_2$, CO, H_2
Arembepe	Brazil	ABP	0-20008-0-ABP	ABP3003	INPE	12.77 S	38.17 W	0	CO_2, CH_4, N_2O, CO

LIST OF OBSERVATIONAL STATIONS (continued)

Station	Country/ Territory	GAW ID	WIGOS ID	WDCGG ID	Organization	Location Latitude (°)	Location Longitude (°)	Elevation (m)	Parameter
Bird Island (South Georgia)	United Kingdom of Great Britain and Northern Ireland	SGI	0-20008-0-SGI	SGI3006	NOAA	54.01 S	38.05 W	30	CO_2, CH_4
Easter Island	Chile	EIC	0-20008-0-EIC	EIC3004	NOAA	27.17 S	109.42 W	41	CO_2, CH_4, N_2O, SF_6, $^{13}CH_4$, $^{13}CO_2$, $C^{18}O_2$, CO, H_2
El Tololo	Chile	TLL	0-20008-0-TLL	TLL3005	DMC	30.17 S	70.80 W	2154	CO_2, CH_4, CO
Huancayo	Peru	HUA	0-20008-0-HUA	HUA3002	IGP	12.15 S	75.57 W	4575	CO_2
Natal	Brazil	NAT	0-20008-0-NAT	NAT3001	NOAA	6.00 S	35.20 W	0	CO_2, CH_4, N_2O, SF_6, $^{13}CO_2$, $C^{18}O_2$, CO, H_2
Ushuaia	Argentina	USH	0-20008-0-USH	USH3007	NOAA	54.85 S	68.31 W	18	CO_2, CH_4, N_2O, SF_6, $^{13}CO_2$, $C^{18}O_2$, CCl_4, CH_3CCl_3, CFCs, CO, H_2
Ushuaia	Argentina	USH	0-20008-0-USH	USH3007	SMNA	54.85 S	68.31 W	18	CO
REGION IV (North and Central America)									
Alert	Canada	ALT	0-20008-0-ALT	ALT4001	NOAA	82.50 N	62.34 W	185	CO_2, CH_4, N_2O, SF_6, $^{13}CH_4$, $^{13}CO_2$, $C^{18}O_2$, CCl_4, CH_3CCl_3, CFCs, HCFCs, HFCs, $CBrClF_2$, $CBrF_3$, $C_2Br_2F_4$, CO, CH_3Cl, CH_2Cl_2, CH_3Br, C_2Cl_4, H_2
Alert	Canada	ALT	0-20008-0-ALT	ALT4001	CSIRO	82.50 N	62.34 W	185	CO_2, CH_4, N_2O, $^{13}CO_2$, CO, H_2
Alert	Canada	ALT	0-20008-0-ALT	ALT4001	ECCC	82.50 N	62.34 W	185	CO_2, CH_4, N_2O, $^{13}CO_2$, $C^{18}O_2$, CO
Argyle (ME)	United States of America	AMT	0-20008-0-AMT	AMT4017	NOAA	45.03 N	68.68 W	50	CH_4, N_2O, SF_6, $^{13}CO_2$, $C^{18}O_2$, CO
Barrow (AK)	United States of America	BRW	0-20008-0-BRW	BRW4003	NOAA	71.32 N	156.61 W	11	CO_2, CH_4, N_2O, SF_6, $^{13}CH_4$, $^{13}CO_2$, $C^{18}O_2$, CCl_4, CH_3CCl_3, CFCs, HCFCs, HFCs, $CBrClF_2$, $CBrF_3$, $C_2Br_2F_4$, CO, CH_3Cl, CH_2Cl_2, CH_3Br, C_2Cl_4, H_2
Behchoko	Canada	BCK	0-20008-0-BCK	BCK4129	ECCC	62.80 N	115.92 W	184	CO_2, CH_4
Bratt's Lake	Canada	BRA	0-20008-0-BRA	BRA4218	ECCC	50.20 N	104.71 W	580	CO_2, CH_4
Cambridge Bay	Canada	CBY	0-20008-0-CBY	CBY4165	ECCC	69.13 N	105.06 W	25	CO_2, CH_4
Candle Lake	Canada	CDL	0-20008-0-CDL	CDL4008	ECCC	53.99 N	105.12 W	591	CO_2, CH_4, CO
Cape Meares (OR)	United States of America	CMO	0-20008-0-CMO	CMO4016	NOAA	45.00 N	124.00 W	30	CO_2, CH_4, $^{13}CO_2$, $C^{18}O_2$, CO
Cape Meares (OR)	United States of America	CMO	0-20008-0-CMO	CMO4016	AGAGE	45.00 N	124.00 W	30	CH_4, N_2O, CCl_4, CH_3CCl_3, CFCs
Chapais	Canada	CPS	0-20008-0-CPS	CPS4245	ECCC	49.82 N	74.97 W	383	CO_2, CH_4
Chibougamau	Canada	CHM	0-20008-0-CHM	CHM4012	ECCC	49.69 N	74.34 W	383	CO_2, CH_4, CO
Churchill	Canada	CHL	0-20008-0-CHL	CHL4004	ECCC	58.74 N	93.82 W	16	CO_2, CH_4, N_2O, $^{13}CO_2$, $C^{18}O_2$, CO
Churchill	Canada	CHL	0-20008-0-CHL	CHL4004	TU	58.74 N	93.82 W	16	$^{13}CH_4$
Cold Bay (AK)	United States of America	CBA	0-20008-0-CBA	CBA4005	NOAA	55.20 N	162.72 W	25	CO_2, CH_4, N_2O, SF_6, $^{13}CH_4$, $^{13}CO_2$, $C^{18}O_2$, CO, H_2
East Trout Lake	Canada	ETL	0-20008-0-ETL	ETL4007	ECCC	54.35 N	104.99 W	500	CO_2, CH_4, $^{13}CO_2$, $C^{18}O_2$, CO
Egbert	Canada	EGB	0-20008-0-EGB	EGB4018	ECCC	44.23 N	79.78 W	255	CO_2, CH_4, CO
Estevan Point	Canada	ESP	0-20008-0-ESP	ESP4013	CSIRO	49.38 N	126.54 W	7	CO_2, CH_4, N_2O, $^{13}CO_2$, CO, H_2
Estevan Point	Canada	ESP	0-20008-0-ESP	ESP4013	ECCC	49.38 N	126.54 W	7	CO_2, CH_4, N_2O, $^{13}CO_2$, $C^{18}O_2$, CO
Esther	Canada	EST	0-20008-0-EST	EST4178	ECCC	51.67 N	110.21 W	707	CO_2, CH_4

LIST OF OBSERVATIONAL STATIONS (continued)

Station	Country/ Territory	GAW ID	WIGOS ID	WDCGG ID	Organization	Location Latitude (°)	Location Longitude (°)	Elevation (m)	Parameter
Fraserdale	Canada	FSD	0-20008-0-FSD	FSD4011	ECCC	49.84 N	81.52 W	210	CO_2, CH_4, $^{13}CO_2$, $C^{18}O_2$, CO
Grifton - Georgia Station (NC)	United States of America	ITN	0-20008-0-ITN	ITN4027	NOAA	35.35 N	77.38 W	505	CH_4, N_2O, SF_6, $^{13}CO_2$, $C^{18}O_2$, CCl_4, CH_3CCl_3, CFCs, CO
Harvard Forest (MA)	United States of America	HFM	0-20008-0-HFM	HFM4020	NOAA	42.90 N	72.30 W	340	N_2O, SF_6, CCl_4, CH_3CCl_3, CFCs, HCFCs, HFCs, $CBrClF_2$, $CBrF_3$, $C_2Br_2F_4$, CH_3Cl, CH_2Cl_2, CH_3Br, C_2Cl_4
Inuvik	Canada	INU	0-20008-0-INU	INU4176	ECCC	68.32 N	133.53 W	107	CO_2, CH_4
Key Biscane (FL)	United States of America	KEY	0-20008-0-KEY	KEY4033	NOAA	25.67 N	80.20 W	3	CO_2, CH_4, N_2O, SF_6, $^{13}CO_2$, $C^{18}O_2$, CO, H_2
Kitt Peak (AZ)	United States of America	KPA	0-20008-0-KPA	KPA4031	NOAA	31.97 N	111.60 W	2083	CH_4
La Jolla (CA)	United States of America	SIO	0-20008-0-SIO	SIO4028	NOAA	32.83 N	117.27 W	14	CH_4
Lac La Biche (Alberta)	Canada	LLB	0-20008-0-LLB	LLB4006	NOAA	54.95 N	112.47 W	548	CO_2, CH_4, N_2O, SF_6, $^{13}CH_4$, $^{13}CO_2$, $C^{18}O_2$, CO, H_2
Lac La Biche (Alberta)	Canada	LLB	0-20008-0-LLB	LLB4006	ECCC	54.95 N	112.47 W	548	CO_2, CH_4, CO
Mex High Altitude Global Climate Observation Center	Mexico	MEX	0-20008-0-MEX	MEX4034	NOAA	18.99 N	97.31 W	4560	CO_2, CH_4, N_2O, SF_6, $^{13}CH_4$, $^{13}CO_2$, $C^{18}O_2$, CO, H_2
Moody (TX)	United States of America	WKT	0-20008-0-WKT	WKT4032	NOAA	31.32 N	97.62 W	723	CH_4, N_2O, SF_6, $^{13}CO_2$, $C^{18}O_2$, CO, H_2
Mould Bay	Canada	MBC	0-20008-0-MBC	MBC4002	NOAA	76.25 N	119.35 W	58	CO_2, CH_4, $^{13}CO_2$, $C^{18}O_2$, CO
Niwot Ridge - T-van (CO)	United States of America	NWR	0-20008-0-NWR	NWR4023	NOAA	40.05 N	105.59 W	3523	CO_2, CH_4, N_2O, SF_6, $^{13}CH_4$, $^{13}CO_2$, $C^{18}O_2$, CCl_4, CH_3CCl_3, CFCs, HCFCs, HFCs, $CBrClF_2$, $CBrF_3$, $C_2Br_2F_4$, CO, CH_3Cl, CH_2Cl_2, CH_3Br, C_2Cl_4, H_2, $^{14}CO_2$
Olympic Peninsula (WA)	United States of America	OPW	0-20008-0-OPW	OPW4014	NOAA	48.25 N	124.42 W	488	CO_2, CH_4
Park Falls (WI)	United States of America	LEF	0-20008-0-LEF	LEF4015	NOAA	45.93 N	90.27 W	868	CO_2, CH_4, N_2O, SF_6, $^{13}CO_2$, $C^{18}O_2$, CCl_4, CH_3CCl_3, CFCs, HCFCs, HFCs, $CBrClF_2$, $CBrF_3$, $C_2Br_2F_4$, CO, CH_3Cl, CH_2Cl_2, CH_3Br, C_2Cl_4, H_2
Point Arena (CA)	United States of America	PTA	0-20008-0-PTA	PTA4025	NOAA	38.95 N	123.73 W	17	CO_2, CH_4, N_2O, SF_6, $^{13}CO_2$, $C^{18}O_2$, CO, H_2
Ragged Point	Barbados	RPB	0-20008-0-RPB	RPB4036	NOAA	13.17 N	59.43 W	45	CO_2, CH_4, N_2O, SF_6, $^{13}CO_2$, $C^{18}O_2$, CO, H_2
Ragged Point	Barbados	RPB	0-20008-0-RPB	RPB4036	AGAGE	13.17 N	59.43 W	45	CH_4, N_2O, SF_6, SO_2F_2, NF_3, CCl_4, CH_3CCl_3, CFCs, HCFCs, HFCs, PFCs, $CBrClF_2$, $CBrF_3$, $C_2Br_2F_4$, $CHCl_3$, CH_3Cl, CH_2Cl_2, CH_3Br, C_2Cl_4
Sable Island	Canada	WSA	0-20008-0-WSA	WSA4019	ECCC	43.93 N	60.01 W	2	CO_2, CH_4, N_2O, $^{13}CO_2$, $C^{18}O_2$, CO
Shemya Island	United States of America	SHM	0-20008-0-SHM	SHM4009	NOAA	52.72 N	174.10 E	40	CO_2, CH_4, N_2O, SF_6, $^{13}CO_2$, $C^{18}O_2$, CO, H_2
Southern Great Plains E13 (OK)	United States of America	SGP	0-20008-0-SGP	SGP4026	NOAA	36.60 N	97.50 W	318	CO_2, CH_4, N_2O, SF_6, $^{13}CO_2$, $C^{18}O_2$, CO, H_2
St. Croix	United States of America	AVI	0-20008-0-AVI	AVI4035	NOAA	17.75 N	64.75 W	3	CO_2, CH_4

LIST OF OBSERVATIONAL STATIONS (continued)

Station	Country/ Territory	GAW ID	WIGOS ID	WDCGG ID	Organization	Location Latitude (°)	Location Longitude (°)	Elevation (m)	Parameter
St. David's Head	United Kingdom of Great Britain and Northern Ireland	BME	0-20008-0-BME	BME4029	NOAA	32.37 N	64.65 W	30	CO_2, CH_4, N_2O, SF_6, $^{13}CO_2$, $C^{18}O_2$, CO, H_2
Trinidad Head (CA)	United States of America	THD	0-20008-0-THD	THD4022	NOAA	41.05 N	124.15 W	107	CO_2, CH_4, N_2O, SF_6, $^{13}CO_2$, $C^{18}O_2$, CCl_4, CH_3CCl_3, CFCs, HCFCs, HFCs, $CBrClF_2$, $CBrF_3$, $C_2Br_2F_4$, CO, CH_3Cl, CH_2Cl_2, CH_3Br, C_2Cl_4, H_2
Trinidad Head (CA)	United States of America	THD	0-20008-0-THD	THD4022	AGAGE	41.05 N	124.15 W	107	CH_4, N_2O, SF_6, SO_2F_2, NF_3, CCl_4, CH_3CCl_3, CFCs, HCFCs, HFCs, PFCs, $CBrClF_2$, $CBrF_3$, $C_2Br_2F_4$, $CHCl_3$, CH_3Cl, CH_2Cl_2, CH_3Br, C_2Cl_4
Tudor Hill (Bermuda)	United Kingdom of Great Britain and Northern Ireland	BMW	0-20008-0-BMW	BMW4030	NOAA	32.27 N	64.88 W	30	CO_2, CH_4, N_2O, SF_6, $^{13}CO_2$, $C^{18}O_2$, CO, H_2
Wendover (UT)	United States of America	UTA	0-20008-0-UTA	UTA4024	NOAA	39.90 N	113.72 W	1320	CO_2, CH_4, N_2O, SF_6, $^{13}CO_2$, $C^{18}O_2$, CO, H_2
West Branch (Iowa)	United States of America	WBI	0-20008-0-WBI	WBI4021	NOAA	41.72 N	91.35 W	242	$C^{18}O_2$
REGION V (South-West Pacific)									
Baring Head	New Zealand	BHD	0-20008-0-BHD	BHD5012	NOAA	41.41 S	174.87 E	85	CO_2, CH_4, N_2O, SF_6, $^{13}CH_4$, $^{13}CO_2$, $C^{18}O_2$, CO, H_2
Baring Head	New Zealand	BHD	0-20008-0-BHD	BHD5012	NIWA	41.41 S	174.87 E	85	CO_2, CH_4, N_2O, $^{13}CH_4$, CO, $^{14}CO_2$
Bukit Kototabang	Indonesia	BKT	0-20008-0-BKT	BKT5007	NOAA	0.20 S	100.32 E	864	CO_2, CH_4, N_2O, SF_6, $^{13}CO_2$, $C^{18}O_2$, CO, H_2
Bukit Kototabang	Indonesia	BKT	0-20008-0-BKT	BKT5007	BMKG	0.20 S	100.32 E	864	CO_2, CH_4, CO
Cape Ferguson	Australia	CFA	0-20008-0-CFA	CFA5010	CSIRO	19.28 S	147.06 E	2	CO_2, CH_4, N_2O, $^{13}CO_2$, CO, H_2
Cape Kumukahi (HI)	United States of America	KUM	0-20008-0-KUM	KUM5003	NOAA	19.52 N	154.82 W	3	CO_2, CH_4, N_2O, SF_6, $^{13}CH_4$, $^{13}CO_2$, $C^{18}O_2$, CCl_4, CH_3CCl_3, CFCs, HCFCs, HFCs, $CBrClF_2$, $CBrF_3$, $C_2Br_2F_4$, CO, CH_3Cl, CH_2Cl_2, CH_3Br, C_2Cl_4, H_2
Christmas Island	Kiribati	CHR	0-20008-0-CHR	CHR5006	NOAA	1.70 N	157.17 W	3	CO_2, CH_4, N_2O, SF_6, $^{13}CO_2$, $C^{18}O_2$, CO, H_2
Danum Valley	Malaysia	DMV	0-20008-0-DMV	DMV5005	MMD	4.98 N	117.84 E	426	CO_2
Guam (Mariana Island)	United States of America	GMI	0-20008-0-GMI	GMI5004	NOAA	13.43 N	144.78 E	2	CO_2, CH_4, N_2O, SF_6, $^{13}CH_4$, $^{13}CO_2$, $C^{18}O_2$, CO, H_2
Gunn Point	Australia	GPA	0-20008-0-GPA	GPA5008	CSIRO	12.25 S	131.05 E	25	CO_2, CH_4, N_2O, $^{13}CO_2$, CO, H_2
Kaitorete Spit	New Zealand	NZL	0-20008-0-NZL	NZL5013	NOAA	43.83 S	172.63 E	3	CH_4
Kennaook / Cape Grim	Australia	CGO	0-20008-0-CGO	CGO5011	NOAA	40.68 S	144.69 E	94	CO_2, CH_4, N_2O, SF_6, $^{13}CH_4$, $^{13}CO_2$, $C^{18}O_2$, CCl_4, CH_3CCl_3, CFCs, HCFCs, HFCs, $CBrClF_2$, $CBrF_3$, $C_2Br_2F_4$, CO, CH_3Cl, CH_2Cl_2, CH_3Br, C_2Cl_4, H_2
Kennaook / Cape Grim	Australia	CGO	0-20008-0-CGO	CGO5011	AGAGE	40.68 S	144.69 E	94	CH_4, N_2O, SF_6, SO_2F_2, NF_3, CCl_4, CH_3CCl_3, CFCs, HCFCs, HFCs,

LIST OF OBSERVATIONAL STATIONS (continued)

Station	Country/ Territory	GAW ID	WIGOS ID	WDCGG ID	Organization	Location Latitude (°)	Location Longitude (°)	Elevation (m)	Parameter
									PFCs, $CBrClF_2$, $CBrF_3$, $C_2Br_2F_4$, CO, $CHCl_3$, CH_3Cl, CH_2Cl_2, CH_3Br, C_2Cl_4, H_2
Kennaook / Cape Grim	Australia	CGO	0-20008-0-CGO	CGO5011	ANSTO	40.68 S	144.69 E	94	^{222}Rn
Kennaook / Cape Grim	Australia	CGO	0-20008-0-CGO	CGO5011	CSIRO	40.68 S	144.69 E	94	CO_2, CH_4, N_2O, $^{13}CO_2$, CO, H_2
Lauder	New Zealand	LAU	0-20008-0-LAU	LAU5014	NIWA	45.04 S	169.68 E	370	CO_2, CH_4, CO
Macquarie Island	Australia	MQA	0-20008-0-MQA	MQA5015	CSIRO	54.50 S	158.94 E	6	CO_2, CH_4, N_2O, $^{13}CO_2$, CO, H_2
Mauna Kea (HI)	United States of America	MKO	0-20008-0-MKO	MKO5026	NOAA	19.83 N	155.48 W	4204	CO_2, CH_4, N_2O, SF_6
Mauna Loa (HI)	United States of America	MLO	0-20008-0-MLO	MLO5002	NOAA	19.54 N	155.58 W	3397	CO_2, CH_4, N_2O, SF_6, $^{13}CH_4$, $^{13}CO_2$, $C^{18}O_2$, CCl_4, CH_3CCl_3, CFCs, HCFCs, HFCs, $CBrClF_2$, $CBrF_3$, $C_2Br_2F_4$, CO, CH_3Cl, CH_2Cl_2, CH_3Br, C_2Cl_4, H_2
Mauna Loa (HI)	United States of America	MLO	0-20008-0-MLO	MLO5002	CSIRO	19.54 N	155.58 W	3397	CO_2, CH_4, N_2O, $^{13}CO_2$, CO, H_2
Samoa (Cape Matatula)	United States of America	SMO	0-20008-0-SMO	SMO5009	NOAA	14.25 S	170.56 W	77	CO_2, CH_4, N_2O, SF_6, $^{13}CH_4$, $^{13}CO_2$, $C^{18}O_2$, CCl_4, CH_3CCl_3, CFCs, HCFCs, HFCs, $CBrClF_2$, $CBrF_3$, $C_2Br_2F_4$, CO, CH_3Cl, CH_2Cl_2, CH_3Br, C_2Cl_4, H_2
Samoa (Cape Matatula)	United States of America	SMO	0-20008-0-SMO	SMO5009	AGAGE	14.25 S	170.56 W	77	CH_4, N_2O, SF_6, SO_2F_2, NF_3, CCl_4, CH_3CCl_3, CFCs, HCFCs, HFCs, PFCs, $CBrClF_2$, $CBrF_3$, $C_2Br_2F_4$, $CHCl_3$, CH_3Cl, CH_2Cl_2, CH_3Br, C_2Cl_4
Sand Island	United States of America	MID	0-20008-0-MID	MID5001	NOAA	28.22 N	177.37 W	4	CO_2, CH_4, N_2O, SF_6, $^{13}CH_4$, $^{13}CO_2$, $C^{18}O_2$, CO, H_2
REGION VI (Europe)									
Adrigole	Ireland	ADR	0-20008-0-ADR	ADR6021	AGAGE	51.68 N	9.73 W	50	N_2O, CCl_4, CH_3CCl_3, CFCs
BEO Moussala	Bulgaria	BEO	0-20008-0-BEO	BEO6045	INRNE	42.18 N	23.59 E	2925	CO_2, CO
Baltic Sea	Poland	BAL	0-20008-0-BAL	BAL6009	NOAA	55.50 N	16.67 E	7	CO_2, CH_4, N_2O, SF_6, $^{13}CH_4$, $^{13}CO_2$, $C^{18}O_2$, CO, H_2
Begur	Spain	BGU	0-20008-0-BGU	BGU6046	LSCE	41.97 N	3.23 E	13	CO_2, CH_4
Bilsdale	United Kingdom of Great Britain and Northern Ireland	BSD	0-20008-0-BSD	BSD6293	UNIVBRIS	54.36 N	1.15 W	380	CO_2, CH_4, N_2O, SF_6, CO
Brotjacklriegel	Germany	BRT	0-20008-0-BRT	BRT6025	UBAG	48.82 N	13.22 E	1016	CO_2
Capo Granitola	Italy	CGR	0-20008-0-CGR	CGR6048	ISAC	37.57 N	12.66 E	5	CO_2, CH_4, CO
Constanta (Black Sea)	Romania	BSC	0-20008-0-BSC	BSC6043	NOAA	44.17 N	28.68 E	3	CO_2, CH_4, N_2O, SF_6, $^{13}CO_2$, $C^{18}O_2$, CO, H_2
Deuselbach	Germany	DEU	0-20008-0-DEU	DEU6023	UBAG	49.77 N	7.05 E	480	CO_2, CH_4
Diabla Gora / Puszcza Borecka	Poland	DIG	0-20008-0-DIG	DIG6012	IOEP	54.15 N	22.07 E	157	CO_2
Dwejra Point	Malta	GOZ	0-20008-0-GOZ	GOZ6050	NOAA	36.05 N	14.18 E	30	CO_2, CH_4, $^{13}CO_2$, $C^{18}O_2$, CO
Finokalia	Greece	FKL	0-20008-0-FKL	FKL6052	LSCE	35.34 N	25.67 E	150	CO_2, CH_4
Fundata	Romania	FDT	0-20008-0-FDT	FDT6041	INMH	45.43 N	25.27 E	1384	CO_2
Gartow	Germany	GAT	0-20008-0-GAT	GAT6058	DWD	53.07 N	11.44 E	69	CO_2, CH_4, N_2O, CO
Giordan Lighthouse	Malta	GLH	0-20008-0-GLH	GLH6049	UMLT	36.07 N	14.22 E	167	CO_2, CH_4, CO, ^{222}Rn

LIST OF OBSERVATIONAL STATIONS (continued)

Station	Country/ Territory	GAW ID	WIGOS ID	WDCGG ID	Organization	Location Latitude (°)	Location Longitude (°)	Elevation (m)	Parameter
Heathfield	United Kingdom of Great Britain and Northern Ireland	HFD	0-20008-0-HFD	HFD6419	NPL	50.98 N	0.23 E	160	CO_2, CH_4, N_2O, SF_6, CO
Hegyhátsál háttérszennyettség-mérő állomás	Hungary	HUN	0-348-4-16307	HUN6034	NOAA	46.96 N	16.65 E	248	CO_2, CH_4, N_2O, SF_6, $^{13}CO_2$, $C^{18}O_2$, CO, H_2
Hegyhátsál háttérszennyettség-mérő állomás	Hungary	HUN	0-348-4-16307	HUN6034	ATOMKI	46.96 N	16.65 E	248	CO_2, CH_4
Helgoland	Germany	HEL	0-276-0-HEL	HEL6415	DWD	54.18 N	7.88 E	43	CO_2, CH_4, N_2O, CO
Hohenpeissenberg	Germany	HPB	0-20008-0-HPB	HPB6028	NOAA	47.80 N	11.01 E	985	CO_2, CH_4, N_2O, SF_6, $^{13}CO_2$, $C^{18}O_2$, CO, H_2
Hohenpeissenberg	Germany	HPB	0-20008-0-HPB	HPB6028	DWD	47.80 N	11.01 E	985	CO_2, CH_4, N_2O, CO, ^{222}Rn
Ile Grande	France	LPO	0-20008-0-LPO	LPO6026	LSCE	48.80 N	3.58 W	20	CO_2, CH_4
Jungfraujoch	Switzerland	JFJ	0-20008-0-JFJ	JFJ6036	AGAGE	46.55 N	7.99 E	3580	SF_6, SO_2F_2, NF_3, CCl_4, CH_3CCl_3, CFCs, HCFCs, HFCs, PFCs, $CBrClF_2$, $CBrF_3$, $C_2Br_2F_4$, $CHCl_3$, CH_3Cl, CH_2Cl_2, CH_3Br, C_2HCl_3, C_2Cl_4
Jungfraujoch	Switzerland	JFJ	0-20008-0-JFJ	JFJ6036	Empa	46.55 N	7.99 E	3580	CO_2, CH_4, N_2O, SF_6, CO
Jungfraujoch	Switzerland	JFJ	0-20008-0-JFJ	JFJ6036	KUP	46.55 N	7.99 E	3580	CO_2
Jülich	Germany	JUE	0-20008-0-JUE	JUE6421	DWD	50.91 N	6.41 E	98	CO_2, CH_4, N_2O, CO
Karlsruhe	Germany	KIT	0-20008-0-KIT	KIT6084	DWD	49.10 N	8.44 E	111	CO_2, CH_4, N_2O, CO
Kecskemét K-puszta háttérszennyettség-mérő állomás	Hungary	KPS	0-348-4-46316	KPS6033	HMS	46.97 N	19.58 E	125	CO_2
Kloosterburen	Kingdom of the Netherlands	KTB	0-20008-0-KTB	KTB6014	RIVM	53.40 N	6.42 E	0	CO
Kollumerwaard	Kingdom of the Netherlands	KMW	0-20008-0-KMW	KMW6015	RIVM	53.33 N	6.27 E	0	CO_2, CH_4, CO
Kosetice Observatory	Czech Republic	KOS	0-20008-0-KOS	KOS6024	CHMI	49.58 N	15.08 E	534	CH_4, CO
Krvavec	Slovenia	KVV	0-20008-0-KVV	KVV6037	ARSO	46.30 N	14.53 E	1740	CO
Lamezia Terme	Italy	LMT	0-20008-0-LMT	LMT6054	ISAC	38.88 N	16.23 E	6	CO_2, CH_4, CO
Lampedusa	Italy	LMP	0-20008-0-LMP	LMP6051	NOAA	35.52 N	12.63 E	45	CO_2, CH_4, N_2O, SF_6, $^{13}CO_2$, $C^{18}O_2$, CO, H_2
Lampedusa	Italy	LMP	0-20008-0-LMP	LMP6051	ENEA	35.52 N	12.63 E	45	CO_2, CH_4, N_2O, SF_6, CCl_4, CH_3CCl_3, CFCs, HCFCs, HFCs, $CBrClF_2$, $CBrF_3$, $CHCl_3$, CH_3Cl, CH_2Cl_2, CH_3I, CH_3Br, CH_2Br_2
Lecce Environmental-Climate Observatory	Italy	ECO	0-20008-0-ECO	ECO6055	ISAC	40.34 N	18.12 E	36	CO_2, CH_4, CO
Lerwick	United Kingdom of Great Britain and Northern Ireland	SIS	0-20008-0-SIS	SIS6008	CSIRO	60.13 N	1.18 W	84	CO_2, CH_4, N_2O, $^{13}CO_2$, CO, H_2
Lindenberg	Germany	LIN	0-20008-0-LIN	LIN6057	DWD	52.22 N	14.12 E	112	CO_2, CH_4, N_2O, CO
Mace Head	Ireland	MHD	0-20008-0-MHD	MHD6016	NOAA	53.33 N	9.90 W	8.4	CO_2, CH_4, N_2O, SF_6, $^{13}CH_4$, $^{13}CO_2$, $C^{18}O_2$, CCl_4, CH_3CCl_3, CFCs, HCFCs, HFCs, $CBrClF_2$, $CBrF_3$, $C_2Br_2F_4$, CO, CH_3Cl, CH_2Cl_2, CH_3Br, C_2Cl_4, H_2
Mace Head	Ireland	MHD	0-20008-0-MHD	MHD6016	AGAGE	53.33 N	9.90 W	8.4	CH_4, N_2O, SF_6, SO_2F_2, NF_3, CCl_4, CH_3CCl_3, CFCs, HCFCs, HFCs, PFCs, $CBrClF_2$, $CBrF_3$, $C_2Br_2F_4$, CO, $CHCl_3$, CH_3Cl, CH_2Cl_2, CH_3Br, C_2HCl_3, C_2Cl_4, H_2
Mace Head	Ireland	MHD	0-20008-0-MHD	MHD6016	LSCE	53.33 N	9.90 W	8.4	CO_2, CH_4
Madonie - Piano Battaglia	Italy	MDN	0-380-0-MDN	MDN6418	ENEA	37.88 N	14.03 E	1650	CO_2, CH_4

LIST OF OBSERVATIONAL STATIONS (continued)

Station	Country/ Territory	GAW ID	WIGOS ID	WDCGG ID	Organization	Location Latitude (°)	Location Longitude (°)	Elevation (m)	Parameter
Monte Cimone	Italy	CMN	0-20008-0-CMN	CMN6042	AGAGE	44.19 N	10.70 E	2165	SF_6, SO_2F_2, NF_3, CCl_4, CH_3CCl_3, CFCs, HCFCs, HFCs, PFCs, $CBrClF_2$, $CBrF_3$, $C_2Br_2F_4$, $CHCl_3$, CH_3Cl, CH_2Cl_2, CH_3Br, C_2Cl_4
Monte Cimone	Italy	CMN	0-20008-0-CMN	CMN6042	IAFMS	44.19 N	10.70 E	2165	CO_2, CH_4
Monte Cimone	Italy	CMN	0-20008-0-CMN	CMN6042	ISAC	44.19 N	10.70 E	2165	CO, H_2
Monte Cimone	Italy	CMN	0-20008-0-CMN	CMN6042	UNIURB	44.19 N	10.70 E	2165	CH_4, N_2O, SF_6, CO
Monte Curcio	Italy	CUR	0-20008-0-CUR	CUR6056	IIA	39.32 N	16.42 E	1796	CO_2, CH_4, CO
Neuglobsow	Germany	NGL	0-20008-0-NGL	NGL6017	UBAG	53.14 N	13.03 E	62	CO_2, CH_4, CO
Ny Ålesund	Norway	NYA	0-20008-0-NYA	NYA6066	TU	78.92 N	11.92 E	0	CH_4, $^{13}CH_4$, CH_3D
Ocean Station Charlie	United States of America	STC	0-20008-0-STC	STC6013	NOAA	54.00 N	35.00 W	0	CO_2
Ocean Station Charlie	United States of America	STC	0-20008-0-STC	STC6013	MGO	54.00 N	35.00 W	0	CO_2
Ocean Station M	Norway	STM	0-20008-0-STM	STM6006	NOAA	66.00 N	2.00 E	4	CO_2, CH_4, N_2O, SF_6, $^{13}CO_2$, $C^{18}O_2$, CO, H_2
Ochsenkopf	Germany	OXK	0-20008-0-OXK	OXK6022	NOAA	50.03 N	11.81 E	1185	CO_2, CH_4, N_2O, SF_6, $^{13}CO_2$, $C^{18}O_2$, CO, H_2
Ochsenkopf	Germany	OXK	0-20008-0-OXK	OXK6022	DWD	50.03 N	11.81 E	1185	CO_2, CH_4, N_2O, CO
Pallas	Finland	PAL	0-20008-0-PAL	PAL6004	NOAA	67.97 N	24.12 E	560	CO_2, CH_4, N_2O, SF_6, $^{13}CO_2$, $C^{18}O_2$, CO, H_2
Pallas	Finland	PAL	0-20008-0-PAL	PAL6004	FMI	67.97 N	24.12 E	560	CO_2, CH_4
Payerne	Switzerland	PAY	0-20008-0-PAY	PAY6035	Empa	46.81 N	6.94 E	490	CO
Pic du Midi	France	PDM	0-20008-0-PDM	PDM6044	LA	42.94 N	0.14 E	2877	CO
Pic du Midi	France	PDM	0-20008-0-PDM	PDM6044	LSCE	42.94 N	0.14 E	2877	CO_2, CH_4
Plateau Rosa	Italy	PRS	0-20008-0-PRS	PRS6039	RSE	45.94 N	7.71 E	3480	CO_2, CH_4
Puy de Dôme	France	PUY	0-20008-0-PUY	PUY6040	LAMP	45.77 N	2.97 E	1465	CO
Puy de Dôme	France	PUY	0-20008-0-PUY	PUY6040	LSCE	45.77 N	2.97 E	1465	CO_2, CH_4
Ridge Hill	United Kingdom of Great Britain and Northern Ireland	RGL	0-20008-0-RGL	RGL6020	UNIVBRIS	52.00 N	2.54 W	204	CO_2, CH_4, N_2O, SF_6
Rigi	Switzerland	RIG	0-20008-0-RIG	RIG6038	Empa	47.07 N	8.46 E	1031	CO
SONNBLICK Observatory	Austria	SNB	0-20000-0-11343	SNB6032	UBAA	47.05 N	12.96 E	3106	CO_2, CH_4, CO
Schauinsland	Germany	SSL	0-20008-0-SSL	SSL6027	UBAG	47.90 N	7.92 E	1205	CO_2, CH_4, N_2O, SF_6, CO
Sede Boker	Israel	WIS	0-20008-0-WIS	WIS6053	NOAA	31.13 N	34.88 E	400	CO_2, CH_4, N_2O, SF_6, $^{13}CO_2$, $C^{18}O_2$, CO, H_2
Serreta (Terceira)	Portugal	AZR	0-20008-0-AZR	AZR6047	NOAA	38.77 N	27.38 W	40	CO_2, CH_4, N_2O, SF_6, $^{13}CH_4$, $^{13}CO_2$, $C^{18}O_2$, CO, H_2
Steinkimmen	Germany	STE	0-20008-0-STE	STE6422	DWD	53.04 N	8.46 E	29	CO_2, CH_4, N_2O, CO
Storhofdi	Iceland	ICE	0-20008-0-ICE	ICE6007	NOAA	63.40 N	20.28 W	118	CO_2, CH_4, N_2O, SF_6, $^{13}CO_2$, $C^{18}O_2$, CO, H_2
Summit	Denmark	SUM	0-20008-0-SUM	SUM6002	NOAA	72.58 N	38.48 W	3238	CO_2, CH_4, N_2O, SF_6, $^{13}CH_4$, $^{13}CO_2$, $C^{18}O_2$, CCl_4, CH_3CCl_3, CFCs, HCFCs, HFCs, $CBrClF_2$, $CBrF_3$, $C_2Br_2F_4$, CO, CH_3Cl, CH_2Cl_2, CH_3Br, H_2
Summit	Denmark	SUM	0-20008-0-SUM	SUM6002	INSTAAR	72.58 N	38.48 W	3238	CH_4
Tacolneston Tall Tower	United Kingdom of Great Britain and Northern Ireland	TAC	0-20008-0-TAC	TAC6019	NOAA	52.52 N	1.14 E	56	CO_2, CH_4, N_2O, SF_6, CO, H_2
Tacolneston Tall Tower	United Kingdom of Great Britain and Northern Ireland	TAC	0-20008-0-TAC	TAC6019	AGAGE	52.52 N	1.14 E	56	SF_6, SO_2F_2, CCl_4, CH_3CCl_3, CFCs, HCFCs, HFCs, PFCs, $CBrClF_2$, $CBrF_3$, $C_2Br_2F_4$, $CHCl_3$, CH_3Cl, CH_2Cl_2, CH_3Br, C_2Cl_4
Tacolneston Tall Tower	United Kingdom of Great Britain and Northern Ireland	TAC	0-20008-0-TAC	TAC6019	UNIVBRIS	52.52 N	1.14 E	56	CO_2, CH_4, N_2O, SF_6, CO, H_2

LIST OF OBSERVATIONAL STATIONS (continued)

Station	Country/ Territory	GAW ID	WIGOS ID	WDCGG ID	Organization	Location Latitude (°)	Location Longitude (°)	Elevation (m)	Parameter
Taunus Observatory	Germany	TOB	0-276-1-TOB	TOB6412	AGAGE	50.22 N	8.45 E	825	SF_6, SO_2F_2, NF_3, CCl_4, CH_3CCl_3, CFCs, HCFCs, HFCs, PFCs, $CBrClF_2$, $CBrF_3$, $C_2Br_2F_4$, $CHCl_3$, CH_3Cl, CH_2Cl_2, C_2Cl_4
Teriberka	Russian Federation	TER	0-20008-0-TER	TER6003	MGO	69.20 N	35.10 E	40	CO_2, CH_4
Torfhaus	Germany	TOH	0-20008-0-TOH	TOH6064	DWD	51.81 N	10.53 E	801	CO_2, CH_4, N_2O, CO
Waldhof-Langenbrügge	Germany	WAL	0-20008-0-WAL	WAL6018	UBAG	52.80 N	10.76 E	74	CO_2
Wank	Germany	WNK	0-20008-0-WNK	WNK6029	IMKIFU	47.51 N	11.14 E	1780	CO_2
Westerland	Germany	WES	0-20008-0-WES	WES6010	UBAG	54.92 N	8.31 E	12	CO_2, CH_4
Zeppelin Mountain (Ny Ålesund)	Norway	ZEP	0-20008-0-ZEP	ZEP6001	NOAA	78.91 N	11.89 E	475	CO_2, CH_4, N_2O, SF_6, $^{13}CH_4$, $^{13}CO_2$, $C^{18}O_2$, CO, H_2
Zeppelin Mountain (Ny Ålesund)	Norway	ZEP	0-20008-0-ZEP	ZEP6001	AGAGE	78.91 N	11.89 E	475	SF_6, SO_2F_2, NF_3, CH_3CCl_3, CFCs, HCFCs, HFCs, PFCs, $CBrClF_2$, $CBrF_3$, $C_2Br_2F_4$, $CHCl_3$, CH_3Cl, CH_2Cl_2, CH_3Br, C_2Cl_4
Zeppelin Mountain (Ny Ålesund)	Norway	ZEP	0-20008-0-ZEP	ZEP6001	ITM	78.91 N	11.89 E	475	CO_2
Zeppelin Mountain (Ny Ålesund)	Norway	ZEP	0-20008-0-ZEP	ZEP6001	NILU	78.91 N	11.89 E	475	CO_2, CH_4, N_2O, CFCs
Zingst	Germany	ZGT	0-20008-0-ZGT	ZGT6011	UBAG	54.44 N	12.72 E	1	CO_2, CH_4
Zugspitze-Gipfel	Germany	ZUG	0-20008-0-ZUG	ZUG6030	IMKIFU	47.42 N	10.99 E	2962	CO_2
Zugspitze-Gipfel	Germany	ZUG	0-20008-0-ZUG	ZUG6030	UBAG	47.42 N	10.99 E	2962	CO_2, CH_4, CO
Zugspitze-Schneefernerhaus	Germany	ZSF	0-20008-0-ZSF	ZSF6031	DWD	47.42 N	10.98 E	2666	^{222}Rn, ^{7}Be
Zugspitze-Schneefernerhaus	Germany	ZSF	0-20008-0-ZSF	ZSF6031	UBAG	47.42 N	10.98 E	2666	CO_2, CH_4, N_2O, SF_6, CO
ANTARCTICA									
Arrival Heights	New Zealand	ARH	0-554-0-89668	ARH7009	NIWA	77.83 S	166.66 E	187.41	CH_4, N_2O, $^{13}CH_4$, CO
Casey	Australia	CYA	0-20008-0-CYA	CYA7004	CSIRO	66.28 S	110.52 E	51	CO_2, CH_4, N_2O, $^{13}CO_2$, CO, H_2
Halley	United Kingdom of Great Britain and Northern Ireland	HBA	0-20008-0-HBA	HBA7008	NOAA	75.57 S	25.50 W	30	CO_2, CH_4, N_2O, SF_6, $^{13}CO_2$, $C^{18}O_2$, CO, H_2
Halley	United Kingdom of Great Britain and Northern Ireland	HBA	0-20008-0-HBA	HBA7008	BAS	75.57 S	25.50 W	30	CO
Jubany	Argentina	JBN	0-20008-0-JBN	JBN7002	IAA	62.24 S	58.67 W	15	CO_2
King Sejong	Republic of Korea	KSG	0-20008-0-KSG	KSG7001	KMA	62.22 S	58.78 W	0	CO_2
Mawson	Australia	MAA	0-20008-0-MAA	MAA7005	CSIRO	67.60 S	62.87 E	20	CO_2, CH_4, N_2O, $^{13}CO_2$, CO, H_2
McMurdo	United States of America	MCM	0-20008-0-MCM	MCM7010	NOAA	77.85 S	166.67 E	11	CH_4
Palmer Station	United States of America	PSA	0-20008-0-PSA	PSA7003	NOAA	64.77 S	64.05 W	10	CO_2, CH_4, N_2O, SF_6, $^{13}CO_2$, $C^{18}O_2$, CCl_4, CH_3CCl_3, CFCs, HCFCs, HFCs, $CBrClF_2$, $CBrF_3$, $C_2Br_2F_4$, CO, CH_3Cl, CH_2Cl_2, CH_3Br, H_2
South Pole	United States of America	SPO	0-20008-0-SPO	SPO7011	NOAA	90.00 S	24.80 W	2841	CO_2, CH_4, N_2O, SF_6, $^{13}CH_4$, $^{13}CO_2$, $C^{18}O_2$, CCl_4, CH_3CCl_3, CFCs, HCFCs, HFCs, $CBrClF_2$, $CBrF_3$, $C_2Br_2F_4$, CO, CH_3Cl, CH_2Cl_2, CH_3Br, C_2Cl_4, H_2

LIST OF OBSERVATIONAL STATIONS (continued)

Station	Country/ Territory	GAW ID	WIGOS ID	WDCGG ID	Organization	Location Latitude (°)	Location Longitude (°)	Elevation (m)	Parameter
South Pole	United States of America	SPO	0-20008-0-SPO	SPO7011	CSIRO	90.00 S	24.80 W	2841	CO_2, CH_4, N_2O, $^{13}CO_2$, CO, H_2
Syowa	Japan	SYO	0-20008-0-SYO	SYO7006	NOAA	69.01 S	39.58 E	29.1	CO_2, CH_4, N_2O, SF_6, $^{13}CO_2$, $C^{18}O_2$, CO, H_2
Syowa	Japan	SYO	0-20008-0-SYO	SYO7006	TU	69.01 S	39.58 E	29.1	CO_2, CH_4, $^{13}CH_4$, CH_3D
MOBILE									
Aircraft (Western North Pacific)	Japan	AOA		AOA8002	JMA				CO_2, CH_4, N_2O, CO
Aircraft (Western North Pacific)	Japan	AOA		AOA8002	AIST				O_2/N_2 ratio
Aircraft (off the Pacific coast of Sendai)	Japan	PIP		PIP8043	TU				CH_4
Aircraft (over Bass Strait and Cape Grim)	Australia	AIA		AIA8003	CSIRO				CO_2, CH_4, N_2O, $^{13}CO_2$, CO, H_2
Aircraft (over Japan and mainland)	Japan	TDA		TDA8042	TU				CH_4
Aircraft (over Japan and surroundings)	Japan	OAS		OAS8001	MRI				CH_4, N_2O, SF_6, CFCs
Aircraft: Orleans	France	ORL		ORL8047	LSCE				CO_2, CH_4
Alligator liberty, M/V	Japan	ALL		ALL8049	JMA				CO_2
Atlantic Ocean	United States of America	AOC		AOC8018	NOAA				CO_2, CH_4
CONTRAIL	Japan	EOM		EOM8007	NIES				CO_2, CH_4, SF_6
CONTRAIL	Japan	EOM		EOM8007	TU				$^{13}CH_4$, CH_3D
Drake Passage	United States of America	DRP		DRP8044	NOAA				CO_2, CH_4, N_2O, SF_6, $^{13}CO_2$, $C^{18}O_2$, CO, H_2
INSTAC	Japan	INS		INS8005	MRI				CO_2, CH_4, $^{13}CO_2$
Keifu Maru, R/V	Japan	KEF		KEF8040	JMA				CO_2, CFCs, TIC
Kofu Maru, R/V	Japan	KOF		KOF8008	JMA				CO_2
MRI Research, Hakuho Maru, R/V	Japan	HKH		HKH8030	MRI				CO_2, CH_4
MRI Research, Kaiyo Maru, R/V	Japan	KIY		KIY8017	MRI				CO_2, CO
MRI Research, Natushima, R/V	Japan	NTU		NTU8028	MRI				CO_2, CH_4
MRI Research, Ryofu Maru, R/V	Japan	RFM		RFM8035	MRI				CO_2, CH_4
MRI Research, Ship observations	Japan	MRI		MRI8031	MRI				CH_4
MRI Research, Wellington Maru, R/V	Japan	WLT		WLT8032	MRI				CO_2
Mirai, R/V	Japan	MMR		MMR8009	MRI				CO_2
Mirai, R/V	Japan	MMR		MMR8009	JAMSTEC				CO_2
NOPACCS - Hakurei Maru -	Japan	HAK		HAK8021	NEDO				TIC
Northern and western Pacific	Japan	NWP		NWP8036	TU				CH_4, N_2O, $^{13}CH_4$, CH_3D
Pacific Ocean	United States of America	POC	0-20008-0-POC	POC8034	NOAA				CO_2, CH_4, N_2O, SF_6, $^{13}CO_2$, $C^{18}O_2$, CO, H_2
Pacific Ocean	New Zealand	BSL		BSL8023	NIWA				CH_4, $^{13}CH_4$
Pacific-Atlantic Ocean	United States of America	PAO		PAO8045	NOAA				CO_2, CH_4, N_2O, SF_6, CO
Ryofu Maru, R/V	Japan	RYF	0-20008-0-RYF	RYF8010	JMA				CO_2, CH_4, N_2O, CFCs, TIC
Santarem	Brazil	SAN		SAN8004	INPE				CO_2, CH_4, N_2O, SF_6, CO
Ship between Ishigaki Island and Hateruma Island	Japan	SIH		SIH8048	TU				CO_2
South China Sea	United States of America	SCS		SCS8038	NOAA				CO_2, CH_4, $^{13}CO_2$, $C^{18}O_2$, CO
Soyo Maru, R/V	Japan	SOY		SOY8039	FRA				CO_2
WEST COSMIC - Hakurei Maru No.2 -	Japan	HRM		HRM8050	NEDO				SF_6, CFCs, TIC
Wakataka-Maru	Japan	WAK		WAK8046	FRA				CO_2

LIST OF OBSERVATIONAL STATIONS (continued)

Station	Country/ Territory	GAW ID	WIGOS ID	WDCGG ID	Organization	Location Latitude (°)	Location Longitude (°)	Location Elevation (m)	Parameter
Western Pacific	United States of America	WPC		WPC8029	NOAA				CO_2, CH_4, N_2O, SF_6, $^{13}CH_4$, $^{13}CO_2$, $C^{18}O_2$, CO, H_2

APPENDIX D LIST OF CONTRIBUTORS†

Station Country/Territory Data Providing Organization	Contact Affiliation
REGION I (Africa)	
Mt. Kenya (Kenya) Kenya Meteorological Department (KMD)	Martin Steinbacher Swiss Federal Laboratories for Materials Science and Technology (Empa) Jörg Klausen Federal Office of Meteorology and Climatology MeteoSwiss (MeteoSwiss) Christoph Zellweger Swiss Federal Laboratories for Materials Science and Technology (Empa) Mathew Mutuku Kenya Meteorological Department (KMD) David Murithi Njiru Kenya Meteorological Department (KMD)
Izaña (Tenerife) (Spain) State Meteorological Agency of Spain (AEMET)	Emilio Cuevas State Meteorological Agency of Spain (AEMET) Pedro Rivas State Meteorological Agency of Spain (AEMET) Carlos Torres State Meteorological Agency of Spain (AEMET)
Cape Point (South Africa) Australian Nuclear Science and Technology Organisation (ANSTO)	Alastair Williams Australian Nuclear Science and Technology Organisation (ANSTO) Scott Chambers Australian Nuclear Science and Technology Organisation (ANSTO)
Assekrem (Algeria) Office National de la Meteorologie (ONM)	Sidi Baika Office National de la Meteorologie (ONM)
CAIRO Farafra (Egypt) Egyptian Meteorological Authority (EMA)	AbdElhamid Gouda Elawadi Egyptian Meteorological Authority (EMA) Zeinab Salah Egyptian Meteorological Authority (EMA) Wael Khaled Egyptian Meteorological Authority (EMA)

† See also the web-based list: https://gaw.kishou.go.jp/search/summary.

LIST OF CONTRIBUTORS (continued)

Station Country/Territory Data Providing Organization	Contact Affiliation
Amsterdam Island (France) Laboratoire des Sciences du Climat et de l'Environnement (LSCE)	Michel Ramonet Laboratoire des Sciences du Climat et de l'Environnement (LSCE) Jean Sciare Laboratoire des Sciences du Climat et de l'Environnement (LSCE)
Cape Point (South Africa) South African Weather Service (SAWS)	Thumeka Mkololo South African Weather Service (SAWS) Casper Labuschagne South African Weather Service (SAWS) Lynwill Martin South African Weather Service (SAWS)
Cape Verde Atmospheric Observatory (Cabo Verde) University of Exeter (UoE)	E Kozlova University of Exeter (UoE)
Cape Verde Atmospheric Observatory (Cabo Verde) University of York (UYRK)	Katie Read University of York (UYRK) Lucy Carpenter University of York (UYRK)
REGION II (Asia)	
Hamamatsu (Japan) Shizuoka University (SHIZU)	Mitsuo Toda Shizuoka University (SHIZU)
Cholpon-Ata (Kyrgyzstan) Agency on Hydrometeorology under Ministry of Emergency Situations of the Kyrgyz Republic (Kyrgyzhydromet)	Martin Steinbacher Swiss Federal Laboratories for Materials Science and Technology (Empa) Gulzhan Esenzhanova Agency on Hydrometeorology under Ministry of Emergency Situations of the Kyrgyz Republic (Kyrgyzhydromet)
Cape Ochiishi Hateruma Island (Japan) National Institute for Environmental Studies (NIES)	Yasunori TOHJIMA National Institute for Environmental Studies (NIES) Hitoshi MUKAI National Institute for Environmental Studies (NIES) Takuya Saito National Institute for Environmental Studies (NIES)

LIST OF CONTRIBUTORS (continued)

Station Country/Territory Data Providing Organization	Contact Affiliation
	Yukio TERAO National Institute for Environmental Studies (NIES)
Memanbetsu Tateno (Tsukuba) (Japan) Meteorological Research Institute (MRI)	Kazuhiro Tsuboi Meteorological Research Institute (MRI)
CHICHIJIMA (Japan) Meteorological Research Institute (MRI)	Kentaro ISHIJIMA Meteorological Research Institute (MRI) Kazuhiro Tsuboi Meteorological Research Institute (MRI)
Minamitorishima Ryori Yonagunijima (Japan) Meteorological Research Institute (MRI)	Kentaro ISHIJIMA Meteorological Research Institute (MRI)
Minamitorishima Ryori Yonagunijima (Japan) Japan Meteorological Agency (JMA)	TAKATSUJI Shinya Japan Meteorological Agency (JMA)
Bering Island Kotelnyj Island Tiksi (Russian Federation) Kyzylcha (Uzbekistan) Voeikov Main Geophysical Observatory (MGO)	Nina Paramonova Voeikov Main Geophysical Observatory (MGO)
Mt. Waliguan (China) China Meteorological Administration (CMA)	LIANG Miao China Meteorological Administration (CMA)
Kisai Mt. Dodaira Urawa (Japan) Center for Environmental Science in Saitama (SAIPF)	Yosuke MUTO Center for Environmental Science in Saitama (SAIPF)
Gosan (Republic of Korea) National Institute of Meteorological Research, KMA (METRI)	SE-HWAN YANG Korea Meteorological Administration (KMA)

LIST OF CONTRIBUTORS (continued)

Station Country/Territory Data Providing Organization	Contact Affiliation
Tiksi (Russian Federation) Finnish Meteorological Institute (FMI)	Ed Dlugokencky Global Monitoring Laboratory, NOAA (NOAA) Juha Hatakka Finnish Meteorological Institute (FMI) Viktor Ivakhov Voeikov Main Geophysical Observatory (MGO) Tuomas Laurila Finnish Meteorological Institute (FMI)
Ryori (Japan) National Institute of Advanced Industrial Science and Technology (AIST)	Shigeyuki Ishidoya National Institute of Advanced Industrial Science and Technology (AIST)
Takayama (Japan) National Institute of Advanced Industrial Science and Technology (AIST)	Shohei Murayama National Institute of Advanced Industrial Science and Technology (AIST)
Nepal Climate Observatory - Pyramid (Nepal) University of Urbino, Dep. of Pure and Applied Sciences (DISPEA) (UNIURB)	Jgor Arduini University of Urbino, Dep. of Pure and Applied Sciences (DISPEA) (UNIURB)
Hok Tsui / Cape d Aguilar King's Park (Hong Kong, China) Hong Kong Observatory (HKO)	W.H. Leung Hong Kong Observatory (HKO) M.C.Lam Hong Kong Observatory (HKO)
Anmyeon-do Gosan (Republic of Korea) Korea Meteorological Administration (KMA)	Daegeun Shin Korea Meteorological Administration (KMA) SE-HWAN YANG Korea Meteorological Administration (KMA)
Ulleungdo (Republic of Korea) Korea Meteorological Administration (KMA)	SE-HWAN YANG Korea Meteorological Administration (KMA)
Hok Tsui / Cape d Aguilar (Hong Kong, China) The Hong Kong Polytechnic University (PolyU)	Ka Se Lam The Hong Kong Polytechnic University (PolyU)

LIST OF CONTRIBUTORS (continued)

Station Country/Territory Data Providing Organization	Contact Affiliation
Pha Din (Viet Nam) Viet Nam Meteorological and Hydrological Administration (VNMHA)	Martin Steinbacher Swiss Federal Laboratories for Materials Science and Technology (Empa) Nguyen Nhat Anh Viet Nam Meteorological and Hydrological Administration (VNMHA)
Issyk-Kul (Kyrgyzstan) Kyrgyz National University (KSNU)	V. Sinyakov Kyrgyz National University (KSNU)
Gosan (Republic of Korea) National Institute of Environmental Research (GERC)	Jiyoung Kim National Institute of Environmental Research (GERC) Eunjung Kim National Institute of Environmental Research (GERC)
Suita (Japan) Osaka University (OSAKAU)	Tomohiro Oda Universities Space Research Association (USRA) Takashi Machimura Osaka University (OSAKAU)
Nagoya (Japan) Nagoya University (NAGOU)	A. Matsunami Nagoya University (NAGOU)
Mikawa-Ichinomiya (Japan) Aichi Air Environment Division (AICH)	Koji Ohno Aichi Air Environment Division (AICH)
REGION III (South America)	
El Tololo (Chile) Direccion Meteorologica de Chile (DMC)	Martin Steinbacher Swiss Federal Laboratories for Materials Science and Technology (Empa) Gaston Torres Direccion Meteorologica de Chile (DMC)
Huancayo (Peru) Instituto Geofisico del Peru (IGP)	Mutsumi Ishitsuka Instituto Geofisico del Peru (IGP)
Arembepe (Brazil) National Institute in Space Research (INPE)	Luciana Vanni Gatti National Institute in Space Research (INPE)

LIST OF CONTRIBUTORS (continued)

Station Country/Territory Data Providing Organization	Contact Affiliation
Ushuaia (Argentina) National Weather Service (SMNA)	Maria Elena Barlasina National Weather Service (SMNA) Lino Condori National Weather Service (SMNA) Gerardo Carbajal Benítez National Weather Service (SMNA)
REGION IV (North and Central America)	
Churchill (Canada) Tohoku University (TU)	Shinji Morimoto Tohoku University (TU)
Alert Churchill East Trout Lake Estevan Point Fraserdale Sable Island (Canada) Environment and Climate Change Canada (ECCC)	Lin Huang Environment and Climate Change Canada (ECCC) Doug Worthy Environment and Climate Change Canada (ECCC)
Behchoko Bratt's Lake Cambridge Bay Candle Lake Chapais Chibougamau Egbert Esther Inuvik Lac La Biche (Alberta) (Canada) Environment and Climate Change Canada (ECCC)	Doug Worthy Environment and Climate Change Canada (ECCC)
REGION V (South-West Pacific)	
Kennaook / Cape Grim (Australia) Australian Nuclear Science and Technology Organisation (ANSTO)	Alastair Williams Australian Nuclear Science and Technology Organisation (ANSTO) Scott Chambers Australian Nuclear Science and Technology Organisation (ANSTO)
Macquarie Island (Australia) Commonwealth Scientific and Industrial Research Organisation (CSIRO)	Paul Krummel Commonwealth Scientific and Industrial Research Organisation (CSIRO)

Station Country/Territory Data Providing Organization	Contact Affiliation
	Zoë Loh Commonwealth Scientific and Industrial Research Organisation (CSIRO) Ann Stavert Commonwealth Scientific and Industrial Research Organisation (CSIRO)
Kennaook / Cape Grim (Australia) Commonwealth Scientific and Industrial Research Organisation (CSIRO)	Paul Krummel Commonwealth Scientific and Industrial Research Organisation (CSIRO) Ray Langenfelds Commonwealth Scientific and Industrial Research Organisation (CSIRO) Zoë Loh Commonwealth Scientific and Industrial Research Organisation (CSIRO)
Lauder (New Zealand) National Institute of Water & Atmospheric Research Ltd. (NIWA)	Sylvia Nichol National Institute of Water & Atmospheric Research Ltd. (NIWA) Gordon Brailsford National Institute of Water & Atmospheric Research Ltd. (NIWA)
Baring Head (New Zealand) National Institute of Water & Atmospheric Research Ltd. (NIWA)	Jocelyn Turnbull GNS Science (GNS) Sylvia Nichol National Institute of Water & Atmospheric Research Ltd. (NIWA) Gordon Brailsford National Institute of Water & Atmospheric Research Ltd. (NIWA)
Danum Valley (Malaysia) Malaysian Meteorological Department (MMD)	Ahmad Fairudz Jamaluddin Malaysian Meteorological Department (MMD) Mohan Kumar Sammathuria Malaysian Meteorological Department (MMD)
Bukit Kototabang (Indonesia) Agency for Meteorology, Climatology and Geophysics (BMKG)	Martin Steinbacher Swiss Federal Laboratories for Materials Science and Technology (Empa) Okaem, Tanti Tritama Agency for Meteorology, Climatology and Geophysics (BMKG)

Station Country/Territory Data Providing Organization	Contact Affiliation
	Nahas, Alberth Christian Agency for Meteorology, Climatology and Geophysics (BMKG) Reza Mahdi Agency for Meteorology, Climatology and Geophysics (BMKG) Arifin, Ikhsan Buyung Agency for Meteorology, Climatology and Geophysics (BMKG)
REGION VI (Europe)	
BEO Moussala (Bulgaria) Institute for Nuclear Research and Nuclear Energy (INRNE)	Todor Arsov Institute for Nuclear Research and Nuclear Energy (INRNE)
Kloosterburen Kollumerwaard (Kingdom of the Netherlands) National Institute of Public Health and the Environment (RIVM)	Ronald Spoor National Institute of Public Health and the Environment (RIVM)
Ny Ålesund (Norway) Tohoku University (TU)	Taku Umezawa National Institute for Environmental Studies (NIES) Shinji Morimoto Tohoku University (TU) Ryo Fujita Meteorological Research Institute (MRI)
Brotjacklriegel Deuselbach Neuglobsow Waldhof-Langenbrügge Zingst (Germany) German Environment Agency (UBAG)	Ludwig Ries German Environment Agency (UBAG)
Westerland Zugspitze-Schneefernerhaus (Germany) German Environment Agency (UBAG)	Cedric Couret German Environment Agency (UBAG)
Schauinsland (Germany) German Environment Agency (UBAG)	Frank Meinhardt German Environment Agency (UBAG)

LIST OF CONTRIBUTORS (continued)

Station Country/Territory Data Providing Organization	Contact Affiliation
Zugspitze-Gipfel (Germany) German Environment Agency (UBAG)	Ludwig Ries German Environment Agency (UBAG) Cedric Couret German Environment Agency (UBAG)
SONNBLICK Observatory (Austria) Federal Environment Agency Austria (UBAA)	Wolfgang Spangl Federal Environment Agency Austria (UBAA) Iris Buxbaum Federal Environment Agency Austria (UBAA) Andreas Wolf Federal Environment Agency Austria (UBAA)
Puy de Dôme (France) Laboratoire de Météorologie Physique (LAMP)	Meyerfeld Yves Laboratoire d'Aérologie (LA) Pichon Jean-Marc Laboratoire de Météorologie Physique (LAMP)
Pallas (Finland) Finnish Meteorological Institute (FMI)	Juha Hatakka Finnish Meteorological Institute (FMI)
Monte Cimone (Italy) University of Urbino, Dep. of Pure and Applied Sciences (DISPEA) (UNIURB)	Jgor Arduini University of Urbino, Dep. of Pure and Applied Sciences (DISPEA) (UNIURB)
Kecskemét K-puszta háttérszennyettség-mérő állomás (Hungary) Hungarian Meteorological Service (HMS)	Laszlo Haszpra Institute for Nuclear Research (ATOMKI)
Giordan Lighthouse (Malta) University of Malta (UMLT)	Martin Saliba University of Malta (UMLT) Marvic Grima University of Malta (UMLT) Alfred Micallef University of Malta (UMLT)
Lampedusa (Italy) Italian National Agency for New Technologies, Energy and Sustainable Economic Development (ENEA)	Salvatore Chiavarini Italian National Agency for New Technologies, Energy and Sustainable Economic Development (ENEA) Damiano Sferlazzo Italian National Agency for New Technologies, Energy and Sustainable Economic Development (ENEA)

LIST OF CONTRIBUTORS (continued)

Station Country/Territory Data Providing Organization	Contact Affiliation
	Alcide di Sarra Italian National Agency for New Technologies, Energy and Sustainable Economic Development (ENEA) Salvatore Piacentino Italian National Agency for New Technologies, Energy and Sustainable Economic Development (ENEA) Tatiana Di Iorio Italian National Agency for New Technologies, Energy and Sustainable Economic Development (ENEA) Francesco Monteleone Italian National Agency for New Technologies, Energy and Sustainable Economic Development (ENEA)
Madonie - Piano Battaglia (Italy) Italian National Agency for New Technologies, Energy and Sustainable Economic Development (ENEA)	Damiano Sferlazzo Italian National Agency for New Technologies, Energy and Sustainable Economic Development (ENEA) Alcide di Sarra Italian National Agency for New Technologies, Energy and Sustainable Economic Development (ENEA) Salvatore Piacentino Italian National Agency for New Technologies, Energy and Sustainable Economic Development (ENEA) Tatiana Di Iorio Italian National Agency for New Technologies, Energy and Sustainable Economic Development (ENEA) Francesco Monteleone Italian National Agency for New Technologies, Energy and Sustainable Economic Development (ENEA) Fabrizio Anello Italian National Agency for New Technologies, Energy and Sustainable Economic Development (ENEA)
Wank Zugspitze-Gipfel (Germany) Fraunhofer-Institute for Atmospheric Environmental Research (IMKIFU)	Thomas Trickl Fraunhofer-Institute for Atmospheric Environmental Research (IMKIFU)
Diabla Gora / Puszcza Borecka (Poland) Institute of Environmental Protection - NRI (IOEP)	Zdzislaw Przadka Institute of Environmental Protection - NRI (IOEP) Anna Degorska Institute of Environmental Protection - NRI (IOEP)

LIST OF CONTRIBUTORS (continued)

Station Country/Territory Data Providing Organization	Contact Affiliation
	Krzysztof Skotak Institute of Environmental Protection - NRI (IOEP)
Monte Curcio (Italy) CNR-Institute of Atmospheric Pollution Research (IIA)	Mariantonia Bencardino CNR-Institute of Atmospheric Pollution Research (IIA)
Jungfraujoch (Switzerland) Physics Institute, Climate and Environmental Physics, University of Bern (KUP)	Markus Leuenberger Physics Institute, Climate and Environmental Physics, University of Bern (KUP)
Bilsdale Ridge Hill Tacolneston Tall Tower (United Kingdom of Great Britain and Northern Ireland) Atmospheric Chemistry Research Group School of Chemistry University of Bristol (UNIVBRIS)	Simon O'Doherty Atmospheric Chemistry Research Group School of Chemistry University of Bristol (UNIVBRIS) Kieran Stanley Atmospheric Chemistry Research Group School of Chemistry University of Bristol (UNIVBRIS) Joseph Pitt Atmospheric Chemistry Research Group School of Chemistry University of Bristol (UNIVBRIS)
Heathfield (United Kingdom of Great Britain and Northern Ireland) National Physical Laboratory (NPL)	Chris Rennick National Physical Laboratory (NPL)
Ocean Station Charlie (United States of America) Voeikov Main Geophysical Observatory (MGO)	Nina Paramonova Voeikov Main Geophysical Observatory (MGO)
Teriberka (Russian Federation) Voeikov Main Geophysical Observatory (MGO)	Nina Paramonova Voeikov Main Geophysical Observatory (MGO) Viktor Ivakhov Voeikov Main Geophysical Observatory (MGO)
Hegyhátsál háttérszennyettség-mérő állomás (Hungary) Institute for Nuclear Research (ATOMKI)	Laszlo Haszpra Institute for Nuclear Research (ATOMKI)
Jungfraujoch (Switzerland) Swiss Federal Laboratories for Materials Science and Technology (Empa)	Martin Steinbacher Swiss Federal Laboratories for Materials Science and Technology (Empa) Thomas Seitz Swiss Federal Laboratories for Materials Science and Technology (Empa)

LIST OF CONTRIBUTORS (continued)

Station Country/Territory Data Providing Organization	Contact Affiliation
Payerne Rigi (Switzerland) Swiss Federal Laboratories for Materials Science and Technology (Empa)	Thomas Seitz Swiss Federal Laboratories for Materials Science and Technology (Empa)
Monte Cimone (Italy) Italian Air Force Mountain Centre (IAFMS)	Stefano Amendola Italian Air Force Mountain Centre (IAFMS) Felice Dipace Italian Air Force Mountain Centre (IAFMS) Luigi Lauria Italian Air Force Mountain Centre (IAFMS)
Plateau Rosa (Italy) Ricerca sul Sistema Energetico - RSE S.p.A. (RSE)	Francesco Apadula Ricerca sul Sistema Energetico - RSE S.p.A. (RSE) Andrea Lanza Ricerca sul Sistema Energetico - RSE S.p.A. (RSE)
Fundata (Romania) National Meteorological Administration (INMH)	Florin Nicodim National Meteorological Administration (INMH)
Kosetice Observatory (Czech Republic) Czech Hydrometeorological Institute (CHMI)	Adéla Holubová Czech Hydrometeorological Institute (CHMI)
Krvavec (Slovenia) Slovenian Environment Agency (ARSO)	Mateja Gjerek Slovenian Environment Agency (ARSO) Tanja Koleša Slovenian Environment Agency (ARSO) Primož Dolenc Slovenian Environment Agency (ARSO)
Zeppelin Mountain (Ny Ålesund) (Norway) Department of Applied Environmental Science, Stockholm University (ITM)	Hans-Christen Department of Applied Environmental Science, Stockholm University (ITM) Birgitta Noone Department of Applied Environmental Science, Stockholm University (ITM)

LIST OF CONTRIBUTORS (continued)

Station Country/Territory Data Providing Organization	Contact Affiliation
Summit (Denmark) Institute of Arctic and Alpine Research, University of Colorado (INSTAAR)	Jacques Hueber Institute of Arctic and Alpine Research, University of Colorado (INSTAAR) Detlev Helmig Institute of Arctic and Alpine Research, University of Colorado (INSTAAR)
Finokalia (Greece) Mace Head (Ireland) Begur (Spain) Ile Grande Pic du Midi Puy de Dôme (France) Laboratoire des Sciences du Climat et de l'Environnement (LSCE)	Michel Ramonet Laboratoire des Sciences du Climat et de l'Environnement (LSCE)
Lamezia Terme (Italy) National Research Council, Institute of Atmospheric Sciences and Climate (ISAC)	Daniel Gullì National Research Council, Institute of Atmospheric Sciences and Climate (ISAC) Claudia Calidonna National Research Council, Institute of Atmospheric Sciences and Climate (ISAC) Ivano Ammoscato National Research Council, Institute of Atmospheric Sciences and Climate (ISAC)
Lecce Environmental-Climate Observatory (Italy) National Research Council, Institute of Atmospheric Sciences and Climate (ISAC)	Adelaide Dinoi National Research Council, Institute of Atmospheric Sciences and Climate (ISAC)
Capo Granitola (Italy) National Research Council, Institute of Atmospheric Sciences and Climate (ISAC)	Paolo Cristofanelli National Research Council, Institute of Atmospheric Sciences and Climate (ISAC) Ignazio Fontana Istituto per lo studio degli impatti Antropici e Sostenibilità in ambiente marino (IASCNR) Giorgio Tranchida Istituto per lo studio degli impatti Antropici e Sostenibilità in ambiente marino (IASCNR)

LIST OF CONTRIBUTORS (continued)

Station Country/Territory Data Providing Organization	Contact Affiliation
	Giovanni Giacalone Istituto per lo studio degli impatti Antropici e Sostenibilità in ambiente marino (IASCNR) Maurizio Busetto National Research Council, Institute of Atmospheric Sciences and Climate (ISAC) Francescopiero Calzolari National Research Council, Institute of Atmospheric Sciences and Climate (ISAC)
Monte Cimone (Italy) National Research Council, Institute of Atmospheric Sciences and Climate (ISAC)	Jgor Arduini University of Urbino, Dep. of Pure and Applied Sciences (DISPEA) (UNIURB) Michela Maione University of Urbino, Dep. of Pure and Applied Sciences (DISPEA) (UNIURB) Paolo Cristofanelli National Research Council, Institute of Atmospheric Sciences and Climate (ISAC) Francescopiero Calzolari National Research Council, Institute of Atmospheric Sciences and Climate (ISAC)
Zugspitze-Schneefernerhaus (Germany) German Meteorological Service (DWD)	Gabriele Frank German Meteorological Service (DWD)
Hohenpeissenberg (Germany) German Meteorological Service (DWD)	Dagmar Kubistin German Meteorological Service (DWD) Robert Holla German Meteorological Service (DWD) Matthias Lindauer German Meteorological Service (DWD) Christian Plass-Dulmer German Meteorological Service (DWD) Jennifer Müller-Williams German Meteorological Service (DWD)
Gartow Helgoland Jülich Karlsruhe Lindenberg	Dagmar Kubistin German Meteorological Service (DWD) Matthias Lindauer German Meteorological Service (DWD)

LIST OF CONTRIBUTORS (continued)

Station Country/Territory Data Providing Organization	Contact Affiliation
Ochsenkopf Steinkimmen Torfhaus (Germany) German Meteorological Service (DWD)	Christian Plass-Dulmer German Meteorological Service (DWD) Jennifer Müller-Williams German Meteorological Service (DWD)
Pic du Midi (France) Laboratoire d'Aérologie (LA)	Meyerfeld Yves Laboratoire d'Aérologie (LA) Gheusi Francois Laboratoire d'Aérologie (LA)
Zeppelin Mountain (Ny Ålesund) (Norway) Norwegian Institute for Air Research (NILU)	Ove Hermansen Norwegian Institute for Air Research (NILU) Tove Svendby Norwegian Institute for Air Research (NILU) Stephen Matthew Platt Norwegian Institute for Air Research (NILU)
ANTARCTICA	
Syowa (Japan) Tohoku University (TU)	Taku Umezawa National Institute for Environmental Studies (NIES) Shinji Morimoto Tohoku University (TU) Daisuke Goto National Institute of Polar Research (NIPR) Ryo Fujita Meteorological Research Institute (MRI)
Jubany (Argentina) Direcion Nacional del Antartico- Istituto Antartico Argentino, Buenos Aires, Argentina (IAA)	Horacio Rodriguez Direcion Nacional del Antartico- Istituto Antartico Argentino, Buenos Aires, Argentina (IAA) Angelo Viola National Research Council, Institute of Atmospheric Sciences and Climate (ISAC)
Arrival Heights (New Zealand) National Institute of Water & Atmospheric Research Ltd. (NIWA)	Sylvia Nichol National Institute of Water & Atmospheric Research Ltd. (NIWA)

LIST OF CONTRIBUTORS (continued)

Station Country/Territory Data Providing Organization	Contact Affiliation
	Gordon Brailsford National Institute of Water & Atmospheric Research Ltd. (NIWA)
King Sejong (Republic of Korea) Korea Meteorological Administration (KMA)	SE-HWAN YANG Korea Meteorological Administration (KMA)
Halley (United Kingdom of Great Britain and Northern Ireland) British Antarctic Survey (BAS)	Freya Squires British Antarctic Survey (BAS)
MOBILE	
Northern and western Pacific (Japan) Tohoku University (TU)	Taku Umezawa National Institute for Environmental Studies (NIES) Kentaro ISHIJIMA Meteorological Research Institute (MRI) Shinji Morimoto Tohoku University (TU) Ryo Fujita Meteorological Research Institute (MRI)
Aircraft (off the Pacific coast of Sendai) Aircraft (over Japan and mainland) CONTRAIL (Japan) Tohoku University (TU)	Taku Umezawa National Institute for Environmental Studies (NIES) Shinji Morimoto Tohoku University (TU)
Ship between Ishigaki Island and Hateruma Island (Japan) Tohoku University (TU)	Shinji Morimoto Tohoku University (TU)
Soyo Maru, R/V Wakataka-Maru (Japan) Fisheries Research Agency (FRA)	Tsuneo Ono Fisheries Research Agency (FRA)
Aircraft (Western North Pacific) (Japan) Japan Meteorological Agency (JMA)	TAKATSUJI Shinya Japan Meteorological Agency (JMA)
Alligator liberty, M/V Keifu Maru, R/V Kofu Maru, R/V	ENYO Kazutaka Japan Meteorological Agency (JMA)

LIST OF CONTRIBUTORS (continued)

Station Country/Territory Data Providing Organization	Contact Affiliation
Ryofu Maru, R/V (Japan) Japan Meteorological Agency (JMA)	ONO Etsuro Japan Meteorological Agency (JMA)
Pacific Ocean (New Zealand) National Institute of Water & Atmospheric Research Ltd. (NIWA)	Sylvia Nichol National Institute of Water & Atmospheric Research Ltd. (NIWA) Gordon Brailsford National Institute of Water & Atmospheric Research Ltd. (NIWA)
CONTRAIL (Japan) National Institute for Environmental Studies (NIES)	Kentaro ISHIJIMA Meteorological Research Institute (MRI) Yousuke Sawa Meteorological Research Institute (MRI) Toshinobu Machida National Institute for Environmental Studies (NIES) Yosuke Niwa National Institute for Environmental Studies (NIES)
Mirai, R/V (Japan) Japan Agency for Marine-Earth Science and Technology (JAMSTEC)	Akihiko Murata Japan Agency for Marine-Earth Science and Technology (JAMSTEC)
MRI Research, Wellington Maru, R/V Mirai, R/V (Japan) Meteorological Research Institute (MRI)	Masao Ishii Meteorological Research Institute (MRI)
Aircraft (over Japan and surroundings) (Japan) Meteorological Research Institute (MRI)	Kazuhiro Tsuboi Meteorological Research Institute (MRI)
INSTAC MRI Research, Hakuho Maru, R/V MRI Research, Kaiyo Maru, R/V MRI Research, Natushima, R/V MRI Research, Ryofu Maru, R/V MRI Research, Ship observations (Japan) Meteorological Research Institute (MRI)	Hidekazu Matsueda Meteorological Research Institute (MRI) Masao Ishii Meteorological Research Institute (MRI) Kazuhiro Tsuboi Meteorological Research Institute (MRI)
Aircraft (Western North Pacific) (Japan) National Institute of Advanced Industrial Science and	Shigeyuki Ishidoya National Institute of Advanced Industrial Science and Technology (AIST)

LIST OF CONTRIBUTORS (continued)

Station Country/Territory Data Providing Organization	Contact Affiliation
Technology (AIST)	
NOPACCS - Hakurei Maru - WEST COSMIC - Hakurei Maru No.2 - (Japan) New Energy and Industrial Technology Development Organization (NEDO)	KANSO TECHNOS KANSO TECHNOS CO., LTD. (Old:Kansai Environmental Engineering Center, Co., Ltd.) (KANSO)
Santarem (Brazil) National Institute in Space Research (INPE)	Luciana Vanni Gatti National Institute in Space Research (INPE)
Aircraft: Orleans (France) Laboratoire des Sciences du Climat et de l'Environnement (LSCE)	Michel Ramonet Laboratoire des Sciences du Climat et de l'Environnement (LSCE)

Data Providing Organization Station Country/Territory	Contact Affiliation

NOAA /GML Flask Network

Global Monitoring Laboratory, NOAA (NOAA)
Institute of Arctic and Alpine Research, University of Colorado (INSTAAR)

Ushuaia
(Argentina)

Kennaook / Cape Grim
(Australia)

Ragged Point
(Barbados)

Arembepe
Natal
(Brazil)

Alert
Lac La Biche (Alberta)
Mould Bay
(Canada)

Easter Island
(Chile)

Mt. Waliguan
Shangdianzi
(China)

Hohenpeissenberg
Ochsenkopf
(Germany)

Summit
(Denmark)

Assekrem
(Algeria)

Izaña (Tenerife)
(Spain)

Pallas
(Finland)

Amsterdam Island
Crozet
(France)

Ascension Island
Bird Island (South Georgia)
Halley
St. David's Head
Tacolneston Tall Tower
Tudor Hill (Bermuda)
(United Kingdom of Great Britain and Northern Ireland)

Kirk Thoning
Global Monitoring Laboratory, NOAA (NOAA)
(CO_2 and CH_4)

Xin Lan
Global Monitoring Laboratory, NOAA (NOAA)
(CO_2, CH_4, N_2O and SF_6)

Colm Sweeney
Global Monitoring Laboratory, NOAA (NOAA)
(CO_2, CH_4, N_2O, SF_6, CO and H_2)

Reid Clark
Institute of Arctic and Alpine Research, University of Colorado (INSTAAR)
($^{13}CH_4$)

Sylvia Michel
Institute of Arctic and Alpine Research, University of Colorado (INSTAAR)

Bruce H Vaughn
Institute of Arctic and Alpine Research, University of Colorado (INSTAAR)
($^{13}CH_4$, $^{13}CO_2$ and $C^{18}O_2$)

James White
Institute of Arctic and Alpine Research, University of Colorado (INSTAAR)
($^{13}CO_2$ and $C^{18}O_2$)

Gabrielle Petron
Global Monitoring Laboratory, NOAA (NOAA)
(CO and H_2)

Scott Lehman
Institute of Arctic and Alpine Research, University of Colorado (INSTAAR)

Jocelyn Turnbull
GNS Science (GNS)
($^{14}CO_2$)

Data Providing Organization Station Country/Territory	Contact Affiliation

Hegyhátsál háttérszennyettség-mérő állomás
(Hungary)

Bukit Kototabang
(Indonesia)

Mace Head
(Ireland)

Sede Boker
(Israel)

Storhofdi
(Iceland)

Lampedusa
(Italy)

Syowa
(Japan)

Mt. Kenya
(Kenya)

Christmas Island
(Kiribati)

Anmyeon-do
Tae-ahn Peninsula
(Republic of Korea)

Plateau Assy
Sary Taukum
(Kazakhstan)

Ulaan Uul
(Mongolia)

Dwejra Point
(Malta)

Kaashidhoo (Male Atoll)
(Maldives)

Mex High Altitude Global Climate Observation Center
(Mexico)

Gobabeb
(Namibia)

Ocean Station M
Zeppelin Mountain (Ny Ålesund)
(Norway)

Baring Head
Kaitorete Spit
(New Zealand)

Data Providing Organization Station Country/Territory	Contact Affiliation
Baltic Sea (Poland)	
Serreta (Terceira) (Portugal)	
Constanta (Black Sea) (Romania)	
Tiksi (Russian Federation)	
Mahé (Seychelles)	
Lulin (Taiwan, province of China)	
Argyle (ME) Atlantic Ocean Barrow (AK) Cape Kumukahi (HI) Cape Meares (OR) Cold Bay (AK) Drake Passage Grifton - Georgia Station (NC) Guam (Mariana Island) Key Biscane (FL) Kitt Peak (AZ) La Jolla (CA) Mauna Kea (HI) Mauna Loa (HI) McMurdo Moody (TX) Niwot Ridge - T-van (CO) Ocean Station Charlie Olympic Peninsula (WA) Pacific Ocean Pacific-Atlantic Ocean Palmer Station Park Falls (WI) Point Arena (CA) Samoa (Cape Matatula) Sand Island Shemya Island South China Sea South Pole Southern Great Plains E13 (OK) St. Croix Trinidad Head (CA) Wendover (UT) West Branch (Iowa) Western Pacific (United States of America)	
Cape Point (South Africa)	

Data Providing Organization Station Country/Territory	Contact Affiliation

NOAA /GML HATS Network

Global Monitoring Laboratory, NOAA (NOAA)
Halocarbons and Other Atmospheric Trace Species Group (HATS)

Ushuaia
(Argentina)

Kennaook / Cape Grim
(Australia)

Alert
(Canada)

Summit
(Denmark)

Mace Head
(Ireland)

Anmyeon-do
(Republic of Korea)

Barrow (AK)
Cape Kumukahi (HI)
Grifton - Georgia Station (NC)
Harvard Forest (MA)
Mauna Loa (HI)
Niwot Ridge - T-van (CO)
Palmer Station
Park Falls (WI)
Samoa (Cape Matatula)
South Pole
Trinidad Head (CA)
(United States of America)

Debra J. Mondeel
Global Monitoring Laboratory, NOAA (NOAA)
J. David Nance
Global Monitoring Laboratory, NOAA (NOAA)
Stephen A. Montzka
Global Monitoring Laboratory, NOAA (NOAA)
Bradley D. Hall
Global Monitoring Laboratory, NOAA (NOAA)
Geoffrey S. Dutton
Global Monitoring Laboratory, NOAA (NOAA)
Isaac Vimont
Global Monitoring Laboratory, NOAA (NOAA)

Data Providing Organization Station Country/Territory	Contact Affiliation

CSIRO Flask Network

Commonwealth Scientific and Industrial Research Organisation (CSIRO)

Aircraft (over Bass Strait and Cape Grim)
Cape Ferguson
Casey
Gunn Point
Kennaook / Cape Grim
Macquarie Island
Mawson
(Australia)

Alert
Estevan Point
(Canada)

Lerwick
(United Kingdom of Great Britain and Northern Ireland)

Cape Rama
(India)

Mauna Loa (HI)
South Pole
(United States of America)

Ann Stavert
Commonwealth Scientific and Industrial Research Organisation (CSIRO)

Zoë Loh
Commonwealth Scientific and Industrial Research Organisation (CSIRO)

Ray Langenfelds
Commonwealth Scientific and Industrial Research Organisation (CSIRO)

Elise Guerette
Commonwealth Scientific and Industrial Research Organisation (CSIRO)

Paul Krummel
Commonwealth Scientific and Industrial Research Organisation (CSIRO)

ALE/GAGE/AGAGE Network

Advanced Global Atmospheric Gases Experiment Science Team(AGAGE) (AGAGE)

Kennaook / Cape Grim
(Australia)

Ragged Point
(Barbados)

Jungfraujoch
(Switzerland)

Taunus Observatory
(Germany)

Tacolneston Tall Tower
(United Kingdom of Great Britain and Northern Ireland)

Adrigole
Mace Head
(Ireland)

Monte Cimone
(Italy)

Gosan
(Republic of Korea)

Jooil Kim
Scripps Institution of Oceanography (SIO)

Dickon Young
Atmospheric Chemistry Research Group School of Chemistry University of Bristol (UNIVBRIS)

Ray Wang
School of Earth and Atmospheric Sciences, Georgia Institute of Technology (EAS)

Simon O'Doherty
Atmospheric Chemistry Research Group School of Chemistry University of Bristol (UNIVBRIS)

Paul Fraser
Commonwealth Scientific and Industrial Research Organisation (CSIRO)

Paul Krummel
Commonwealth Scientific and Industrial Research Organisation (CSIRO)

Jens Mühle
Scripps Institution of Oceanography (SIO)

Ray F. Weiss
Scripps Institution of Oceanography (SIO)

LIST OF CONTRIBUTORS (continued)

Data Providing Organization Station Country/Territory	Contact Affiliation
Zeppelin Mountain (Ny Ålesund) (Norway)	Christina Harth Scripps Institution of Oceanography (SIO) Stefan Reimann Swiss Federal Laboratories for Materials Science and Technology (Empa) Martin Vollmer Swiss Federal Laboratories for Materials Science and Technology (Empa) Michela Maione University of Urbino, Dep. of Pure and Applied Sciences (DISPEA) (UNIURB) Jgor Arduini University of Urbino, Dep. of Pure and Applied Sciences (DISPEA) (UNIURB) Andreas Engel Goethe University Frankfurt (GU) Thomas Wagenhäuser Goethe University Frankfurt (GU) Chris Lunder Norwegian Institute for Air Research (NILU) Ove Hermansen Norwegian Institute for Air Research (NILU) Kieran Stanley Atmospheric Chemistry Research Group School of Chemistry University of Bristol (UNIVBRIS) Sunyoung Park Kyungpook National University (KNU)
Cape Meares (OR) Samoa (Cape Matatula) Trinidad Head (CA) (United States of America)	

APPENDIX E LIST OF ABBREVIATIONS

ORGANIZATIONS:

AEMET	State Meteorological Agency of Spain (Spain)
AGAGE	Advanced Global Atmospheric Gases Experiment Science Team
AICH	Aichi Air Environment Division (Japan)
AIST	National Institute of Advanced Industrial Science and Technology (Japan)
ANSTO	Australian Nuclear Science and Technology Organisation (Australia)
ARSO	Slovenian Environment Agency (Slovenia)
ATOMKI	Institute for Nuclear Research (Hungary)
BAS	British Antarctic Survey (United Kingdom)
BMKG	Agency for Meteorology, Climatology and Geophysics (Indonesia)
CHMI	Czech Hydrometeorological Institute (Czech Republic)
CMA	China Meteorological Administration (China)
CSIRO	Commonwealth Scientific and Industrial Research Organisation (Australia)
DMC	Dirección Meteorológica de Chile (Chile)
DWD	German Meteorological Service (Germany)
ECCC	Environment and Climate Change Canada (Canada)
EMA	Egyptian Meteorological Authority (Egypt)
Empa	Swiss Federal Laboratories for Materials Science and Technology (Switzerland)
ENEA	Italian National Agency for New Technologies, Energy and Sustainable Economic Development (Italy)
FMI	Finnish Meteorological Institute (Finland)
FRA	Fisheries Research Agency (Japan)
GAGE	Global Atmospheric Gases Experiment
GAW	Global Atmosphere Watch (WMO)
GERC	National Institute of Environmental Research (Republic of Korea)
HATS	Halocarbons and other Atmospheric Trace Species Group, NOAA/GML (USA)
HKO	Hong Kong Observatory (Hong Kong, China)
HMS	Hungarian Meteorological Service (Hungary)
IAA	Dirección Nacional del Antártico - Instituto Antartico Argentino, Buenos Aires, Argentina (Argentina)
IAFMS	Italian Air Force Mountain Centre (Italy)
ICOS	Integrated Carbon Observation System (European Union)
IGP	Instituto Geofísico del Perú (Peru)
IIA	CNR - Institute of Atmospheric Pollution Research (Italy)
IMKIFU	Fraunhofer - Institute for Atmospheric Environmental Research (Germany)
INMH	National Meteorological Administration (Romania)
INPE	National Institute in Space Research (Brazil)
INRNE	Institute for Nuclear Research and Nuclear Energy (Bulgaria)
INSTAAR	Institute of Arctic and Alpine Research, University of Colorado (USA)
IOEP	Institute of Environmental Protection - NRI (Poland)
ISAC	National Research Council, Institute of Atmospheric Sciences and Climate (Italy)
ITM	Department of Applied Environmental Science, Stockholm University (Sweden)
JAMSTEC	Japan Agency for Marine - Earth Science and Technology (Japan)
JMA	Japan Meteorological Agency (Japan)

KIT	Karlsruhe Institute of Technology (Germany)
KMA	Korea Meteorological Administration (Republic of Korea)
KMD	Kenya Meteorological Department (Kenya)
KRISS	Korea Research Institute of Standards and Science (Republic of Korea)
KSNU	Kyrgyz National University (Kyrgyzstan)
KUP	Physics Institute, Climate and Environmental Physics, University of Bern (Switzerland)
Kyrgyzhydromet	Agency on Hydrometeorology under Ministry of Emergency Situations of the Kyrgyz Republic (Kyrgyzstan)
LA	Laboratoire d'Aérologie (France)
LAMP	Laboratoire de Météorologie Physique (France)
LSCE	Laboratoire des Sciences du Climat et de l'Environnement (France)
METAS	Federal Institute of Metrology (Switzerland)
METRI	National Institute of Meteorological Research, KMA (Republic of Korea)
MGO	Voeikov Main Geophysical Observatory (Russian Federation)
MMD	Malaysian Meteorological Department (Malaysia)
MPI-BGC	Max-Planck Institute (MPI) for Biogeochemistry in Jena (Germany)
MRI	Meteorological Research Institute (Japan)
NAGOU	Nagoya University (Japan)
NEDO	New Energy and Industrial Technology Development Organization (Japan)
NIES	National Institute for Environmental Studies (Japan)
NILU	Norwegian Institute for Air Research (Norway)
NIST	National Institute of Standards and Technology (USA)
NIWA	National Institute of Water & Atmospheric Research Ltd. (New Zealand)
NOAA	National Oceanic and Atmospheric Administration (USA)
NOAA/GML	Global Monitoring Laboratory, NOAA (USA)
NPL	National Physical Laboratory (United Kingdom)
ONM	Office National de la Météorologie (Algeria)
OSAKAU	Osaka University (Japan)
PolyU	The Hong Kong Polytechnic University (Hong Kong, China)
RIVM	National Institute of Public Health and the Environment (Kingdom of the Netherlands)
RSE	Ricerca sul Sistema Energetico - RSE S.p.A. (Italy)
SAIPF	Center for Environmental Science in Saitama (Japan)
SAWS	South African Weather Service (South Africa)
SHIZU	Shizuoka University (Japan)
SIO	Scripps Institution of Oceanography (USA)
SMNA	National Weather Service (Argentina)
TU	Tohoku University (Japan)
UBAA	Federal Environment Agency Austria (Austria)
UBAG	German Environment Agency (Germany)
UMLT	University of Malta (Malta)
UNIURB	University of Urbino, Dep. of Pure and Applied Sciences (DISPEA) (Italy)
UNIVBRIS	Atmospheric Chemistry Research Group School of Chemistry University of Bristol (United Kingdom)
UoE	University of Exeter (United Kingdom)
UYRK	University of York (United Kingdom)
VNMHA	Viet Nam Meteorological and Hydrological Administration (Viet Nam)
WCC	World Calibration Centre
WDCGG	World Data Centre for Greenhouse Gases (WMO)
WMO	World Meteorological Organization

ATMOSPHERIC SPECIES:

Be	beryllium
CCl_4	tetrachloromethane (carbon tetrachloride)
C_2Cl_4	tetrachloroethene (tetrachloroethylene)
CFC-11	trichlorofluoromethane (chlorofluorocarbon-11, CCl_3F)
CFC-12	dichlorodifluoromethane (chlorofluorocarbon-12, CCl_2F_2)
CFC-113	1,1,2-trichloro-1,2,2-trifluoroethane (chlorofluorocarbon-113, CCl_2FCClF_2)
CFCs	chlorofluorocarbons
CH_4	methane
$CHBr_3$	tribromomethane (bromoform)
CH_2Br_2	dibromomethane (methylene bromide)
CH_3Br	bromomethane (methyl bromide)
CH_3CCl_3	1,1,1-trichloroethane (methyl chloroform)
CH_3D	deuterated methane
CH_3I	iodomethane (methyl iodide)
$CHCl_3$	trichloromethane (chloroform)
CH_2Cl_2	dichloromethane (methylene chloride)
CH_3Cl	chloromethane (methyl chloride)
C_2HCl_3	trichloroethene (trichloroethylene)
CO	carbon monoxide
CO_2	carbon dioxide
COS	carbon oxide sulfide (carbonyl sulfide)
H_2	hydrogen
Halon-1211	bromochlorodifluoromethane ($CBrClF_2$)
Halon-1301	bromotrifluoromethane ($CBrF_3$)
HCFC-141b	1,1-dichloro-1-fluoroethane (hydrochlorofluorocarbon-141b, CH_3CCl_2F)
HCFC-142b	1-chloro-1,1-difluoroethane (hydrochlorofluorocarbon-142b, CH_3CClF_2)
HCFC-22	chlorodifluoromethane (hydrochlorofluorocarbon-22, $CHClF_2$)
HCFCs	hydrochlorofluorocarbons
HFC-134a	1,1,1,2-tetrafluoroethane (hydrofluorocarbon-134a, CH_2FCF_3)
HFC-152a	1,1-difluoroethane (hydrofluorocarbon-152a, CHF_2CH_3)
HFCs	hydrofluorocarbons
N_2O	nitrous oxide
NF_3	nitrogen trifluoride
PFCs	perfluorocarbons
Rn	radon
SF_6	sulfur hexafluoride
SO_2F_2	sulfuryl fluoride

UNITS:

ppm	parts per million
ppb	parts per billion
ppt	parts per trillion

Others:

TIC	total inorganic carbon
M/V	merchant vessel
R/V	research vessel

APPENDIX F LIST OF WMO/WDCGG PUBLICATIONS

DATA REPORTING MANUAL:

WDCGG No. 1	January	1991

WMO WDCGG DATA REPORT:

			(period of data accepted)				
WDCGG No. 2 Part A	October	1992	October	1990	~	August	1992
WDCGG No. 2 Part B	October	1992	October	1990	~	August	1992
WDCGG No. 3	October	1993	September	1992	~	March	1993
WDCGG No. 5	March	1994	April	1993	~	September	1993
WDCGG No. 6	September	1994	September	1993	~	March	1994
WDCGG No. 7	March	1995	April	1994	~	December	1994
WDCGG No. 9	September	1995	January	1995	~	June	1995
WDCGG No.10	March	1996	July	1995	~	December	1995
WDCGG No.11	September	1996	January	1996	~	June	1996
WDCGG No.12	March	1997	July	1996	~	November	1996
WDCGG No.14	September	1997	December	1996	~	June	1997
WDCGG No.16	March	1998	July	1997	~	December	1997
WDCGG No.17	September	1998	January	1998	~	June	1998
WDCGG No.18	March	1999	July	1998	~	December	1998
WDCGG No.20	September	1999	January	1999	~	June	1999
WDCGG No.21	March	2000	July	1999	~	December	1999
WDCGG No.23	September	2000	January	2000	~	June	2000
WDCGG No.25	March	2001	July	2000	~	December	2000

WMO WDCGG DATA CATALOGUE:

WDCGG No. 4	December	1993
WDCGG No.13	March	1997
WDCGG No.19	March	1999
WDCGG No.24	March	2001

WMO WDCGG DATA SUMMARY:

WDCGG No. 8	October	1995
WDCGG No.15	March	1998
WDCGG No.22	March	2000
WDCGG No.26	March	2002
WDCGG No.27	March	2003
WDCGG No.28	March	2004
WDCGG No.29	March	2005
WDCGG No.30	March	2006
WDCGG No.31	March	2007
WDCGG No.32	March	2008
WDCGG No.33	March	2009
WDCGG No.34	March	2010
WDCGG No.35	March	2011
WDCGG No.36	March	2012
WDCGG No.37	March	2013
WDCGG No.38	March	2014
WDCGG No.39	March	2015
WDCGG No.40	March	2016
WDCGG No.41	March	2017
WDCGG No.42	October	2018
WDCGG No.43	March	2020
WDCGG No.44	November	2020
WDCGG No.45	September	2021
WDCGG No.46	August	2022

WDCGG No.47	August	2023
WDCGG No.48	August	2024

WMO WDCGG CD-ROM: (period of data accepted)

CD-ROM No. 1	March	1995	October	1990	~	December	1994
CD-ROM No. 2	March	1996	October	1990	~	June	1995
CD-ROM No. 3	March	1997	October	1990	~	June	1996
CD-ROM No. 4	March	1998	October	1990	~	December	1997
CD-ROM No. 5	March	1999	October	1990	~	December	1998
CD-ROM No. 6	March	2000	October	1990	~	December	1999
CD-ROM No. 7	March	2001	October	1990	~	December	2000
CD-ROM No. 8	March	2002	October	1990	~	January	2002
CD-ROM No. 9	March	2003	October	1990	~	December	2002
CD-ROM No.10	March	2004	October	1990	~	December	2003
CD-ROM No.11	March	2005	October	1990	~	December	2004
CD-ROM No.12	March	2006	October	1990	~	December	2005
CD-ROM No.13	March	2007	October	1990	~	November	2006
CD-ROM No.14	March	2008	October	1990	~	November	2007

WMO WDCGG DVD: (period of data accepted)

DVD No. 1	March	2009	October	1990	~	November	2008
DVD No. 2	March	2010	October	1990	~	November	2009
DVD No. 3	March	2011	October	1990	~	November	2010
DVD No. 4	March	2012	October	1990	~	November	2011
DVD No. 5	March	2013	October	1990	~	November	2012
DVD No. 6	March	2014	October	1990	~	November	2013
DVD No. 7	March	2015	October	1990	~	November	2014
DVD No. 8	March	2016	October	1990	~	November	2015

REFERENCES

References

Alden, C. B., J. B. Miller, and J. W. C. White, Can Bottom-up Ocean CO2 Fluxes Be Reconciled with Atmospheric 13C Observations? *Tellus* **62B** (5), 369–388, https://doi.org/10.1111/j.1600-0889.2010.00481.x, 2010.

Ballantyne, A. P., C. B. Alden, J. B. Miller, P. P. Tans, and J. W. C. White, Increase in observed net carbon dioxide uptake by land and oceans during the past 50 years, *Nature*, **488**, 70–72, https://doi.org/10.1038/nature11299, 2012.

Basu, S., X. Lan, E. Dlugokencky, S. Michel, S. Schwietzke, J. B. Miller, L. Bruhwiler, Y. Oh, P. P. Tans, F. Apadula, L. V. Gatti, A. Jordan, J. Necki, M. Sasakawa, S. Morimoto, T. Di Iorio, H. Lee, J. Arduini, and G. Manca, Estimating emissions of methane consistent with atmospheric measurements of methane and $\delta^{13}C$ of methane, *Atmos. Chem. Phys.*, **22**, 15351-15377, https://doi.org/10.5194/acp-2022-317, 2022.

Blunden, J. and T. Boyer (eds.), State of the Climate in 2023, Bulletin of the American Meteorological Society, **105** (8) special supplement, https://doi.org/10.1175/2024BAMSStateoftheClimate.1, 2024.

Byrne, B., J. Liu, K. W. Bowman, M. Pascolini-Campbell, A. Chatterjee, S. Pandey, K. Miyazaki, G. R. van der Werf, D. Wunch, P. O. Wennberg, C.M. Roehl and S. Sinha, Carbon Emissions from the 2023 Canadian Wildfires. *Nature*, **633**, 835–839. https://doi.org/10.1038/s41586-024-07878-z, 2024.

Chandra, N., P. K. Patra, J. S. H. Bisht, A. Ito, T. Umezawa, N. Saigusa, S. Morimoto, S. Aoki, G. Janssens-Maenhout, R. Fujita, M. Takigawa, S. Watanabe, N. Saitoh, and J. G. Canadell, Emissions from the Oil and Gas Sectors, Coal Mining and Ruminant Farming Drive Methane Growth over the Past Three Decades, *Journal of the Meteorological Society of Japan. Ser. II*, **99**, https://doi.org/10.2151/jmsj.2021-015, 2021.

Cleveland, W. S., and S. J. Devlin, Locally weighted regression: an approach to regression analysis by local fitting, *J. Amer. Statist. Assn.*, **83**, 596–610, https://doi.org/10.1080/01621459.1988.10478639, 1988.

Conway, T. J., P. P. Tans, L. S. Waterman, K. W. Thoning, D. R. Kitzis, K. A. Masarie, and N. Zhang, Evidence for interannual variability of the carbon cycle from the National Oceanic and Atmospheric Administration/Climate Monitoring and Diagnostics Laboratory global air sampling network, *J. Geophys. Res.*, **99**, 22831–22855, https://doi.org/10.1029/94JD01951, 1994.

Crippa, M., E. Solazzo, G. Huang, D. Guizzardi, E. Koffi, M. Muntean, C. Schieberle, R. Friedrich, and G. Janssens-Maenhout, High resolution temporal profiles in the Emissions Database for Global Atmospheric Research, *Scientific Data*, **7**, 121, https://doi.org/10.1038/s41597-020-0462-2, 2020.

Dlugokencky, E. J., B. P. Walter, K. A. Masarie, P. M. Lang, and E. S. Kasischke, Measurements of an anomalous global methane increase during 19 98, *Geophys. Res. Lett.*, **28**, 499–502, https://doi.org/10.1029/2000GL012119, 2001.

Dlugokencky, E. J., S. Houweling, L. Bruhwiler, K. A. Masarie, P. M. Lang, J. B. Miller, and P. P. Tans, Atmospheric methane levels off: Temporary pause or a newsteady-state?, *Geophys. Res. Lett.*, **30**, 1992, https://doi.org/10.1029/2003GL018126, 2003.

Dlugokencky, E. J., R. C. Myers, P. M. Lang, K. A. Masarie, A. M. Crotwell, K. W. Thoning, B. D. Hall, J. W. Elkins, and L. P. Steele, Conversion of NOAA atmospheric dry air CH_4 mole fractions to a gravimetrically prepared standard scale, *J. Geophys. Res.*, **110**, D18306, https://doi.org/10.1029/2005JD006035, 2005.

Duchon, C. E., Lanczos filtering in one and two dimensions, *J. Appl. Meteor.*, **18**, 1016-1022, https://doi.org/10.1175/1520-0450(1979)018%3C1016:LFIOAT%3E2.0.CO;2, 1979.

Feng, L., P. I. Palmer, S. Zhu, R. J. Parker, and Y. Liu, Tropical Methane Emissions Explain Large Fraction of Recent Changes in Global Atmospheric Methane Growth Rate. *Nature Communications* **13**, 1378. https://doi.org/10.1038/s41467-022-28989-z, 2022.

Feng, L., P. I. Palmer, R. J. Parker, M. F. Lunt, and H. Bösch, Methane emissions are predominantly responsible for record-breaking atmospheric methane growth rates in 2020 and 2021, *Atmos. Chem. Phys.*, **23**, 4863–4880, https://doi.org/10.5194/acp-23-4863-2023, 2023.

Friedlingstein, P., M. O'Sullivan, M. W. Jones, R. M. Andrew, J. Hauck, P. Landschützer, C. Le Quéré, H. Li, I. T. Luijkx, A. Olsen, G. P. Peters, W. Peters, J. Pongratz, C. Schwingshackl, S. Sitch, J.G. Canadell, P. Ciais, R. B. Jackson, S. R. Alin, A. Arneth, V. Arora, N. R. Bates, M. Becker, N. Bellouin, C. F. Berghoff, H. C. Bittig, L. Bopp, P. Cadule, K. Campbell, M. A. Chamberlain, N. Chandra, F. Chevallier, L. P. Chini, T. Colligan, J. Decayeux, L. Djeutchouang, X. Dou, C. Duran Rojas, K. Enyo, W. Evans, A. Fay, R. A. Feely, D. J. Ford, A. Foster, T. Gasser, M. Gehlen, T. Gkritzalis, G. Grassi, L. Gregor, N. Gruber, Ö. Gürses, I. Harris, M. Hefner, J. Heinke, G. C. Hurtt, Y. Iida, T. Ilyina, A. R. Jacobson, A. Jain, T. Jarníková, A. Jersild, F. Jiang, Z. Jin, E. Kato, R. F. Keeling, K. Klein Goldewijk, J. Knauer, J. I. Korsbakken, S. K. Lauvset, N. Lefèvre, Z. Liu, J. Liu, L. Ma, S. Maksyutov, G. Marland, N. Mayot, P. McGuire, N. Metzl, N. M. Monacci, E. J. Morgan, S.-I. Nakaoka, C. Neill, Y.

Niwa, T. Nützel, L. Olivier, T. Ono, P. I. Palmer, D. Pierrot, Z. Qin, L. Resplandy, A. Roobaert, T. M. Rosan, C. Rödenbeck, J. Schwinger, T. L. Smallman, S. Smith, R. Sospedra-Alfonso, T. Steinhoff, Q. Sun, A. J. Sutton, R. Séférian, S. Takao, H. Tatebe, H. Tian, B. Tilbrook, O. Torres, E. Tourigny, H. Tsujino, F. Tubiello, G. van der Werf, R. Wanninkhof, X. Wang, D. Yang, X. Yang, Z. Yu, W. Yuan, X. Yue, S. Zaehle, N. Zeng, and J. Zheng, Global Carbon Budget 2024, *Earth Syst. Sci. Data*, **17**, 965–1039, https://doi.org/10.5194/essd-17-965-2025, 2025.

Fujita, R., S. Morimoto, T. Umezawa, K. Ishijima, P. K. Patra, D. E. J. Worthy, D. Goto, S. Aoki, and T. Nakazawa, Temporal Variations of the Mole Fraction, Carbon, and Hydrogen Isotope Ratios of Atmospheric Methane in the Hudson Bay Lowlands, Canada, *J. Geophys. Res.*, **123**, 4695–4711, https://doi.org/10.1002/2017JD027972, 2018.

Haan, D., and D. Raynaud, Ice core record of CO variations during the last two millennia: atmospheric implications and chemical interactions within the Greenland ice, *Tellus*, **50B**, 253–262, https://doi.org/10.3402/tellusb.v50i3.16101, 1998.

Hall, B. D. (ed.), J. W. Elkins, J. H. Butler, S. A. Montzka, T. M. Thompson, L. Del Negro, G. S. Dutton, D. F. Hurst, D. B. King, E. S. Kline, L. Lock, D. MacTaggart, D. Mondeel, F. L. Moore, J. D. Nance, E. A. Ray, and P. A. Romashkin, Halocarbons and Other Atmospheric Trace Species, Section 5 in Climate Monitoring and Diagnostics Laboratory Summary Report No. 25, 1998–1999, R. S. Schnell, D. B. King, and R. M. Rosson (eds.), NOAA-CMDL, Boulder, CO., USA, 2001.

Hall, B. D., G. S. Dutton, and J. W. Elkins, The NOAA nitrous oxide standard scale for atmospheric observations, *J. Geophys. Res.*, **112**, D09305, https://doi.org/10.1029/2006JD007954, 2007.

Hall, B. D., G. S. Dutton, D. J. Mondeel, J. D. Nance, M. Rigby, J. H. Butler, F. L. Moore, D. F. Hurst, and J. W. Elkins, Improving measurements of SF_6 for the study of atmospheric transport and emissions, *Atmospheric Measurement Techniques*, **4**, 2441-2451, https://doi.org/10.5194/amt-4-2441-2011, 2011.

Hall, B. D., A. M. Crotwell, D. R. Kitzis, T. Mefford, B. R. Miller, M. F. Schibig, and P. P. Tans, Revision of the World Meteorological Organization Global Atmosphere Watch (WMO/GAW) CO_2 calibration scale, *Atmos. Meas. Tech.*, **14**, 3015–3032, https://doi.org/10.5194/amt-14-3015-2021, 2021.

Höglund-Isaksson, L., A. Gómez-Sanabria, Z. Klimont, P. Rafaj, and W. Schöpp, Technical potentials and costs for reducing global anthropogenic methane emissions in the 2050 timeframe – results from the GAINS model, *Environmental Research Communications*, **2**, 025004, https://doi.org/10.1088/2515-7620/ab7457, 2020.

IPCC, Climate Change 2021: The Physical Science Basis. Contribution of Working Group I to the Sixth Assessment Report of the Intergovernmental Panel on Climate Change [Masson-Delmotte, V., P. Zhai, A. Pirani, S. L. Connors, C. Péan, S. Berger, N. Caud, Y. Chen, L. Goldfarb, M. I. Gomis, M. Huang, K. Leitzell, E. Lonnoy, J. B. R. Matthews, T. K. Maycock, T. Waterfield, O. Yelekçi, R. Yu, and B. Zhou (eds.)]. Cambridge University Press, Cambridge, United Kingdom and New York, NY, USA, 2391 pp., https://doi.org/10.1017/9781009157896, 2021.

Jackson, R. B., M. Saunois, P. Bousquet, J. G. Canadell, B. Poulter, A. R. Stavert, P. Bergamaschi, Y. Niwa, A. Segers, and A. Tsuruta, Increasing anthropogenic methane emissions arise equally from agricultural and fossil fuel sources, *Environmental Research Letters*, **15**, 071002, https://doi.org/10.1088/1748-9326/ab9ed2, 2020.

Ji, Q., M. A. Altabet, H. W. Bange, M. I. Graco, X. Ma, D. L. Arévalo-Martínez, and D. S. Grundle, Investigating the effect of El Niño on nitrous oxide distribution in the eastern tropical South Pacific, *Biogeosciences*, **16**, 2079–2093, https://doi.org/10.5194/bg-16-2079-2019, 2019.

Keeling, C. D., and R. Revelle, Effects of El Nino/Southern Oscillation on the Atmospheric Content of Carbon Dioxide. *Meteoritics*, **20**, 437–450, 1985.

Lan, X., P. Tans, C. Sweeney, A. Andrews, E. Dlugokencky, S. Schwietzke, J. Kofler, K. McKain, K. Thoning, M. Crotwell, S. Montzka, B. R. Miller, and S. C. Biraud, Long-Term Measurements Show Little Evidence for Large Increases in Total U.S. Methane Emissions Over the Past Decade, *Geophysical Research Letters*, **46**, 4991–4999, https://doi.org/10.1029/2018GL081731, 2019.

Laube, J. C. and S. Tegtmeier (Lead Authors), R. P. Fernandez, J. Harrison, L. Hu, P. Krummel, E. Mahieu, S. Park, L. Western, Update on Ozone-Depleting Substances (ODSs) and Other Gases of Interest to the Montreal Protocol, Chapter 1 in *Scientific Assessment of Ozone Depletion: 2022*, GAW Report No. **278**, 509 pp., WMO, Geneva, 2022.

Lee, H., S. Kim, H. Yoo, H. Choe, S.-O. Han, S.-B. Ryoo, B. Hall, G. Forster, Y. K. Camille, F. Meinhardt, I. Levin, L. Ries, C. Couret, M. Guillevic, S. A. Wyss, D. Rzesanke, A. Jordan, R. Moss, J. Lee, and J. Yu, The report of the result on SF_6 Inter-Comparison Experiment, 2016 – 2017, World Calibration Centre for SF_6, National Institute of Meteorological Sciences, Korea Meteorological Administration, 2017.

Michel, S. E., X. Lan, J. Miller, P. Tans, J. R. Clark, H. Schaefer, P. Sperlich, G. Brailsford, S. Morimoto, H. Moossen, and J. Li, Rapid Shift in Methane Carbon Isotopes Suggests Microbial Emissions Drove Record High Atmospheric Methane Growth in 2020–2022. *Proceedings of the National Academy of Sciences*, **121**,

https://doi.org/10.1073/pnas.2411212121, 2024.

Montzka, S. A., G. S. Dutton, P. Yu, E. Ray, R. W. Portmann, J. S. Daniel, L. Kuijpers, B. D. Hall, D. Mondeel, C. Siso, J. D. Nance, M. Rigby, A. J. Manning, L. Hu, F. Moore, B. R. Miller, and J. W. Elkins, An unexpected and persistent increase in global emissions of ozone-depleting CFC-11, *Nature*, **557**, 413–417, https://doi.org/10.1038/s41586-018-0106-2, 2018.

Montzka, S. A., G. S. Dutton, R. W. Portmann, M. P. Chipperfield, S. Davis, W. Feng, A. J. Manning, E. Ray, M. Rigby, B. D. Hall, C. Siso, J. D. Nance, P. B. Krummel, J. Mühle, D. Young, S. O'Doherty, P. K. Salameh, C. M. Harth, R. G. Prinn, R. F. Weiss, J. W. Elkins, H. Walter-Terrinoni, and C. Theodoridi, A decline in global CFC-11 emissions during 2018−2019, *Nature*, **590**, 428–432, https://doi.org/10.1038/s41586-021-03260-5, 2021.

Nisbet, E. G., E. J. Dlugokencky, M. R. Manning, D. Lowry, R. E. Fisher, J. L. France, S. E. Michel,J. B. Miller, J. W. C. White, B. Vaughn, P. Bousquet, J. A. Pyle, N. J. Warwick, M. Cain, R. Brownlow, G. Zazzeri, M. Lanoisellé, A. C. Manning, E. Gloor, D. E. J. Worthy, E.-G. Brunke, C. Labuschagne, E. W. Wolff, and A. L. Ganesan, Rising atmospheric methane: 2007-2014 growth and isotopic shift, *Global Biogeochemical Cycles*, **30**, 1356–1370, https://doi.org/10.1002/2016GB005406, 2016.

Novelli, P. C., K. A. Masarie, and P. M. Lang, Distributions and recent changes of carbon monoxide in the lower troposphere, *J. Geophys. Res.*, **103**, 19015–19033, https://doi.org/10.1029/98JD01366, 1998.

Novelli, P. C., K. A. Masarie, P. M. Lang, B. D. H all, R. C. Myers, and J. W. Elkins, Reanalysis of tropospheric CO trends: Effects of the 1997–199 8 wildfires, *J. Geophys. Res.,* **108**, 4464, https://d oi.org/10.1029/2002JD003031, 2003.

Oh, Y., Q. Zhuang, L. R. Welp, L. Liu, X. Lan, S. Basu, E. J. Dlugokencky, L. Bruhwiler, J. B. Miller, S. E. Michel, S. Schwietzke, P. Tans, P. Ciais, J. P. Chanton, Improved global wetland carbon isotopic signatures support post-2006 microbial methane emission increase, *Commun. Earth Environ.*, **3**, 159, https://doi.org/10.1038/s43247-022-00488-5, 2022.

Patra, P. K., T. Saeki, E. J. Dlugokencky, K. Ishijima, T. Umezawa, A. Ito, S. Aoki, S. Morimoto, E. A. Kort, A. Crotwell, K. Ravi Kumar, and T. Nakazawa, Regional methane emission estimation based on observed atmospheric concentrations (2002-2012), *Journal of the Meteorological Society of Japan. Ser. II*, **94**, 91–113, https://doi.org/10.2151/jmsj.2016-006, 2016.

Peng, S., X. Lin, R. L. Thompson, Y. Xi, G. Liu, D. Hauglustaine, X. Lan, B. Poulter, M. Ramonet, M. Saunois, Y. Yin, Z. Zhang, B. Zheng and P. Ciais, Wetland Emission and Atmospheric Sink Changes Explain Methane Growth in 2020. *Nature*, **612**, 477–482, https://doi.org/10.1038/s41586-022-05447-w, 2022.

Prinn, R. G., R. F. Weiss, P. J. Fraser, P. G. Simmonds, D. M. Cunnold, F. N. Alyea, S. O'Doherty, P. Salameh, B. R. Miller, J. Huang, R. H. J. Wang, D. E. Hartley, C. Harth, L. P. Steele, G. Sturrock, P. M. Midgley, A. McCulloch, A history of chemically and radiatively important gases in air deduced from ALE/GAGE/AGAGE, *Journal of Geophysical Research*, **105**, 17751-17792, https://doi.org/10.1029/2000JD900141, 2000.

Prinn, R. G., R. F. Weiss, J. Arduini, T. Arnold, H. L. DeWitt, P. J. Fraser, A. L. Ganesan, J. Gasore, C. M. Harth, O. Hermansen, J. Kim, P. B. Krummel, S. Li, Z. M. Loh, C. R. Lunder, M. Maione, A. J. Manning, B. R. Miller, B. Mitrevski, J. Mühle, S. O'Doherty, S. Park, S. Reimann, M. Rigby, T. Saito, P. K. Salameh, R. Schmidt, P. G. Simmonds, L. P. Steele, M. K. Vollmer, R. H. Wang, B. Yao, Y. Yokouchi, D. Young, and L. Zhou, History of chemically and radiatively important atmospheric gases from the Advanced Global Atmospheric Gases Experiment (AGAGE), *Earth Syst. Sci. Data*, **10**, 985–1018, https://doi.org/10.5194/essd-10-985-2018, 2018.

Rice, A. L., C. L. Butenhoff, D. G. Teama, F. H. Röger, M. A. K. Khalil, and R. A. Rasmussen, Atmospheric methane isotopic record favors fossil sources flat in 1980s and 1990s with recent increase, *Proceedings of the National Academy of Sciences*, **113**, 10791–10796, https://doi.org/10.1073/pnas.1522923113, 2016.

Saunois, M., A. Martinez, B. Poulter, Z. Zhang, P. Raymond, P. Regnier, J. G. Canadell, R. B. Jackson, P. K. Patra, P. Bousquet, P. Ciais, E. J. Dlugokencky, X. Lan, G. H. Allen, D. Bastviken, D. J. Beerling, D. A. Belikov, D. R. Blake, S. Castaldi, M. Crippa, B. R. Deemer, F. Dennison, G. Etiope, N. Gedney, L. Höglund-Isaksson, M. A. Holgerson, P. O. Hopcroft, G. Hugelius, A. Ito, A. K. Jain, R. Janardanan, M. S. Johnson, T. Kleinen, P. Krummel, R. Lauerwald, T. Li, X. Liu, K. C. McDonald, J. R. Melton, J. Mühle, J. Müller, F. Murguia-Flores, Y. Niwa, S. Noce, S. Pan, R. J. Parker, C. Peng, M. Ramonet, W. J. Riley, G. Rocher-Ros, J. A. Rosentreter, M. Sasakawa, A. Segers, S. J. Smith, E. H. Stanley, J. Thanwerdas, H. Tian, A. Tsuruta, F. N. Tubiello, T. S. Weber, G. van der Werf, D. E. Worthy, Y. Xi, Y. Yoshida, W. Zhang, B. Zheng, Q. Zhu, Q. Zhu, and Q. Zhuang, Global Methane Budget 2000-2020, *Earth Syst. Sci. Data*, **17**, 1873-1958, https://doi.org/10.5194/essd-17-1873-2025, 2025.

Schaefer, H., S. E. Mikaloff Fletcher, C. Veidt, K. R. Lassey, G. W. Brailsford, T. M. Bromley, E. J. Dlugokencky, S. E. Michel, J. B. Miller, I. Levin, D. C. Lowe, R. J. Martin, B. H. Vaughn, and J. W. C. White, A 21st-century shift from fossil-fuel to biogenic methane emissions indicated by $^{13}CH_4$, *Science*, **352**, 80–84, https://doi.org/10.1126/science.aad2705, 2016.

Schwietzke, S., O. A. Sherwood, L. M. P. Bruhwiler, J. B. Miller, G. Etiope, E. J. Dlugokencky, S. E. Michel, V. A. Arling, B. H. Vaughn, J. W. C. White, and P. P. Tans, Upward revision of global fossil fuel methane emissions based on isotope database, *Nature*, **538**, 88–91, https://doi.org/10.1038/nature19797, 2016.

Simpson, I.J., M. P. Sulbaek Andersen, S. Meinardi, L. Bruhwiler, N. J. Blake, D. Helmig, F. S. Rowland, and D. R. Blake, Long-term decline of global atmospheric ethane concentrations and implications for methane. *Nature*, **488**, 490–494, https://doi.org/10.1038/nature11342, 2012.

Solomon, S., J. Alcamo and A. R. Ravishankara, Unfinished business after five decades of ozone-layer science and policy, *Nature Communications*, **11**, 4272, https://doi.org/10.1038/s41467-020-18052-0, 2020.

Thompson, R. L., E. G. Nisbet, I. Pisso, A. Stohl, D. Blake, E. J. Dlugokencky, D. Helmig, and J. W. C. White, Variability in Atmospheric Methane From Fossil Fuel and Microbial Sources Over the Last Three Decades, *Geophysical Research Letters*, **45**, 11,499–11,508, https://doi.org/10.1029/2018GL078127, 2018.

Thompson, R. L., L. Lassaletta, P. K. Patra, C. Wilson, K. C. Wells, A. Gressent, E. N. Koffi, M. P. Chipperfield, W. Winiwarter, E. A. Davidson, H. Tian, and J. G. Canadell, Acceleration of global N_2O emissions seen from two decades of atmospheric inversion, *Nat. Clim. Chang.*, **9**, 993–998, https://doi.org/10.1038/s41558-019-0613-7, 2019.

Tian, H., N. Pan, R. L. Thompson, J. G. Canadell, P. Suntharalingam, P. Regnier, E. A. Davidson, M. Prather, P. Ciais, M. Muntean, S. Pan, W. Winiwarter, S. Zaehle, F. Zhou, R. B. Jackson, H. W. Bange, S. Berthet, Z. Bian, D. Bianchi, A. F. Bouwman, E. T. Buitenhuis, G. Dutton, M. Hu, A. Ito, A. K. Jain, A. Jeltsch-Thömmes, F. Joos, S. Kou-Giesbrecht, P. B. Krummel, X. Lan, A. Landolfi, R. Lauerwald, Y. Li, C. Lu, T. Maavara, M. Manizza, D. B. Millet, J. Mühle, P. K. Patra, G. P. Peters, X. Qin, P. Raymond, L. Resplandy, J. A. Rosentreter, H. Shi, Q. Sun, D. Tonina, F. N. Tubiello, G. R. van der Werf, N. Vuichard, J. Wang, K. C. Wells, L. M. Western, C. Wilson, J. Yang, Y. Yao, Y. You, and, Q. Zhu, Global nitrous oxide budget (1980–2020), *Earth Syst. Sci. Data*, **16**, 2543–2604, https://doi.org/10.5194/essd-16-2543-2024, 2024.

van der Woude, A. M., W. Peters, E. Joetzjer, S. Lafont, G. Koren, P. Ciais, M. Ramonet, Y. Xu, A. Bastos, S. Botía, S. Sitch, R. de Kok, T. Kneuer, D. Kubistin, A. Jacotot, B. Loubet, P. H. Herig-Coimbra, D. Loustau, and I. T. Luijkx, Temperature extremes of 2022 reduced carbon uptake by forests in Europe. *Nature Communications* **14**, 6218, https://doi.org/10.1038/s41467-023-41851-0, 2023.

Weiss, R. F., C. D. Keeling, and H. Craig, The determination of tropospheric nitrous oxide, *J. Geophys. Res. -Oceans*, **86**, 7197–7202, https://doi.org/10.1029/JC086iC08p07197, 1981.

WMO, Technical Report of Global Analysis Method for Major Greenhouse Gases by the World Data Center for Greenhouse Gases, GAW Report No. 184, WMO TD No. 1473, 2009.

WMO, WMO Global Atmosphere Watch (GAW) Implementation Plan: 2016-2023, GAW Report No.228, 2017.

WMO, 19th WMO/IAEA Meeting on Carbon Dioxide, Other Greenhouse Gases and Related Measurement Techniques (GGMT-2017), GAW Report No.242, 2018.

WMO, 20th WMO/IAEA Meeting on Carbon Dioxide, Other Greenhouse Gases and Related Measurement Techniques (GGMT-2019), GAW Report No.255, 2020.

WMO, Twenty-First WMO/IAEA Meeting on Carbon Dioxide, Other Greenhouse Gases and Related Measurement Techniques (GGMT-2022), GAW Report No. 292, WMO, 2024.

WMO, Report on the Unexpected Emissions of CFC-11, WMO-No.1268, 2021.

WMO, WMO Greenhouse Gas Bulletin No.19, 2023.

WMO, WMO Greenhouse Gas Bulletin No.20, 2024.

Worden, J. R., A. A. Bloom, S. Pandey, Z. Jiang, H. M. Worden, T. W. Walker, S. Houweling, and T. Röckmann, Reduced biomass burning emissions reconcile conflicting estimates of the post-2006 atmospheric methane budget, *Nature Communications*, **8**, 2227, https://doi.org/10.1038/s41467-017-02246-0, 2017.

Worthy, D. E. J., I. Levin, N. B. A. Trivett, A. J. Kuhlmann, J. F. Hopper, and M. K. Ernst, Seven years of continuous methane observations at a remote boreal site in Ontario, Canada, *J. Geophys. Res.*, **103**, 15995–16007, https://doi.org/10.1029/98JD00925, 1998.

Wu, Z., A. Vermeulen, Y. Sawa, U. Karstens, W. Peters, R. de Kok, X. Lan, Y. Nagai, A. Ogi, and O. Tarasova, Investigating the differences in calculating global mean surface CO_2 abundance: the impact of analysis methodologies and site selection, *Atmos. Chem. Phys*., **24**, 1249–1264, https://doi.org/10.5194/acp-24-1249-2024, 2024.

Yang S., B. X. Chang, M. J. Warner, T. S. Weber, A. M. Bourbonnais, A. E. Santoro, A. Kock, R. E. Sonnerup, J. L. Bullister, S. T. Wilson, and D. Bianchi, Global reconstruction reduces the uncertainty of oceanic nitrous oxide emissions and reveals a vigorous seasonal cycle, *Proceedings of the National Academy of Sciences*, **117(22)**, 11954–11960, https://doi.org/10.1073/pnas.1921914117, 2020.

Zhang, Z., B. Poulter, A. F. Feldman, Q. Ying, P. Ciais, S. Peng, and X. Li, Recent intensification of wetland methane feedback, *Nature Climate Change*, **13**, 430–433, https://doi.org/10.1038/s41558-023-01629-0, 2023.

Zheng, B., F. Chevallier, Y. Yin, P. Ciais, A. Fortems-

Cheiney, M. N. Deeter, R. J. Parker, Y. Wang, H. M. Worden, and Y. Zhao, Global atmospheric carbon monoxide budget 2000–2017 inferred from multi-species atmospheric inversions, *Earth Syst. Sci. Data*, **11**, 1411–1436, https://doi.org/10.5194/essd-11-1411-2019, 2019.

Zhao, C. L., P. P. Tans, and K. W. Thoning, A high precision manometric system for absolute calibrations of CO_2 in dry air, *J. Geophys. Res.*, **102**, 5885–5894, https://doi.org/10.1029/96JD03764, 1997.